



DIABETIC RETINOPATHY CLASSIFICATION AND INTERPRETATION USING DEEP LEARNING TECHNIQUES

Jordi De la Torre Gallart

ADVERTIMENT. L'accés als continguts d'aquesta tesi doctoral i la seva utilització ha de respectar els drets de la persona autora. Pot ser utilitzada per a consulta o estudi personal, així com en activitats o materials d'investigació i docència en els termes establerts a l'art. 32 del Text Refós de la Llei de Propietat Intel·lectual (RDL 1/1996). Per altres utilitzacions es requereix l'autorització prèvia i expressa de la persona autora. En qualsevol cas, en la utilització dels seus continguts caldrà indicar de forma clara el nom i cognoms de la persona autora i el títol de la tesi doctoral. No s'autoritza la seva reproducció o altres formes d'explotació efectuades amb finalitats de lucre ni la seva comunicació pública des d'un lloc aliè al servei TDX. Tampoc s'autoritza la presentació del seu contingut en una finestra o marc aliè a TDX (framing). Aquesta reserva de drets afecta tant als continguts de la tesi com als seus resums i índexs.

ADVERTENCIA. El acceso a los contenidos de esta tesis doctoral y su utilización debe respetar los derechos de la persona autora. Puede ser utilizada para consulta o estudio personal, así como en actividades o materiales de investigación y docencia en los términos establecidos en el art. 32 del Texto Refundido de la Ley de Propiedad Intelectual (RDL 1/1996). Para otros usos se requiere la autorización previa y expresa de la persona autora. En cualquier caso, en la utilización de sus contenidos se deberá indicar de forma clara el nombre y apellidos de la persona autora y el título de la tesis doctoral. No se autoriza su reproducción u otras formas de explotación efectuadas con fines lucrativos ni su comunicación pública desde un sitio ajeno al servicio TDR. Tampoco se autoriza la presentación de su contenido en una ventana o marco ajeno a TDR (framing). Esta reserva de derechos afecta tanto al contenido de la tesis como a sus resúmenes e índices.

WARNING. Access to the contents of this doctoral thesis and its use must respect the rights of the author. It can be used for reference or private study, as well as research and learning activities or materials in the terms established by the 32nd article of the Spanish Consolidated Copyright Act (RDL 1/1996). Express and previous authorization of the author is required for any other uses. In any case, when using its content, full name of the author and title of the thesis must be clearly indicated. Reproduction or other forms of for profit use or public communication from outside TDX service is not allowed. Presentation of its content in a window or frame external to TDX (framing) is not authorized either. These rights affect both the content of the thesis and its abstracts and indexes.



UNIVERSITAT
ROVIRA i VIRGILI

Diabetic Retinopathy Classification and Interpretation using Deep Learning Techniques

JORDI DE LA TORRE GALLART



DOCTORAL THESIS
2018

UNIVERSITAT ROVIRA I VIRGILI

DIABETIC RETINOPATHY CLASSIFICATION AND INTERPRETATION USING DEEP LEARNING TECHNIQUES

Jordi De la Torre Gallart

Diabetic Retinopathy Classification and Interpretation using Deep Learning Techniques

DOCTORAL THESIS

Author:

Jordi DE LA TORRE GALLART

Supervisors:

Dra. Aïda VALLS MATEU and

Dr. Domènec Savi PUIG VALLS

Department d'Enginyeria Informàtica i Matemàtiques



UNIVERSITAT ROVIRA i VIRGILI

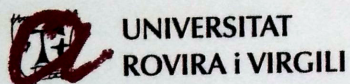
Tarragona

2018

UNIVERSITAT ROVIRA I VIRGILI

DIABETIC RETINOPATHY CLASSIFICATION AND INTERPRETATION USING DEEP LEARNING TECHNIQUES

Jordi De la Torre Gallart



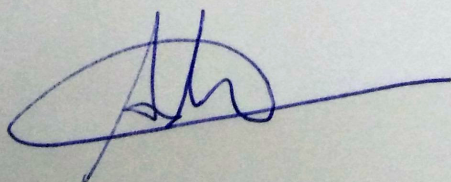
Departament d'Enginyeria Informàtica
i Matemàtiques

Av. Països Catalans, 27
43007 Tarragona
Tel. +34 977 55 95 95
Fax. +34 977 55 95 97

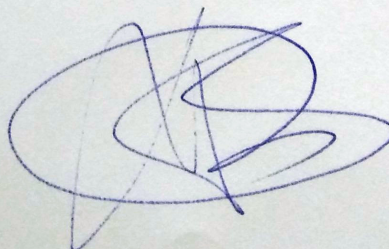
We STATE that the present study, entitled "Diabetic Retinopathy Classification and Interpretation using Deep Learning Techniques", presented by Jordi DE LA TORRE GALLART, for the award of the degree of Doctor, has been carried out under our supervision at the Department d'Enginyeria Informàtica i Matemàtiques.

Tarragona, November 2018.

Doctoral Thesis Supervisors,



Dra. Aida Valls Mateu



Dr. Domènec Savi Puig Valls

UNIVERSITAT ROVIRA I VIRGILI

DIABETIC RETINOPATHY CLASSIFICATION AND INTERPRETATION USING DEEP LEARNING TECHNIQUES

Jordi De la Torre Gallart

*To my wife Ana,
my children Pol & Alba,
my parents José & Tere and
my siblings Sonia, Xavi & Sergi.*

UNIVERSITAT ROVIRA I VIRGILI

DIABETIC RETINOPATHY CLASSIFICATION AND INTERPRETATION USING DEEP LEARNING TECHNIQUES

Jordi De la Torre Gallart

“Study hard what interests you the most in the most undisciplined, irreverent and original manner possible.”

Richard Feynman

“El amor al saber, la curiosidad, el asombro, es lo que puede sostener a cualquier ser humano.”

Antonio Escotado

“The process of creativity and genius are inherent in human consciousness.”

David R. Hawkins

“Nada para mí que no sea para los otros.”

Alejandro Jodorowsky

UNIVERSITAT ROVIRA I VIRGILI

DIABETIC RETINOPATHY CLASSIFICATION AND INTERPRETATION USING DEEP LEARNING TECHNIQUES

Jordi De la Torre Gallart

Acknowledgements

This work is supported by the URV grant 2015PFR-URV-B2-60 and the Spanish research projects PI15/01150 and PI12/01535 (Instituto Salud Carlos III).

I would like to express my gratitude to my supervisors Dra. Aida Valls and Dr. Domènec Puig for their useful guidance, insightful comments, and considerable encouragement to complete this thesis.

I would also like to express my gratitude to Dr. Pere Romero-Aroca and his team of collaborators of the Hospital Universitari Sant Joan de Reus, for their trust, passion and for providing the medical interpretation assessment required in this thesis.

I would also like to thank to all the Artificial Intelligence Community, specially to Geoffrey Hinton, Yann LeCun, Yoshua Bengio and Andrew Ng, an example to follow for their proved generosity sharing their knowledge in benefit of all Humanity.

My gratitude also for Facebook Inc. and Google Inc., technological leader companies in favor of public research, collaborating, designing and publicly sharing freely important part of their research and their machine learning tools: PyTorch and Tensorflow, helping to speed up immensely the creation of greatly beneficial products for all of us.

My gratitude for all the Open Source Community. Culture of collaboration is key for our success as Civilization.

Without all of them this thesis would not be possible.

UNIVERSITAT ROVIRA I VIRGILI

DIABETIC RETINOPATHY CLASSIFICATION AND INTERPRETATION USING DEEP LEARNING TECHNIQUES

Jordi De la Torre Gallart

Contents

| | |
|--|-------------|
| Acknowledgements | ix |
| List of Figures | xvii |
| List of Tables | xxi |
| Abstract | xxv |
| 1 Introduction | 1 |
| 1.1 Motivation | 1 |
| 1.2 Objectives | 3 |
| 1.2.1 Design of a DR classifier | 3 |
| 1.2.2 Design of a system for results interpretation | 4 |
| 1.2.3 Design a model for facilitating the understanding of explanations | 4 |
| 1.3 Contributions | 5 |
| 1.4 Thesis organization | 6 |
| 2 Background | 7 |
| 2.1 Diabetic retinopathy | 7 |
| 2.1.1 Retina health evaluation | 9 |
| Fundus photography | 10 |
| 2.1.2 Diabetic retinopathy grading and classification | 11 |
| 2.2 Evaluation measures for disease grading | 14 |
| 2.2.1 Confusion matrix | 15 |
| 2.2.2 Sensitivity and Specificity | 16 |
| 2.2.3 Positive and Negative Predictive Value | 16 |
| 2.2.4 False Positive and Negative Rates | 17 |
| 2.2.5 False Discovery and Omission Rates | 17 |

| | | |
|----------|---|-----------|
| 2.2.6 | Accuracy | 18 |
| 2.2.7 | Balanced measures | 18 |
| 2.2.8 | The Kappa family of statistics | 19 |
| 2.2.9 | How to define human performance | 21 |
| 2.3 | Machine Learning | 21 |
| 2.3.1 | Supervised Learning | 22 |
| | Classification vs Regression | 22 |
| | Dataset management | 23 |
| | Strategies for hyper-parameter optimization | 23 |
| 2.3.2 | Algorithms used in supervised machine learning | 24 |
| 2.3.3 | Pattern recognition | 26 |
| | Traditional models of pattern recognition | 26 |
| | Deep Learning for pattern recognition | 26 |
| | Types of Deep Learning architectures | 27 |
| | Convolutional neural networks | 27 |
| 2.3.4 | Prediction error: bias vs variance | 31 |
| 2.3.5 | Model ensembling | 32 |
| 2.4 | Data | 33 |
| 2.4.1 | Datasets | 33 |
| 2.4.2 | EyePACS dataset | 34 |
| 2.4.3 | Messidor-2 dataset | 34 |
| 2.4.4 | HUSJR dataset | 34 |
| 2.5 | Summary of the data and methods used in this thesis | 35 |
| I | Classification | 37 |
| 3 | Preliminary Models | 39 |
| 3.1 | Introduction | 39 |
| 3.2 | Related work | 40 |
| 3.3 | Data | 41 |
| 3.4 | Methodology for retinal image classification | 41 |
| | 3.4.1 Evaluation function | 42 |
| | 3.4.2 Data pre-processing and data augmentation | 43 |
| | 3.4.3 Model | 43 |
| | 3.4.4 Training procedure | 44 |
| | 3.4.5 Testing procedure | 45 |

| | | |
|----------|---|-----------|
| 3.4.6 | Probabilistic combination of the models of both eyes | 46 |
| 3.5 | Experiments | 48 |
| 3.6 | Conclusions | 49 |
| 4 | Kappa a Loss Function for Ordinal Regression | 51 |
| 4.1 | Introduction | 51 |
| 4.2 | Deep learning method | 54 |
| 4.3 | Weighted kappa as loss function in deep learning | 56 |
| 4.3.1 | Mathematical foundation | 57 |
| 4.3.2 | Partial derivatives of the weighted kappa loss function | 59 |
| 4.4 | Experiments | 60 |
| 4.4.1 | Case 1. Search results relevance | 60 |
| | Problem definition | 60 |
| | Data | 61 |
| | Procedure | 61 |
| 4.4.2 | Case 2. Life insurance assessment | 61 |
| | Problem definition | 61 |
| | Data | 62 |
| | Procedure | 62 |
| 4.4.3 | Case 3. Diabetic retinopathy detection | 63 |
| | Problem definition | 63 |
| | Data | 63 |
| | The models | 64 |
| | Procedure | 65 |
| 4.5 | Results | 66 |
| 4.5.1 | Case 1. Search results relevance | 66 |
| 4.5.2 | Case 2. Life insurance assessment | 66 |
| 4.5.3 | Case 3. Diabetic retinopathy detection | 67 |
| 4.5.4 | Overall discussion on the performance improvement | 70 |
| 4.6 | Conclusions | 71 |
| 5 | Enhanced Models | 79 |
| 5.1 | Introduction | 79 |
| 5.2 | Related work | 82 |
| 5.3 | Classification model for DR | 83 |
| 5.3.1 | Data | 83 |

| | | |
|-----------|---|------------|
| 5.3.2 | Construction of the classifier | 83 |
| | Design guidelines for DR classification | 84 |
| | Classification model description | 88 |
| 5.3.3 | Training procedure | 88 |
| 5.4 | Results | 89 |
| 5.5 | Conclusions | 91 |
| 6 | Classification Stability | 93 |
| 6.1 | Introduction | 93 |
| 6.2 | Methods | 94 |
| 6.3 | Results | 95 |
| | 6.3.1 Rotation | 95 |
| | 6.3.2 Lightness | 99 |
| | 6.3.3 Saturation | 100 |
| | 6.3.4 Hue | 101 |
| 6.4 | Conclusions | 101 |
| II | Interpretation | 119 |
| 7 | Explanation Maps Generation | 121 |
| 7.1 | Introduction | 121 |
| 7.2 | Related work | 123 |
| | 7.2.1 Sensitivity maps | 123 |
| | 7.2.2 Layer-wise relevance propagation | 123 |
| | 7.2.3 Taylor-type decomposition | 124 |
| | 7.2.4 Deep Taylor decomposition | 125 |
| 7.3 | Receptive field score distribution model | 125 |
| | 7.3.1 Score propagation through an activation function node | 128 |
| | 7.3.2 Score propagation through a batch normalization node | 129 |
| | 7.3.3 Score propagation through a convolutional layer | 129 |
| | 7.3.4 Score propagation through pooling layers | 130 |
| | 7.3.5 Score propagation through a fully connected layer | 131 |
| | 7.3.6 Score propagation through a dropout layer | 131 |
| | 7.3.7 Mapping the score of hidden layers and S_k into input-space | 132 |
| 7.4 | Results | 132 |
| | 7.4.1 Pixel and receptive field map generation | 133 |

| | | |
|------------|---|------------|
| 7.5 | Conclusions | 137 |
| 8 | Feature Space Compression | 139 |
| 8.1 | Introduction | 139 |
| 8.2 | ICA based interpretation procedure | 140 |
| 8.2.1 | Mathematical formalization | 142 |
| 8.3 | Results | 144 |
| 8.3.1 | Data | 144 |
| 8.3.2 | Baseline model | 144 |
| 8.3.3 | Model modifications | 144 |
| 8.3.4 | Score components contribution for a test sample | 146 |
| 8.4 | Conclusions | 147 |
| III | Experimental Application and Conclusions | 151 |
| 9 | Inference using HUSJR data | 153 |
| 9.1 | Introduction | 153 |
| 9.2 | Methods | 155 |
| 9.2.1 | Original model evaluation | 155 |
| 9.2.2 | Category standardization | 155 |
| 9.2.3 | Model and dataset adaptations | 155 |
| 9.2.4 | Final evaluation | 156 |
| 9.3 | Results | 156 |
| 9.3.1 | Original model evaluation | 156 |
| 9.3.2 | Category standardization | 158 |
| 9.3.3 | Model adaptation | 158 |
| 9.3.4 | Results re-evaluation | 158 |
| 9.4 | Conclusions | 159 |
| 10 | Conclusions | 161 |
| 10.1 | Summary of contributions | 161 |
| 10.2 | Future research lines | 165 |
| | Bibliography | 167 |

UNIVERSITAT ROVIRA I VIRGILI

DIABETIC RETINOPATHY CLASSIFICATION AND INTERPRETATION USING DEEP LEARNING TECHNIQUES

Jordi De la Torre Gallart

List of Figures

| | | |
|------|---|----|
| 2.1 | Schematic diagram of the human eye | 8 |
| 2.2 | Typical aspect of a fundus eye camera | 10 |
| 2.3 | Eye fundus images taken from a healthy patient | 11 |
| 2.4 | Sample image of a Mild NPDR (class 1) | 12 |
| 2.5 | Sample image of a Moderate NPDR (class 2) | 13 |
| 2.6 | Sample image of a Severe NPDR (class 3) | 14 |
| 2.7 | Sample image of a PDR (class 4) | 15 |
| 2.8 | Traditional pattern recognition scheme | 26 |
| 2.9 | Deep Learning pattern recognition scheme | 27 |
| 2.10 | High level representation of a typical convolutional neural network | 28 |
| 2.11 | Convolution operator of 3x3, stride 2, padding 1 | 29 |
| 2.12 | Max-pooling operator of 3x3, stride 1, padding 0 | 29 |
| 2.13 | Typical activation functions used in Deep Learning | 30 |
| 2.14 | Bias vs Variance extreme possible scenarios | 32 |
| 2.15 | Datasets class percentage distribution | 35 |
| 3.1 | Architecture of a 4 layer CNN | 44 |
| 3.2 | Testing ensemble used for evaluation | 46 |
| 4.1 | High level description of a deep learning image classification scheme | 54 |
| 4.2 | QWK_{val} vs BS - Search results relevance use case | 67 |
| 4.3 | QWK_{val} vs BS - Life insurance assessment use case | 68 |
| 4.4 | QWK_{val} vs BS - Diabetic Retinopathy detection use case | 69 |
| 4.5 | Histograms of DR prediction (qwk-loss vs log-loss) | 71 |
| 4.6 | QWK use cases confidence intervals | 72 |
| 5.1 | Model RF growth | 86 |

| | | |
|------|--|-----|
| 5.2 | Feature space cumulative PCA variance of training set . . . | 87 |
| 5.3 | Prediction model | 92 |
| 6.1 | Hue-Lightness-Saturation color space cone | 95 |
| 6.2 | Images used for testing model robustness (Tag: 0) | 96 |
| 6.3 | Images used for testing model robustness (Tag: 1) | 97 |
| 6.4 | Images used for testing model robustness (Tag: 2) | 98 |
| 6.5 | Images used for testing model robustness (Tag: 3) | 99 |
| 6.6 | Score vs Rotation (Tag: 0) | 103 |
| 6.7 | Score vs Rotation (Tag: 1) | 104 |
| 6.8 | Score vs Rotation (Tag: 2) | 105 |
| 6.9 | Score vs Rotation (Tag: 3) | 106 |
| 6.10 | Score vs Lightness (Tag: 0) | 107 |
| 6.11 | Score vs Lightness (Tag: 1) | 108 |
| 6.12 | Score vs Lightness (Tag: 2) | 109 |
| 6.13 | Score vs Lightness (Tag: 3) | 110 |
| 6.14 | Score vs Saturation (Tag: 0) | 111 |
| 6.15 | Score vs Saturation (Tag: 1) | 112 |
| 6.16 | Score vs Saturation (Tag: 2) | 113 |
| 6.17 | Score vs Saturation (Tag: 3) | 114 |
| 6.18 | Score vs Hue (Tag: 0) | 115 |
| 6.19 | Score vs Hue (Tag: 1) | 116 |
| 6.20 | Score vs Hue (Tag: 2) | 117 |
| 6.21 | Score vs Hue (Tag: 3) | 118 |
| 7.1 | Score distribution through layers | 127 |
| 7.2 | Score propagation through an activation function node . . . | 128 |
| 7.3 | Score propagation through an batch normalization node . . | 129 |
| 7.4 | Convolution score calculation | 130 |
| 7.5 | Score propagation through different pooling layers | 130 |
| 7.6 | Score propagation through a fully connected node | 131 |
| 7.7 | Score propagation through a dropout node | 132 |
| 7.8 | Class 4 sample image | 133 |
| 7.9 | Class 4 sample intermediate score maps | 134 |
| 7.10 | Total score maps | 136 |
| 8.1 | Model changes done for improving explainability | 142 |

| | | |
|-----|--|-----|
| 8.2 | Contribution of each ICA component in the classification final score | 144 |
| 8.3 | Original and ICA feature space visualization | 146 |
| 8.4 | ICA score maps generated for a class 2 image RF 61x61 | 146 |
| 8.5 | ICA score maps generated for a class 4 image | 147 |
| 8.6 | ICA_2 score map for a class 3 image | 148 |
| 9.1 | Feature space visualization of HUSJR dataset | 157 |

UNIVERSITAT ROVIRA I VIRGILI

DIABETIC RETINOPATHY CLASSIFICATION AND INTERPRETATION USING DEEP LEARNING TECHNIQUES

Jordi De la Torre Gallart

List of Tables

| | |
|---|-----|
| 2.1 Binary confusion matrix | 16 |
| 2.2 List of the most successful classification architectures used for Imagenet prediction | 31 |
| 3.1 Testing scheme performance results | 45 |
| 3.2 Frequencies of combined occurrence of classes in both eyes . | 47 |
| 3.3 Conditional probabilities of occurrence of DR | 47 |
| 3.4 Best classification results for different input sizes | 48 |
| 3.5 Best classification results adding the probabilistic information of both eyes | 49 |
| 3.6 Best performing DCNN architecture | 50 |
| 4.1 Interpretation of Weighted Kappa | 53 |
| 4.2 Search results relevance experiments | 74 |
| 4.3 Life insurance assessment experiments | 75 |
| 4.4 DR detection experiments | 76 |
| 4.5 Summary of the difference in performance between qwk-loss and log-loss trained models in function of input size for the DR detection case | 77 |
| 5.1 Prediction performance & model complexity comparison of our proposal vs the state-of-the-art model (Messidor-2 data set) | 90 |
| 7.1 Class 4 score map statistics for the analyzed image | 135 |
| 9.1 CM of HUSJR data using EyePACS trained model | 157 |
| 9.2 CM of HUSJR data using EyePACS trained model finetuned with Messidor | 158 |

UNIVERSITAT ROVIRA I VIRGILI

DIABETIC RETINOPATHY CLASSIFICATION AND INTERPRETATION USING DEEP LEARNING TECHNIQUES

Jordi De la Torre Gallart

List of Abbreviations

| | |
|-------------|---|
| ML | Machine Learning |
| DL | Deep Learning |
| CNN | Convolutional Neural Network |
| DCNN | Deep Convolutional Neural Network |
| BS | Batch Size |
| RF | Receptive Field |
| PCA | Principal Components Analysis |
| ICA | Independent Components Analysis |
| IC | Independent Component |
| | |
| DM | Diabetes Mellitus |
| DR | Diabetic Retinopathy |
| DME | Diabetic Macular Edema |
| NPDR | Non-Proliferative Diabetic Retinopathy |
| PDR | Proliferative Diabetic Retinopathy |
| | |
| QWK | Quadratic Weighted Kappa |
| CM | Confusion Matrix |
| TP | True Positive |
| TN | True Negative |
| FP | False Positive |
| FN | False Negative |
| ACC | Accuracy |
| PPV | Positive Predictive Value |
| NPV | Negative Predictive Value |
| FPR | False Positive Rate |
| FNR | False Negative Rate |
| FDR | False Discovery Rate |
| FOR | False Omission Rate |

UNIVERSITAT ROVIRA I VIRGILI

DIABETIC RETINOPATHY CLASSIFICATION AND INTERPRETATION USING DEEP LEARNING TECHNIQUES

Jordi De la Torre Gallart

Abstract

Diabetic Retinopathy (DR) is a leading disabling chronic disease and one of the main causes of blindness and visual impairment in developed countries for diabetic patients. Studies reported that 90% of the cases can be prevented through early detection and treatment. Eye screening through retinal images is used by physicians to detect the lesions related with this disease. Due to the increasing number of diabetic people, the amount of images to be manually analyzed is becoming unaffordable. Moreover, training new personnel for this type of image-based diagnosis is long, because it requires to acquire expertise by daily practice.

In this thesis, we explore different novel methods for the automatic diabetic retinopathy disease grade classification using retina fundus images. For this purpose, we explore methods based in automatic feature extraction and classification, based on deep neural networks.

Furthermore, as results reported by these models are difficult to interpret, we design a new method for results interpretation. The model is designed in a modular manner in order to generalize its possible application to other networks and classification domains. We experimentally demonstrate that our interpretation model is able to detect retina lesions in the image solely from the classification information.

Additionally, we propose a method for compressing model feature-space information. The method is based on a independent component analysis over the disentangled feature space information generated by the model for each image and serves also for identifying the mathematically independent elements causing the disease. Using our previously mentioned interpretation method is also possible to visualize such components on the image.

Finally, we present an experimental application of our best model for classifying retina images of a different population, concretely from the Hospital de Reus. We study the possible presence of co-variate shift and present the results obtained from such a new population.

The methods proposed, achieve ophthalmologist performance level and are able to identify with great detail lesions present on images, inferred only from image classification information.

Chapter 1

Introduction

1.1 Motivation

Computer Science is the field of knowledge that deals with the study of computers and computational systems. Its principal areas include artificial intelligence & machine learning, computer systems & networks, security, databases, human-machine interaction, computer vision, numerical analysis, programming languages, software engineering, bioinformatics and theory of computing.

Computer vision is an interdisciplinary sub-field of Computer Science that deals with methods for understanding relevant information present in images. From an engineering perspective, its main purpose is developing methods and algorithms for automatically acquiring, processing, analyzing and understanding images. Typical problems addressed by computer vision include image classification, object detection, segmentation, semantic segmentation and text explanation generation.

Pattern recognition is a sub-field of Computer Vision which purpose is the design of methods for extracting information from images. It uses machine learning techniques for extracting the relevant information. Although its methods can be generally applied to any signal, a significant part of the field is devoted to extract information from image data.

Medical Imaging is the term used for describing the set of techniques used for obtaining visual representations of the interior of a body with the objective of being used for clinical analysis and medical intervention.

It seeks to reveal internal structures hidden inside the body for detecting possible pathologies, facilitating diagnosis. Such discipline incorporates radiology, magnetic resonance imaging, medical ultrasonography, endoscopy, elastography, tactile imaging, thermography, medical photography and nuclear medicine functional imaging techniques as positron emission tomography (PET) and Single-photon emission computed tomography (SPECT) (Bushberg and Boone, 2011). Such techniques have been essential for improving probability of early detection of many diseases and in this way, reducing also the resources required for treating patients, due to the fact that early stages of many diseases require milder treatments.

Diabetes mellitus (DM) is a chronic disease that affects nearly 400 million patients worldwide and is expected to increase up to 600 million adults by 2035 (Aguiree et al., 2013). Spain is expected to have nearly 3 million DM patients by 2030 (Shaw, Sicree, and Zimmet, 2010). Patients affected by DM can develop other diseases derived from diabetes. The most serious DM ocular derived disease is Diabetic Retinopathy (DR). DR is a leading disabling chronic disease and one of the main causes of blindness and visual impairment in developed countries for diabetic patients (Fong et al., 2004). Studies reported that 90% of the cases can be prevented through early detection and treatment. Eye screening through retinal image analysis is used by physicians to detect lesions related with this disease. Due to the increasing number of diabetic people, the amount of images to be manually analyzed is becoming unaffordable. Moreover, training new personnel for this type of image-based diagnosis is long, because it requires to acquire expertise by daily practice. Disease detection using non-mydratic fundus cameras results to be a very cost effective method for DR screening (Romero-Aroca et al., 2018).

Design of automatic diagnostics systems for Medical Imaging in general and for DR in particular, could help reducing the prevalence of most severe disease cases, increasing the cost effectiveness of diagnostic systems, reducing its associated costs and increasing patients life quality. The motivation of this thesis is the exploration of new and effective methods for the diabetic retinopathy disease detection, classification and lesion detection through automatic analysis of retina fundus images.

Traditionally, pattern recognition automatic systems have been based on the extraction of hand-crafted engineered features or fixed kernels from

the image object of study and the use of a trainable classifier on top of them for obtaining the final classification. Using this scheme the problem of the DR detection has been based on hand engineering the features for detection of disease related lesions, ie. microaneurisms, hemorrhages and exudates in retinal images that maximize the performance of classifiers. This type of approach requires a good understanding of the disease mechanism, requiring a lot of labor time and being very task-specific and thereby not reusable in other classification domains.

In this thesis, we explore a completely different approach consisting on automatic feature learning. We explore the use deep convolutional neural network models for predicting disease classification.

1.2 Objectives

The objectives of this thesis are the creation of a human performance level diabetic retinopathy automatic classifier using Machine Learning techniques based on Deep Learning. The classifier should be able not only of reporting good classification indexes (near or better than human performance) but also to give additional information to the physicians about the important elements that the model took into account to arrive to every particular conclusion.

To reach this final objective, we need to achieve other intermediate goals that are described in the following sections. Such intermediate goals are (1) design a classifier with good balance between performance and required hardware resources, (2) design a method for explaining the results reported by the model and finally (3) design a way to express as concisely as possible the results in order to facilitate the interpretation by human experts.

1.2.1 Design of a DR classifier

Deep learning classifier is known to be the best available technique for classification in general applications based on natural images recognition. At the beginning of the elaboration of this thesis, deep learning for medical imaging was in its infancy and it was not clear that such models were able

to evaluate the small lesions present in images and to infer from them a statistically relevant disease classification. Another challenge at the beginning of the elaboration of this thesis was the reduced number of available resources and the limitation of deep learning software libraries. Although having a big enough public dataset, we did not had enough computation capability for experimenting with big networks. The first attempts were focused on designing different types of networks, with different input sizes, in order to find the correct balance between size of the network and size of the input image, in order to maximize performance. Another challenge was choosing the right minimization function for training the network. As an ordinal regression problem, the evaluation function used for measuring classification performance was different from the traditional multi-class classification loss function, the log-loss. First networks were trained with log-loss. Afterwards we explored the possibility of directly optimizing some ordinal based evaluation function, like quadratic weighted kappa.

1.2.2 Design of a system for results interpretation

Deep learning classifiers use to work as black box intuition machines. When trained in the right way, they are able to have high statistical confidence but they do not give any clue of the reasons behind each decision. In medical imaging, it is critical to be able to explain the reasons behind a conclusion, because part of the curing process can be related with some kind of treatment over the disease causal elements. So, our goal for the case of DR disease was helping in the process of lesion location, facilitating an eventual treatment of surgery over local elements.

1.2.3 Design a model for facilitating the understanding of explanations

Machines treat the information in a way different than humans. Computers can handle efficiently multi-dimensional representations. Humans interpret data better when presented in reduced dimensional spaces (2D if possible). The last objective of the thesis is related with the design of techniques for compression representation.

1.3 Contributions

The main contributions of this thesis are:

1. Design of automatic classifiers based on deep neural networks able to reach ophthalmologist performance level.

Jordi de la Torre, Aïda Valls, and Domenec Puig (2016a). “Diabetic Retinopathy Detection Through Image Analysis Using Deep Convolutional Neural Networks”. In: *Artificial Intelligence Research and Development - Proceedings of the 19th International Conference of the Catalan Association for Artificial Intelligence, Barcelona, Catalonia, Spain, October 19-21, 2016*. Ed. by Àngela Nebot, Xavier Binefa, and Ramon López de Mántaras. Vol. 288. Frontiers in Artificial Intelligence and Applications. IOS Press, pp. 58–63. ISBN: 978-1-61499-695-8

2. Study of the usage of Quadratic Weighted Kappa index as a Deep Learning Loss Function for the optimization of ordinal regression problems.

Jordi de la Torre, Domenec Puig, and Aida Valls (2018). “Weighted kappa loss function for multi-class classification of ordinal data in deep learning”. In: *Pattern Recognition Letters* 105, pp. 144–154 Impact Factor: 1.952 (Q2)

3. Design of a generalized model for the interpretation of results reported by deep learning classifiers.

Jordi de la Torre, Aida Valls, and Domenec Puig (2017). “A Deep Learning Interpretable Classifier for Diabetic Retinopathy Disease Grading”. In: *arXiv preprint arXiv:1712.08107* Accepted for publication in Neurocomputing. Impact Factor: 3.241 (Q1)

4. Design of a method for compressing feature space internal representations of deep learning models.

Jordi de La Torre et al. (2018). “Identification and Visualization of the Underlying Independent Causes of the Diagnostic of Diabetic Retinopathy made by a Deep Learning Classifier”. In: *CoRR* abs/1809.08567. arXiv: 1809.08567. URL: <http://arxiv.org/abs/1809.08567>

5. Study of the feature space manifold stability of the designed diabetic retinopathy classifiers.
6. Application of designed classifiers into a real use case in Hospital de Reus. A software has been implemented for DR classification and lesion identification. Registered in Benelux Office for Intellectual Property. Reference number 109999.

1.4 Thesis organization

This thesis is organized as follows: In chapter 1 a brief description of the work motivation is presented. Main contributions done during thesis elaboration are described and journal publications are cited. In chapter 2 scope of the work is briefly explained, defining the challenges and tools & techniques used for solving them. The following chapters are organized in three differentiated parts: the first part groups chapters related with *Classification* (3, 4, 5 and 6), the second part groups chapters related with *Interpretation* (chapters 7 and 8) and finally, the third part groups *Experimental Applications and Conclusions* (chapters 9 and 10). In chapter 3 first designed classifiers are presented followed by some ensembling techniques used for improving results achieved, near human expert performance. In chapter 4 a new loss function for ordinal regression optimization is presented accompanied with experimental studies validating the increase of performance achieved against conventional optimization losses. In chapter 5 an improved version of first classifiers is presented, using the new derived loss function and other changes, achieving ophthalmologist level performance. In chapter 6 a feature-space manifold stability study is also presented for evaluation of the stability of the model internal representation to changes in input structure. In chapter 7 a general interpretation model for deep learning classifiers is presented and applied to the specific case of our diabetic retinopathy classifiers achieving an excellent performance in lesion detection. In chapter 8 a system for feature-space compression is presented. In chapter 9 a research results case study application is presented, applying the classifiers for prediction of *Hospital Universitari Sant Joan de Reus* population. A set of studies for evaluation of covariate shift of training and new test set population are also presented. Finally, in chapter 10 thesis conclusions and future work directions are described.

Chapter 2

Background

2.1 Diabetic retinopathy

Eyes are globular organs of sight present in humans and vertebrates with the function of capturing the light coming from the environment and convert it into signals that are interpreted by the brain as images. From this images the brain is able to extract information and construct abstractions from the external world. Eyes are composed of different parts, each one having a differentiated function (see figure 2.1). Light coming from the environment travels through the cornea, iris and lens, reaching the retina, situated in the internal back side of the eyeball. Retina is continuous with the optic nerve, and consists of several layers, one of which contains the rods and cones that are sensitive to light. Activated rods and cones transfer information through the optic nerve, that is interpreted by the brain as an image.

Diabetes is a disorder of the body due to its inability of producing or responding to the hormone insulin, resulting in abnormal metabolism of carbohydrates and elevated levels of glucose in the blood. Such high blood glucose levels can damage blood vessels and nerves, increasing the probability in diabetic patients of developing other derived diseases, like Diabetic Retinopathy.

Diabetes can be of two different types: type 1 and 2. Type 1 is an autoimmune disease that causes the insulin producing beta cells in the pancreas to be destroyed, preventing the body from being able to produce enough insulin to adequately regulate blood glucose levels. Because type

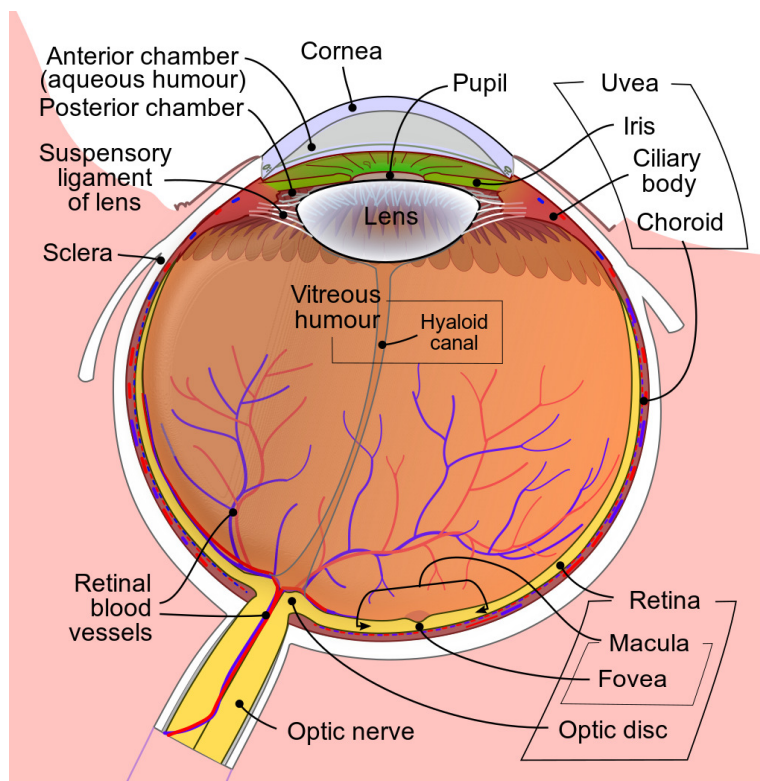


FIGURE 2.1: Schematic diagram of the human eye (source commons.wikimedia.org)

1 diabetes causes the loss of insulin production, it therefore requires regular insulin administration. Type 2 is a metabolic disorder that results in hyperglycemia, ie. high blood glucose levels, due to the body either being ineffective at using the insulin it has produced or being unable to produce enough insulin. Type 2 diabetes is characterized by the body being unable to metabolize glucose, leading to high levels of blood glucose, which over time, may damage the organs of the body. (www.diabetes.co.uk, 2018)

Diabetic Retinopathy is an associated disease derived from diabetes. It is caused by the damage of the small blood vessels of the retina. Due to diabetes disease related secondary effects, retinal blood vessels can break

down, leak or become blocked; affecting the transport of nutrients and oxygen to parts of the retina, causing impaired vision over time. Due to the blockages, abnormal blood vessels can grow on the retina surface, causing an increment of the probability of bleeding and liquid leakages. Such structural changes can result initially in vision blurring and in last stages, even in retinal detachment and/or glaucoma.

During the first two decades of the diabetes disease, nearly all patients with type 1 and more than 60% of patients with type 2 diabetes, will develop a retinopathy (Fong et al., 2004).

2.1.1 Retina health evaluation

There are several tests that a doctor may perform to evaluate retina eye health:

An *ophthalmoscope* is a specialized type of microscope that allows the inspection of the vitreous, retina and other internal structures of the eye. With this instrument is possible to create a mirrored image of the various portions of the eye.

A *visual field* or *perimetry test*, measures the ability of the examined eye to see straight ahead and the peripheral vision. The purpose of this test is to determine if there are any peripheral vision areas that are developing blind spots.

Fluorescein angiography allows the doctor to inspect retina blood vessels. A vegetable-based dye is injected into patient blood stream. As blood circulates in the retina, a series of quick, sequential photographs of the eye are taken. These photographs provide useful information about its condition. Fluorescein angiography is one of the most important tests performed for determining the diagnosis and treatment of retinal disorders.

B-scan ultrasound uses high frequency sound waves to view the back portions of the eye. This technology provides a full surface view of the eye that can be also used for retina condition evaluation.

Fundus photography utilizes special cameras to document and track the progress of certain retinal diseases, like diabetic retinopathy, as well as monitor its treatment. This type of images are the used in this thesis for creating the automatic diagnostic system.

Fundus photography

Fundus photography is a technique for capturing the internal part of the back of the eye. This technique allows the visualization of main structures present in the back of eye interior, ie. center and peripheral retina, the optic disc and the macula.

Figure 2.2 shows a photography of a typical camera used for capturing eye fundus images.



FIGURE 2.2: Typical aspect of a fundus eye camera (source commons.wikimedia.org)

Figure 2.3 shows an example of the fundus photography of both eyes of a healthy patient. In such images, it can be identified zones like central and peripheral retina, macula (darker part located at the center) and the optic disc (white spherical structure inside the retina).

With this type of photography is possible to identify, if they exist, the location and type of lesions and to infer from them a diagnostic.

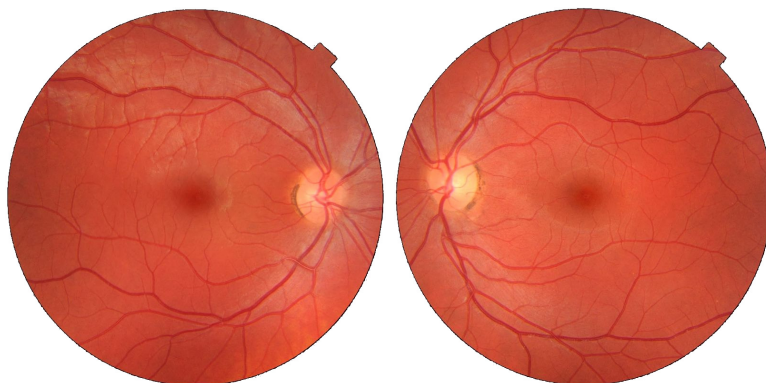


FIGURE 2.3: Left and right eye fundus images taken from a healthy patient (source commons.wikimedia.org)

2.1.2 Diabetic retinopathy grading and classification

Accurately grading diabetic retinopathy can be a significant challenge for a untrained person. Medical community establishes a standardized classification based on four severity stages (Wilkinson et al., 2003) determined by the type and number of lesions (as micro-aneurysms, hemorrhages and exudates) present in the retina: class 0 referring to no apparent Retinopathy, class 1 as a Mild Non-Proliferative Diabetic Retinopathy (NPDR), class 2 as Moderate NPDR, class 3 as a Severe NPDR and class 4 as a Proliferative DR.

Any of the stages can have no or few symptoms. Therefore, periodic dilated eye examinations are crucial for the detection and evolution study of the disease. Furthermore, diabetic macular edema can develop at any of these stages due to damaged and leaky blood vessels, affecting patient vision quality.

In the following sections diabetic retinopathy disease levels (Wilkinson et al., 2003) are described:

No apparent diabetic retinopathy (class 0)

The exams done to the fundus images of this class does not show any abnormality, either in the form of micro-aneurysms or in more complex

forms. A diabetic patient with no retinopathy has a $< 1\%$ chance of developing a PDR in the next four years (Klein et al., 2009).

Mild non-proliferative diabetic retinopathy (class 1)

This is the earliest stage of the disease. In this stage, micro-aneurysms are the only abnormality found in exams. Class 1 diabetic patients have a $< 5\%$ chance of developing a PDR in the next four years (Klein et al., 2009).



FIGURE 2.4: Sample image of a Mild NPDR (class 1)

Figure 2.4 shows image EyePACS 11736_left, tagged as 1 and classified as 1 by our best predictive model. We show lesion map generated by our models described in chapter 7.

Moderate non-proliferative diabetic retinopathy (class 2)

Moderate NPDR contains dot blot hemorrhages or microaneurysms in at least one quadrant with or without cotton-wool spots, venous beading, or intraretinal microvascular abnormalities (IrMA) but less than the 4:2:1 rule that defines the severe case and that is explained below.

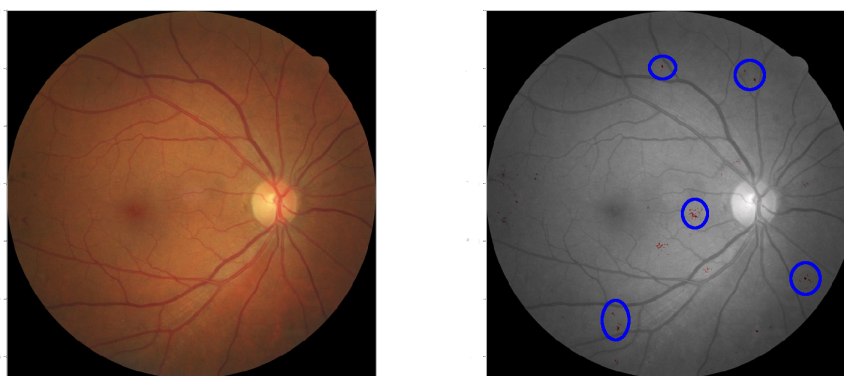


FIGURE 2.5: Sample image of a Moderate NPDR (class 2)

Figure 2.5 shows image EyePACS 681_right, tagged as 2 and classified as 2 by our best predictive model. We show lesion map generated by our models described in chapter 7.

Severe non-proliferative diabetic retinopathy (class 3)

Exam findings of the severe NPDR are characterized by any of the following cases:

- 20 or more intraretinal hemorrhages (dot blot hemorrhages) in each of all four quadrants
- Definite venous beading in 2 or more quadrants
- Prominent intraretinal microvascular abnormality (IRMA) in one or more quadrants

These three points are called the 4:2:1 rule because the abnormalities are required to be present in at least 4, 2 and 1 retina quadrants respectively. Patients with severe NPDR have a 17% chance of developing high-risk PDR within one year, and 40% chance of high-risk PDR within three years.

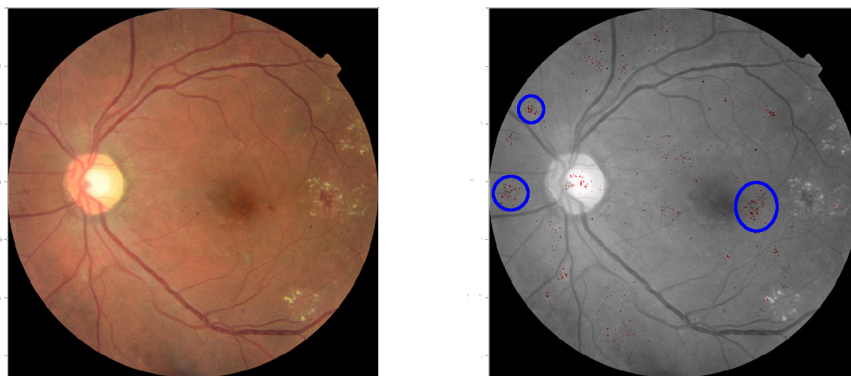


FIGURE 2.6: Sample image of a Severe NPDR (class 3)

Figure 2.6 shows image EyePACS 1561_left, tagged as 3 and classified as 3 by our best predictive model. We show lesion map generated by our models described in chapter 7.

Proliferative diabetic retinopathy (class 4)

This is the most advanced stage of the disease. In this stage, new, fragile & abnormal blood vessels grow on the retina or optic nerve. These blood vessels can leak, affecting vision quality. Exams find either a definite neovascularization, or pre-retinal or vitreous hemorrhages.

Figure 2.7 shows image EyePACS 11854_left, tagged as 4 and classified as 4 by our best predictive model. We show lesion map generated by our models described in chapter 7.

2.2 Evaluation measures for disease grading

An objective measure of the classification capabilities of a human or machine system requires the derivation of index measures that enable an exact measure of its performance. Even the most easiest classification task, ie. binary classification, requires the usage of many different indexes to

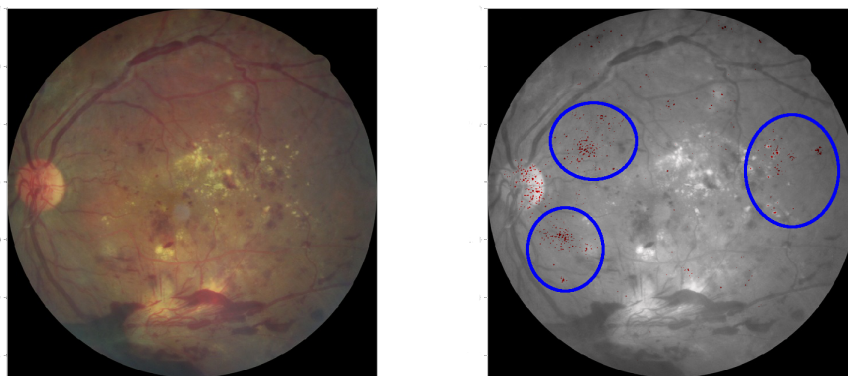


FIGURE 2.7: Sample image of a PDR (class 4)

find a good approximation of classification performance. For binary classification, instances of a set are classified as belonging or not to a class. Four possible outcomes can occur: a positive class being correctly classified (true positive, TP), a positive class being incorrectly classified (false positive, FP), a negative class being correctly classified (true negative, TN) and a negative class being incorrectly classified (false negative, FN). Furthermore, the prediction set can be balanced, ie. having the same number of elements of true positive and negative class or can be unbalanced having more instances of one class than another, producing a difference between absolute and relative results. All these variables make difficult to use a unique index for measuring the prediction capabilities. This is the reason why many different indexes exist, even for binary classification. Here below a brief description of the more used indexes for binary classification is presented.

2.2.1 Confusion matrix

The four possible outcomes, defined above, can be represented in a contingency table, known as *confusion matrix*. Table 2.1 shows how information is represented in the table.

Confusion matrix summarizes all information about the problem. All

| | | True class | | Total |
|-----------------|----------|------------|-----------|-----------|
| | | Positive | Negative | |
| Predicted class | Positive | TP | FN | $TP + FN$ |
| | Negative | FP | TN | $FP + TN$ |
| Total | | $TP + FP$ | $TN + FN$ | $Total$ |

TABLE 2.1: Binary confusion matrix

other indexes are derived from the information showed in this table. Confusion matrix can be easily generalized for its usage in multi-class classification cases, just adding as many rows and columns as classes to predict.

2.2.2 Sensitivity and Specificity

Sensitivity and Specificity are the most important indexes derived from confusion matrix. Sensitivity (eq. 2.1), also known as recall, hit rate or true positive rate, measures the proportion of actual positives that are correctly identified as such. Specificity (eq. 2.2), also known as selectivity or true negative rate, measures the proportion of actual negatives that are correctly identified as such. Mathematically is expressed as: .

$$Sensitivity = \frac{TP}{P} \tag{2.1}$$

$$Specificity = \frac{TN}{N} \tag{2.2}$$

In medical diagnosis, sensitivity measures the model ability to correctly identify those with the disease, whereas specificity measures the model ability to correctly identify those without the disease.

2.2.3 Positive and Negative Predictive Value

Positive Predictive Value (PPV) (eq. 2.3), also known as precision, measures of the proportion of correctly classified positive cases over the total

2.2. Evaluation measures for disease grading

17

number of predicted positives. It allows the identification of too conservative models. Negative Predictive Value (NPV) (eq. 2.4) measures the same in negative cases.

$$PPV = \frac{TP}{TP + FP} \quad (2.3)$$

$$NPV = \frac{TN}{TN + FN} \quad (2.4)$$

2.2.4 False Positive and Negative Rates

False Positive Rate (eq. 2.5) and False Negative Rate (eq. 2.6) indexes measure the rate of false values reported by the model. In statistical hypothesis testing these indexes are known as type I and II errors respectively. They are of common use in medical diagnosis, being a very important indexes for defining strategies of screening or testing.

$$FPR = \frac{FP}{N} \quad (2.5)$$

$$FNR = \frac{FN}{P} \quad (2.6)$$

2.2.5 False Discovery and Omission Rates

False Discovery Rate (eq. 2.7) measures the proportion false positives which are incorrectly accepted. False omission rate (eq. 2.8) measures the proportion of false negatives which are incorrectly rejected. Both measures complement FPR and FNR.

$$FDR = \frac{FP}{FP + TP} \quad (2.7)$$

$$FOR = \frac{FN}{FN + TN} \quad (2.8)$$

2.2.6 Accuracy

Accuracy (eq. 2.9) measures the proportion of true predictions (positive or negative) over the total of population. This measure can be misleading in unbalanced data sets giving too optimistic results due to the weight of predominant class.

$$ACC = \frac{TP + TN}{Total} \quad (2.9)$$

2.2.7 Balanced measures

Each one of the indexes defined above give a partial information about the classification, this is the reason why a combination of some of them, and not its individual values alone, must be taken into account to make a correct evaluation of model performance. In the quest of finding a unique index that summarizes global performance, a set of meta-indexes have been proposed. These meta-indexes combine the information given by a set of indexes to, in this way, give a unique index with an overall performance evaluation. In between these indexes are: F_β , Matthews correlation coefficient (MCC) (Sammut and Webb, 2011).

F_β (eq. 2.10) is an harmonic mean between specificity and sensitivity. β is a constant that allows to weight the relative importance of both components. For giving the same importance to both variables, β is set to 1.

$$F_\beta = (1 + \beta^2) \frac{sensitivity \cdot specificity}{\beta^2 \cdot specificity + sensitivity} \quad (2.10)$$

MCC (eq. 2.11) acts as a correlation coefficient between observed and predicted values. MCC is related to the chi-square statistic for a 2x2 contingency table.

$$MCC = \frac{TP \cdot TN + FP \cdot FN}{\sqrt{(TP \cdot FP)(TP \cdot FN)(TN \cdot FP)(TN \cdot FN)}} \quad (2.11)$$

2.2.8 The Kappa family of statistics

Ordinal Regression is a particular case of multi-class classification where an ordering of the classes can be established a priori, based on some underlying properties present in data.

In medical diagnosis, it is a typical situation the use of an ordinal or nominal classification scale for defining the severity of patient diseases. Frequently, such scales are designed for identifying the gradation of disease level from mild cases to the most severe, being then a particular case of an ordinal regression.

A typical situation in the definition of such gradation classes is the inherent existence of some subjectivity. Normally, the underlying properties that define the classification are not completely observable or cannot be completely identified, causing even experts to differ to some extent in its conclusions, requiring the usage of an index that allows the objective measure of the level of agreement between experts.

Kappa family of statistics (Sim and Wright, 2005) are a way of measuring such inter-rater and intra-rater agreement, ie. diagnostics reliability. Main purpose of the kappa derived statistics is to measure of "true" agreement. When a set of experts evaluate a fact, there are mainly two sources of possible agreement: one coming from expertise and another from chance. Kappa index discounts the probability of agreement by chance, being then a pure measure of "true" agreement.

In its binary classification form and for evaluation of two experts, kappa can be expressed as eq. 2.12.

$$\kappa = \frac{P_o - P_c}{1 - P_c} \quad (2.12)$$

being P_o the proportion of observed agreement and P_c the proportion of agreement by chance. The range of possible values of kappa is of -1 to +1. Denoting $\kappa = -1$ complete disagreement, $\kappa = 0$ random agreement and $\kappa = +1$ complete agreement between raters.

Kappa for multi-class classification. Kappa coefficient can be extended for its use with more than 2 ordinal categories. When more than two classes

are present, disagreement can be expressed by the distance between predictions of both raters. Weighted kappa is the multi-class version of original kappa, where the discrepancy is penalized by a weight that is a function of the distance between both predictions. The most common weight strategy used is the quadratic, where weights used are proportional to the square of the distance between predictions of both raters. In such case, the index is known as *Quadratic Weighted Kappa*, QWK or κ indistinctly (Cohen, 1968). This index is the most commonly used by medical community and it is the main one used in this thesis for performance evaluation.

$$\kappa = \frac{\sum \omega f_o - \omega f_c}{n - \sum \omega f_c} \quad (2.13)$$

Equation 2.13 shows the expression of quadratic weighted kappa, where $\sum \omega f_o$ is the sum of weighted observed frequencies in the confusion matrix cells, and $\sum \omega f_c$ the sum of weighted frequencies expected by chance in the confusion matrix cells. In case of using linear weights, $\omega = 1 - \frac{|i-j|}{k-1}$ and in case of quadratic weights, $\omega = 1 - \left(\frac{i-j}{k-1}\right)^2$.

Alternatively, QWK can be defined in terms of observation and expectation histogram matrices. For N classes, a $N \times N$ observation matrix O is constructed, such that $O_{i,j}$ correspond to the number of elements rated as class i by rater 1 and as class j by rater 2. A $N \times N$ expectation matrix E is also calculated as the outer product between each rater's histogram vector, normalized such that E and O have the same sum. Representing the weights as $\omega = \frac{(i-j)^2}{(N-1)^2}$, kappa can be calculated as:

$$\kappa = 1 - \frac{\sum_{i,j} \omega_{i,j} O_{i,j}}{\sum_{i,j} \omega_{i,j} E_{i,j}} \quad (2.14)$$

Kappa interpretation. In (Landis and Koch, 1977) the next standards of agreement are proposed: $\kappa \leq 0$ indicating poor agreement, $0.01 \leq \kappa \leq 0.20$ slight, $0.21 \leq \kappa \leq 0.40$ fair, $0.41 \leq \kappa \leq 0.60$ moderate, $0.61 \leq \kappa \leq 0.80$ substantial and $\kappa \geq 0.81$ almost perfect. Value of *kappa* is influenced by the weighting applied and by the number of classes, bias and prevalence, this is the reason why kappa values are not comparable across variables having different prevalence or bias (Sim and Wright, 2005). In the case of

diabetic retinopathy disease grading, using QWK, the inter-rating agreement between expert ophthalmologists is about 0.80. For the purpose of this thesis, such value ($\kappa = 0.80$) is the standard of reference our models are compared against.

2.2.9 How to define human performance

A key factor for evaluation of machine performance against humans is the standard used to measure the last one. In the context of medical classification, the next comparison standards can be used:

1. A person (not a doctor)
2. A general doctor
3. A specialized doctor
4. A highly experienced specialized doctor
5. A team of highly experienced specialized doctors

The team of highly experienced specialized doctors can be approximated to the *Bayes Optimal Error* (Fukunaga, 2013), (Tumer and Ghosh, 1996). In any case, it is important to define the standard we are comparing against. For the purpose of this thesis, human performance is established as the given by a *highly experienced specialized doctor*.

2.3 Machine Learning

Machine Learning is a Computer Science discipline, sub-field of Artificial Intelligence, that include all the tools and techniques used for enabling computers to learn from data and, from a more ambitious perspective, giving computers the ability of acting without being explicitly programmed.

All tools and techniques available in the discipline can be classified according on the type of learning algorithm that they implement: supervised, unsupervised and reinforced learning.

Supervised learning algorithms require all the instances of the training set to be labeled. From this previous knowledge the algorithm is able to learn and generalize, being able to predict new never seen before samples. From a probability perspective these type of algorithms learn a conditional distribution, ie. $P(c|X)$, being c the class to predict and X the sample.

Unsupervised learning algorithms allow the learning of underlying regularities present in the training set without requiring labeling of the individual instances. From a probability perspective, such models are able to learn the joint distribution of the population represented by the training set, ie. $P(X)$, being X the sample.

Reinforcement learning algorithms give models the capacity of learning from environment, ie. accumulating experience from its interaction with the surroundings. Such models are goal oriented, having an internal representation of the environment that is updated periodically with the objective of maximizing gain.

2.3.1 Supervised Learning

In this thesis we used supervised learning techniques for learning from data. As previously stated, in this learning paradigm a *labeled training set* is used as a foundation for learning general representations that can be used for generalizing behaviors and inferring then new labels in never seen before data.

Classification vs Regression

The objective of supervised learning is the learning of a conditional probability distribution in the form of $P(c|X)$. Depending on the nature of the variable to be predicted, it can be differentiated between classification or regression. Fundamentally, classification is about a disjoint class label prediction and regression is about a quantity prediction. Ordinal regression is a particular case of classification, where some a priori class ordinality can be established.

Dataset management

In supervised learning, the source of knowledge is represented by a labeled data set. The probability distribution of the population that it is supposed to be predicted is assumed to be represented by a sample, ie. a labeled data set. The design process of a predictive model has two parts: building the model (ie. training) and statistical evaluation of its performance. Performance evaluation require the usage of a never seen before data set, so the original full data set is required to be split in two parts: one for training (called *training set*) and another for testing (called *test set*). Both train and test set must be big enough either for training good models or for having a high statistical confidence of its generalization capabilities.

Strategies for hyper-parameter optimization

Frequently, supervised learning models have parameters that must be fixed before learning. In such cases, model performance can change dramatically depending on the selected parameters, requiring also a meta-learning parameter optimization for selection of the highest performance model, more commonly known as hyper-parameter optimization.

Different strategies can be followed in order to optimize such meta-parameters:

Hold Out method: This method splits original training data set using random sampling without repetition into 2 subsets. The first called training set is used for fitting the model/s, the second one, called validation set is used for hyper-parameter optimization and for model selection, not only between hyper-parameters but also between different types of models. As a rule of thumb, training set use to have between 50% to 70% of the data and validation set between 50% to 30%.

K-fold cross validation: The original training set is split in K folds of the same size using random sampling without repetition. The model/s are trained K times, each one of them using as training set $K - 1$ folds and 1 (the not used one) as a validation set. Prediction error is the average of K individual errors. Error variance can be used as a measure of the model

stability. The advantage of this method is that it matters less how the data is divided, ie. the model is less prone of having selection bias. After choosing the best model hyper-parameters and/or model, a retrain with the whole data set is recommended.

Leave one out cross-validation: It is a type of K-fold cross validation where it is hold out only one sample each time. It is a good way to validate, but requires a high computation time.

Bootstrap methods: It randomly draws data sets from the original sample. Each sample size is equal to the original training size. Each model/s with its particular hyper-parameters is fitted using the bootstrapped samples. Model/s are examined with the out-of-bag data, ie. data not selected in each bootstrap.

2.3.2 Algorithms used in supervised machine learning

The most widely used learning algorithms can be divided into the next categories:

- Linear / Logistic regression
- Support Vector Machines
- Probabilistic Graphical Models
- Decision trees related algorithms
- Deep Learning (Multilayer Perceptron, Neural Networks)
- Others (clustering, association rules, inductive logic, representation learning, similarity and metric learning, sparse dictionary learning, genetic algorithms, etc.)

Linear/Logistic Regression are regression and classification algorithms, where a linear combination of the inputs is optimized for least squares error minimization in the first case and for cross entropy minimization in the second.

Support Vector Machines are similar to linear/logistic regression but using a different optimization function. They minimize the Hinge loss, giving as a result maximum-margin classifiers. Support vector machines can be used as linear classifiers but also as a non-linear ones, substituting its features with so-called kernels, that are non-linear functions of the features and training set samples.

Probabilistic Graphical Models are a set of models based on probabilistic conditional dependency graphs that use bayesian rules for model construction and inference.

Decision Trees based models are a set of very effective algorithms based on the usage of weak learners like decision trees for constructing very powerful predictors combining them using bagging or boosting techniques. This category include algorithms like Random Forest or Gradient Boosting.

Deep Learning also known as Artificial Neural Networks or Multilayer Perceptrons, is a set of Machine Learning techniques for automatically constructing models from the underlying distribution represented by a large set of examples, using multiple levels of representation (in the form of layers), with the final objective of mapping a high-multidimensional input into a smaller multidimensional output ($f: \mathbb{R}^n \mapsto \mathbb{R}^m, n \gg m$). This mapping allows the classification of multidimensional objects into a small number of categories. The model is composed by many neurons that are organized in layers and blocks of layers, using a cascade of layers in a hierarchical way. Every neuron receives the input from a predefined set of neurons. Every connection has a parameter that corresponds to the weight of the connection. The function of every neuron is to make a transformation of the received inputs into a calculated output value. For every incoming connection, the weight is multiplied by the input value received by the neuron and the aggregated value that used by an activation function that calculates the output of the neuron. Parameters are usually optimized using a stochastic gradient descent algorithm that minimizes a predefined loss function. Network parameters are updated after back-propagating the loss function gradients through the network. These hierarchical models are

able to learn multiple levels of representation that correspond to different levels of abstraction, which enables the representation of complex concepts in a compressed way (Lecun, Bengio, and Hinton, 2015), (Schmidhuber, 2015), (Bengio, Courville, and Vincent, 2013), (Bengio, 2009). The models used in this thesis are based mainly in Deep Learning.

2.3.3 Pattern recognition

Traditional models of pattern recognition

The traditional model for pattern recognition since the 50's were based on a fix design of a set of important features manually engineered or derived from a fixed kernel (Fig. 2.8). Such kernels allowed the extraction of texture, statistic, position, geometry features that were posteriously combined with a simple classifier. A great diversity of methods for feature extraction exist as the local binary pattern, histogram of oriented gradients, gray level co-occurrence matrix, gabor filters, between others. In the classification phase it was common practice to use k-nearest neighbors, linear discriminant analysis, support vector machines or decision trees derived algorithms like random forest or gradient boosting.

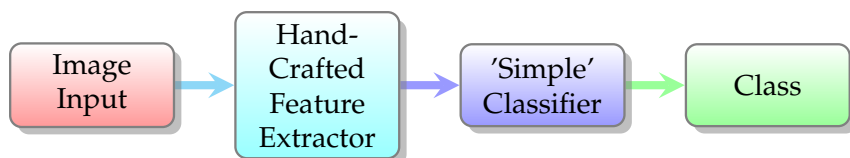


FIGURE 2.8: Traditional pattern recognition scheme

Such pattern recognition pipeline required a lot of labor time for designing the appropriate filters for every particular application.

Deep Learning for pattern recognition

Deep learning for pattern recognition represents a change of the design paradigm. Instead of hand-crafting features, a fully trainable model is designed, that is the combination of a trainable feature extractor and a trainable classifier (Fig 2.9), creating a end-to-end automatic learner.

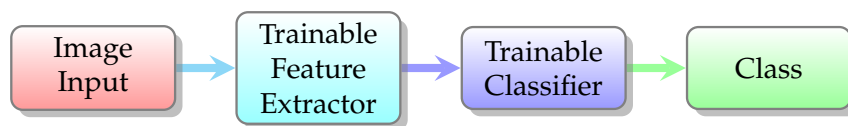


FIGURE 2.9: Deep Learning pattern recognition scheme (end-to-end learning)

Types of Deep Learning architectures

Neural networks are the architectures lying under the term of deep learning. They are directed graphical models with a defined architecture formed by their building block, the neuron. We can differentiate between three typical base architectures: fully connected, convolutional and recurrent neural networks. Every designed network can be classified into one of such architectures or as combinations of them. Each one is suitable for different types of problems. Recurrent neural networks are optimized to be used for serially organized information, for example text or sound related problems. Convolutional neural networks are designed for local correlation exploitation, for example in the case of images. Fully connected layers are designed to be used in cases where all the information is equally important, for example in classification layers. The models designed in this thesis use mainly convolutional neural networks.

Convolutional neural networks

Convolutional neural networks (fig. 2.10), firstly proposed successfully in (LeCun et al., 1989) for handwritten image recognition, are the main type of network used in this thesis for diabetic retinopathy image classification and interpretation.

CNNs are a type of neural network specialized in exploiting the natural local correlations present in images. They are able to create local abstractions that are combined layer-by-layer forming more elaborated meta-abstractions, hopefully, being able to disentangle the information contained in the image, forming features that are useful for solving a particular classification/regression problem.

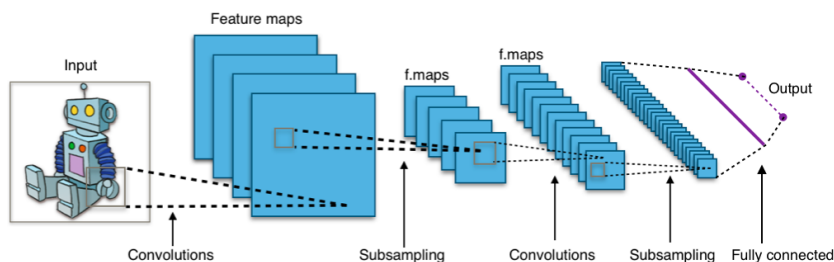


FIGURE 2.10: High level representation of a typical convolutional neural network (source: commons.wikimedia.org)

As conventional neural networks, they are formed by a set of layers that are piled together. Each layer has a convolutional operator that allows the transformation of a input tensor into another one. The output tensor can pass through other transformations inside the same layer, like a batch-normalization, an activation function or reducing size functions like max-pooling or average pooling blocks. All these functions are parametric, ie. they have learnable parameters, that are tuned through a loss function optimization process with the objective of enhancing the classification/regression capabilities of the network. The characteristic building block of such type of network is the convolution operator.

Convolution operator (fig. 2.11) is repeatedly applied to different localizations of the input. Parameters that define such operator are: a tensor of *number of feature inputs* \times *convolution width* \times *convolution height* \times *number of outputs*, *horizontal and vertical padding* and *horizontal and vertical stride*. Padding defines the number of pixels that must be added to the width and height of the input before applying it, ie. if the input has a *width* \times *height* original size, is extended for applying the operator to $(width + 2 \times padding\ width) \times (height + 2 \times padding\ height)$. The operator is applied in every location of the input with a separation between initial points of *horizontal stride* and *vertical stride*. The output value correspond to the linear combination of the convolution parameters with input values.

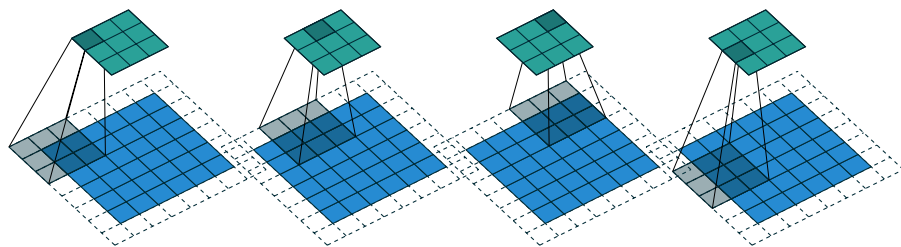


FIGURE 2.11: Convolution operator of 3x3 with stride 2 and padding 1 in both directions applied to a 6x6 input. Only one input and output features are shown (Dumoulin and Visin, 2016).

Pooling operators (fig. 2.12) are other typical elements used in CNNs. They are used for reducing the size of feature maps. Max-pooling operators select from a predefined window the maximum value and discards the others. Average-pooling, selects the average. Both, are the most common strategies for reducing the size of feature maps.

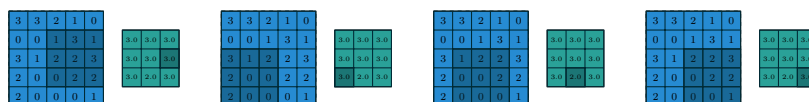


FIGURE 2.12: Max-pooling operator of 3x3 with stride 1 and padding 0 in both directions applied to a 5x5 input. Only one input and output features are shown (Dumoulin and Visin, 2016).

Batch normalization are another typical element used in CNN layers. It applies a normalization to the inputs that help to reduce covariate shift, increasing stability and acting as a regularizer (Ioffe and Szegedy, 2015).

Activation function (fig. 2.13) is a key element of neural networks. ReLU is the most versatile, stable and used one. Sigmoid function, the most used one in the 80's, only used nowadays for certain types of output layers, due to its gradient descent vanishing problems. Without them, deep learning

models would behave just like linear functions. In the 80s the most used activation function was the sigmoid, a smooth non-linear function, that is continuously differentiable. Despite its interesting properties, it has a very important concern, called gradient vanishing problem (Glorot and Bengio, 2010). Sigmoid first derivative becomes flat not far from the origin, affecting network loss optimization due to near-to-zero gradients. In (Nair and Hinton, 2010) ReLUs were used for improving Restricted Boltzmann Machines (RBMs), approximating stepped sigmoid units with ReLUs. In (Glorot, Bordes, and Bengio, 2011) the authors compared the performance of Sigmoid, Tanh and ReLU arriving to the conclusion that despite Sigmoid being more plausible biologically, Tanh and ReLU were more suitable to be used as activation function for training multi-layer perceptrons. ReLU networks have better performance in general, despite its non-differentiability at zero and its hard non-linearity. Furthermore, ReLU networks lead to sparse representations, being beneficial, both because information is represented in a more robust manner and because it leads to significant computational efficiency. Moreover, the simplicity of the function and its derivative reduces calculation time, being of significant importance when working with big networks. The constant value of the gradient, helps avoiding the gradient vanishing problem, allowing the design of deeper networks. For then on, ReLU has become the default activation function for deep learning. Many other activation functions have been published, like LeakyReLU, but not introducing significant performance gains.

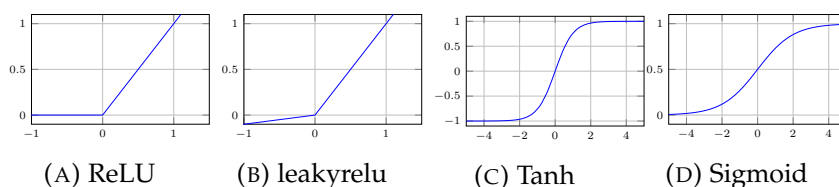


FIGURE 2.13: Typical activation functions used in Deep Learning

Typical CNN architectures. CNNs have been demonstrated to be very effective in solving complex classification, detection and segmentation problems. Table 2.2 shows a summary of the most successful Imagenet (Deng et al., 2009) prediction standardized architectures sorted by its performance

solving the complex Imagenet classification task. The more successful network presented in the table is *InceptionResNetV2* having more than 55 million of parameters. *Xception* has a similar accuracy using less than a half of parameters. *MobileNetV2*, an architecture designed to be used in mobile devices, with only 3.4 million of parameters has an accuracy similar to the achieved with older architectures as *VGG16* and *VGG19*, that used more than 100 million of parameters.

| Model | Input size | Imagenet | | Depth | Residual | Publication | Source |
|-------------------|-------------|----------------|--------|-------|----------|-------------|--|
| | | Top-1 Accuracy | Params | | | | |
| InceptionResNetV2 | (299,299,3) | 0.804 | 55.9M | 572 | Yes | 2016-02 | (Szegedy et al., 2017) |
| InceptionV4 | (299,299,3) | 0.802 | 55.9M | | No | 2016-02 | (Szegedy et al., 2017) |
| Xception | (299,299,3) | 0.790 | 22.9M | 126 | Yes | 2016-10 | (Chollet, 2017) |
| InceptionV3 | (299,299,3) | 0.788 | 23.8M | 159 | No | 2015-12 | (Szegedy et al., 2016) |
| DenseNet201 | (224,224,3) | 0.770 | 20.2M | 201 | Dense | 2016-08 | (Huang et al., 2017) |
| ResNet50 | (224,224,3) | 0.759 | 25.6M | 168 | Yes | 2015-12 | (He et al., 2016) |
| DenseNet169 | (224,224,3) | 0.759 | 14.3M | 169 | Dense | 2016-08 | (Huang et al., 2017) |
| MobileNetV2 (1.4) | (224,224,3) | 0.747 | 6.9M | | Yes | 2018-01 | (Sandler et al., 2018) |
| DenseNet121 | (224,224,3) | 0.745 | 8M | 121 | Dense | 2016-08 | (Huang et al., 2017) |
| VGG19 | (224,224,3) | 0.727 | 143.7M | 26 | No | 2014-09 | (Simonyan and Zisserman, 2015) |
| MobileNetV2 | (224,224,3) | 0.720 | 3.4M | | Yes | 2018-01 | (Sandler et al., 2018) |
| VGG16 | (224,224,3) | 0.715 | 138.3M | 23 | No | 2014-09 | (Simonyan and Zisserman, 2015) |
| MobileNetV1 | (224,224,3) | 0.706 | 4.2M | | Yes | 2017-06 | (Howard et al., 2017) |
| SqueezeNet | (227,227,3) | 0.575 | 1.2M | | Yes | 2016-02 | (Iandola et al., 2016) |
| AlexNet | (227,227,3) | 0.571 | 62M | 8 | No | 2012-00 | (Krizhevsky, Sutskever, and Hinton, 2012a) |

TABLE 2.2: List of the most successful classification architectures used for Imagenet prediction

2.3.4 Prediction error: bias vs variance

Prediction error has two sources of error: bias and variance. *Bias* is the difference between expected average prediction and the real value. *Variance* is a measure of the model variability prediction for a given data point. Figure 2.14 show visual examples of different scenarios of bias and variance combinations.

A low bias - high variance model gives predictions where its expected average is near the true value, but its individual predictions are highly dispersed around the true value. A high bias - low variance model gives predictions far from the true value but with small variability between the predictions. A high bias - high variance model gives predictions far from the true value and with high variability between them. Finally a low bias - low variance model is the best one having close to the true value predictions and low variability between individual predictions.

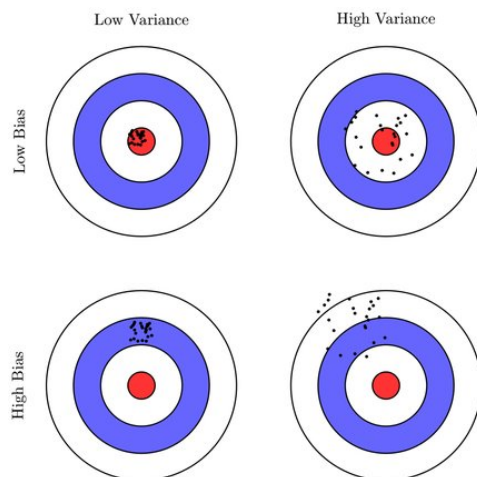


FIGURE 2.14: Bias vs Variance extreme possible scenarios

2.3.5 Model ensembling

Model ensembling (Zhou, 2012) is a way of improving accuracy of predictions using a combination of classifiers that are trained using different models, data, hyper-parameters or parameter initializations. Every difference introduced in the ensembling increases diversity and improves generalization capabilities of final model. The drawbacks are loss of interpretability and the increase in complexity of evaluation of ensembled model.

Classifiers can be combined using different techniques: bagging, boosting and model stacking.

Bagging: Bagging uses a base predictor, ie. a weak learner, for creating a pool of N weak predictors. Every predictor is generated using a random sampling with replacement from the original dataset. In the classifier phase, all predictions are averaged (regression) or selected by majority vote (classification). Model predictions obtained have lower variance than the coming from original predictors.

Boosting: Boosting predictor generation process is sequential, building multiple incremental models to decrease bias, while keeping variance small. In every step, Boosting increases the weights of miss-classified data to emphasize the importance of the most difficult cases. Boosting also assigns weights in the classification stage to predictors giving more importance to best predictors. Due to this weighting strategy, boosting is able not only to reduce variance but also to reduce bias. In counterpart, boosting can over-fit training data, problem that is not present in bagging predictors.

Model stacking: allows the combination of model predictors of completely different nature. It fits a meta-model such as for example, a logistic regression, using cross validation predictions coming from multiple models, achieving better results than source predictors.

2.4 Data

Data is at the core of any machine learning model, its quality determines the validity and generalization capabilities of any model derived from it. Machine learning paradigm is based, precisely, in the design of models that are able to learn from data. In this section, we aim to make an exploratory analysis of the data sets that have been used for the elaboration of this thesis.

2.4.1 Datasets

Three different datasets have been used: EyePACS, Messidor-2 and Reus. EyePACS, the biggest dataset available, have been used for model training, validation and testing. Messidor-2 and Reus have been used for testing purposes and for checking validity of trained models over alternative populations.

2.4.2 EyePACS dataset

EyePACS dataset (EyePACS, 2018) is formed by the images of 44,346 different patients. For each one of them, left and right eye images are available, having a total of 88,692 retina fundus images. Each one of the images is classified according to the standards defined in (Wilkinson et al., 2003). The images are taken in variable conditions: by different cameras, in different illumination conditions and have different resolutions. The dataset is highly imbalanced having 65,343 class 0 images; 6,195 of class 1; 13,153 of class 2; 2,087 of class 3 and 1,914 of class 4. Figure 2.15a shows a graphical representation of the class distribution of the dataset.

2.4.3 Messidor-2 dataset

Messidor-2 dataset (Decencière et al., 2014) is formed by a total of 1,748 retina fundus images. Each one of the images has adjudicated grades for Diabetic Retinopathy Severity following (Wilkinson et al., 2003), Diabetic Macular Edema (DME) based on hard exudates classification, and Gradability. The grades were adjudicated by a panel of three Retina Specialists (Brain, 2018). This fact gives high confidence to the tagging (being near Bayes Optimal Error), making the dataset suitable to be used as a high confidence test set. The dataset is also highly imbalanced having 1,017 class 0 images; 270 of class 1; 347 of class 2; 75 of class 3 and 35 of class 4. No explicit differentiation between eyes of the same patient is given. Figure 2.15b shows a graphical representation of its class distribution.

2.4.4 HUSJR dataset

We have been able to obtain a third dataset from a reference hospital in Catalonia region: Hospital Universitari Sant Joan de Reus (HUSJR). It is located in Tarragona province, concretely in the city of Reus. The ophthalmology unit of this hospital has collected data from population of Caucasian, T2DM patients between January 1, 2007 and December 31, 2016. This included 85.33% of T2DM patients of this area. Patients have been screened with the nonmydriatic fundus camera units (NMCU) at HUSJR. Screening was carried out with one 45° field retinography, centered on the fovea. If DR was diagnosed, the patient was sent to the Ophthalmology

service at our hospital and another 2 retinographs of 45° were taken according to EURODIAB guidelines (Aldington et al., 1995).

This dataset is used in chapter 9 for evaluation of the performance of designed models. It consist of 19,230 tagged retinograhies: 15,123 with no apparent DR, 2,576 with mild DR, 944 with moderate DR and 587 with severe proliferative or non-proliferative DR. This dataset has a higher number of the most severe cases of the disease, allowing the extraction of finer statistical measures is such cases. In this dataset, no differentiation between class 3 and class 4 is given, considering that they belong to the same class 3. Figure 2.15c shows a graphical representation of its class distribution. Figure 2.15c shows a graphical representation of its class distribution.

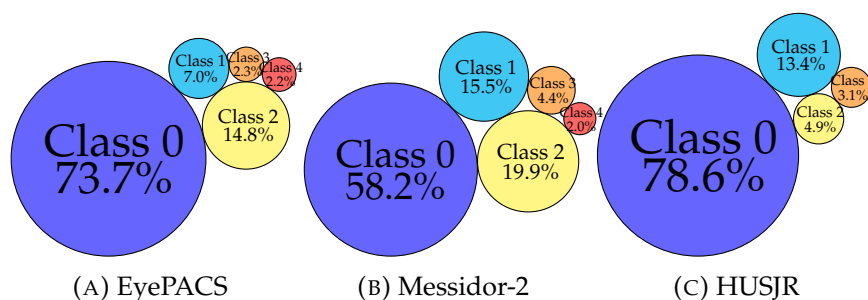


FIGURE 2.15: Datasets class percentage distribution

2.5 Summary of the data and methods used in this thesis

All classification and interpretation models used in this thesis are based on convolutional neural networks. For its optimization, different loss functions are used, including a new contribution for ordinal regression based on the quadratic weighted kappa (see chapter 4). Ensembling methods are also used for obtaining better predictions, based either on averaging different rotated versions of the same image or on bayesian inference (see chapter 3). As a evaluation function we use mainly quadratic weighted kappa.

Relating to data, all models are trained using different subsets of Eye-PACS dataset and tested using another subset of the same dataset. Messidor-2 is used for testing purposes in chapter 5 and for model fine-tuning of the last classification layer in chapter 9. Reus dataset is used only for testing purposes in chapter 9.

Part I

Classification

UNIVERSITAT ROVIRA I VIRGILI

DIABETIC RETINOPATHY CLASSIFICATION AND INTERPRETATION USING DEEP LEARNING TECHNIQUES

Jordi De la Torre Gallart

Chapter 3

Preliminary Models

In this chapter we present the models that were designed in the early stage of the thesis. The aim of this work was to understand better the problem, ie. explore different input sizes, types of models, data augmentation techniques and hyper-parameters and explore the possibilities of using deep learning for successfully solving this task. They were published in (Torre, Valls, and Puig, [2016a](#)).

3.1 Introduction

In the last decade, several attempts to automatize the DR diagnosis through images of the eye fundus have been tested. They are basically focused on applying well-known pattern recognition models. In this work, we want to apply a Deep Convolutional Neural Network (DCNN) model, as it has been proven to be a very effective algorithm to solve general image classification problems. DCNN is a supervised learning model for automatic classification that does not require any pretreatment of the images, nor any feature analysis.

Deep learning techniques are focused on learning multiple levels of representation and abstraction that help to make sense of the hidden information in data such as images. In this way having a complete set of correctly classified images and without having any a priori understanding of the features required to make the classification, the system is able to learn the properties of the image that minimize a defined cost function that is direct or indirectly related with the classification score index that has to

be optimized. In this chapter we show that a DCNN is able to learn from data the most important features to make the classification of retinal images into the five DR categories, without the need of a hand-crafted feature extraction process.

In this chapter we explore methods for classifying retina images into the five different classes of DR defined in chapter 2, that are:

0. - No apparent retinopathy
1. - Mild Non-Proliferative Diabetic Retinopathy (NPDR)
2. - Moderate NPDR
3. - Severe NPDR
4. - Proliferative DR

The chapter is organized as follows: we present the related work, next we explain the characteristics of the available data and why deep learning techniques can be applied over them, next we explain the methodology used for solving the problem, we show the obtained results and finally we expose the conclusions and further steps for improving the results.

3.2 Related work

Traditional models of pattern recognition in images since the late 50s have been based on extracting hand-crafted fixed engineered features or fixed kernels from the image and, then, using a trainable classifier on top of those features to get the final classification. Using this model, the problem of the DR detection has been tackled by feature extraction using on hand models targeted to the detection of microaneurisms, haemorrhages and exudates in retinal images (e.g. (Sudha and Thirupurasundari, 2014), (Torrents-Barrena et al., 2015), etc).

This type of approach requires a good understanding of disease mechanisms to be able to find the important features present in the image. This knowledge is specific of the problem to be solved, requires a lot of labor

time and is task specific and thereby not reusable for other different classification problems.

Deep learning is a new powerful method for supervised learning. By adding more layers and more units within a layer of a neural network, we can represent functions of increasing complexity. Training must be done on sufficiently large annotated image data sets. In computer vision classification problems, neural networks have largely displaced the traditional approaches based on handcrafted features. They have proved to be the best available method for solving the biggest classification challenges, like for example IMAGENET (Russakovsky et al., 2015). In this previous type of image analysis problems, distinct objects should be recognized on different types of images. In the case of DR classification, all images are very similar (as they are retina photos) and very small and vague lesions have to be detected at different locations in order to find the correct severity category of DR. This chapter, thus, wants to study the performance of DCNNs for this kind of medical image analysis.

3.3 Data

We use the EyePACS dataset presented in chapter 2. We split the dataset using random selection in two disjoint sets. The training set contains 35,126 images; 25,810 of class 0, 2,443 of class 1, 5,292 of class 2, 873 of class 3 and 708 of class 4. The test set contains a total of 53,576 images; 39,533 of class 0, 3,762 of class 1, 7,861 of class 2, 1,214 of class 3 and 1,206 of class 4.

3.4 Methodology for retinal image classification

All the state-of-the-art architectures for supervised deep learning over images (e.g. AlexNet (Krizhevsky, Sutskever, and Hinton, 2012b), GoogleNet (Szegedy et al., 2015) and VGGNet (Simonyan and Zisserman, 2015)) are based on convolutional neural networks (CNNs). A set of convolutional layers with dimensional down-sizing blocks between them, also known as pooling layers, extract the statistical information from the data (feature extraction) that is passed to the posterior layers to construct more elaborate abstractions (features of features) that are useful for the classification.

As a final stage a fully connected set of layers perform the classification based on the information coming from the last layers of the convolutional network. This kind of structure provides an end to end learning process, where either the classes or the features are learned from data with no human intervention.

Next we explain the different phases of the DCNN construction for performing DR detection based on the available data: evaluation function, data pre-processing and data augmentation, model, training, testing and probabilistic combination of the models of both eyes.

3.4.1 Evaluation function

The performance of the classification model is measured using the quadratic weighted kappa (QWK) index (see eq. 3.1), defined previously in chapter 2. As a brief summary, QWK, also known as Cohen's Kappa, measures inter-rater agreement for categorical items in multi-class classification problems (Fleiss, Cohen, and Everitt, 1969), penalizing the discrepancy quadratically with the distance from the correct class. It is generally thought to be a more robust measure than simple percent agreement calculation, since QWK takes into account the agreement occurring by chance. This metric typically varies from 0 (random agreement) to 1 (complete agreement). Negative values are also possible, the maximum possible negative value (-1) indicates a complete disagreement between classes. Being $O_{i,j}$ the observed values, $E_{i,j}$ the expected ones and C number of classes, QWK is defined as:

$$\kappa = 1 - \frac{\sum_{i=1}^C \sum_{j=1}^C \omega_{i,j} O_{i,j}}{\sum_{i=1}^C \sum_{j=1}^C \omega_{i,j} E_{i,j}} \quad \text{where} \quad \omega_{i,j} = \frac{(i-j)^2}{(C-1)^2} \quad (3.1)$$

The QWK coefficient is used to compare the performance of different prediction models and with the performance of the human experts (SE et al., 1985). Individual human experts report values of QWK of about 0.80 in the prediction of the correct class in the DR disease. This value is considered excellent because small discrepancies between the class prediction does not affect the treatment of the disease. The most important is the differentiation between presence or absence of the disease.

3.4.2 Data pre-processing and data augmentation

Firstly, DCNNs require large data-sets in order to avoid overfitting. A class balanced data-set is also desirable as well (MA et al., 2008). One of the proven approaches that has good results to get more data from small data-sets is to use data augmentation techniques (Krizhevsky, Sutskever, and Hinton, 2012b). The data augmentation is done in two stages: first a copy of the training examples of the small classes is done until they have the same number of images as the biggest class. This generates an equilibrated training set. After this first step, to every image the next transformations are applied in order to diversify the training examples:

- Cropping, random uniform
- Rotation (0° to 360°), random uniform
- Mirroring (X and Y axes), random uniform
- Brightness correction, random gaussian ($\sigma = 0.1$)
- Contrast correction, random gaussian ($\sigma = 0.1$)

All these transformations are applied to every image of the balanced training set and redone for every training epoch. This transformations assure that every image of the training set is different between each other for every epoch, making the final prediction invariant to rotation, brightness and contrast over the training set.

Secondly, DCNNs perform better when then input data is normalized by having mean equal to 0 and standard deviation equal to 1, on each channel (RGB). Thus, a normalization must be done on each image.

3.4.3 Model

The well-known LeCun et al. architecture has been taken (LeCun et al., 1998). It is composed by a series of convolutional layers followed by activation function blocks, with some max-pooling dimensional reducing blocks. At the end, a final fully connected layer performs the classification and, finally, a softmax output layer gives a probability estimation of every class (Figure 3.1).

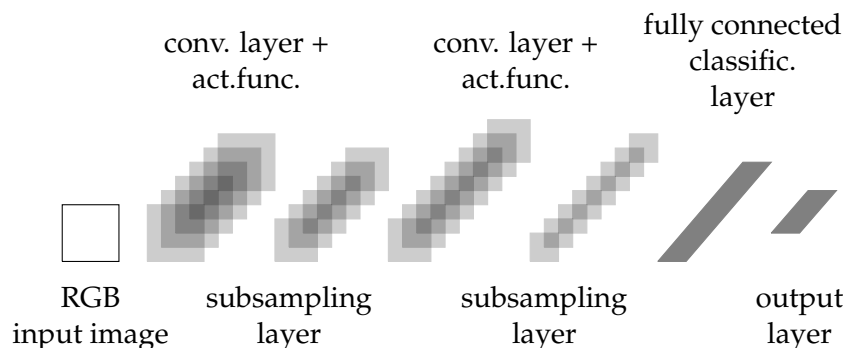


FIGURE 3.1: Architecture of a 4 layer CNN: two convolutional layers, one fully connected classification layer and the final output layer

Some of the parameters of this model are the following: input size, number of layers, number of filters per convolution layer, size of the convolution, number and size of classification layers, activation function, optimization and regularization methods to be used. Due to the high number of parameters involved, these systems have a lot of versatility and there is not a unique solution to a problem. Different configurations can perform well solving the same problem.

3.4.4 Training procedure

As a multi-class classification problem, a log-loss function is used to perform the optimization in the learning stage. The original training set is splitted in two random subsets: one with 90% of the data and other with 10%. The last one is used as a cross validation set for hyperparameter selection. QWK results are calculated every epoch either for the training or the test set. The model chosen is the one that maximizes the QWK over the cross validation set. In all models a ReLU or leaky ReLU (Dahl, Sainath, and Hinton, 2013) activation function is used. In all layers a batch normalization (Ioffe and Szegedy, 2015) is applied before the activation function in order to reduce the gradient vanishing problem that occurs in deep networks, reduce the internal covariance shift and improve the regularization. As an additional regularizer a dropout (Baldi and Sadowski, 2013)

3.4. Methodology for retinal image classification

45

($p=0.5$) is performed before the final classification layer. L2 regularization has been tested with no significant improvements in the final classification results. A random initialization based in the Kaiming&He approach (He et al., 2015) is used for all the networks. When deep networks are randomly initialized using fixed standard deviations (e.g., 0.01), very deep models (e.g., >8 conv layers) have difficulties to converge, as reported by the VGG team (Simonyan and Zisserman, 2014). Kaiming method takes into account the particularities of rectifier non-linearities. Initializing the weights of every layer randomly with 0 mean and $\sqrt{2/n_l}$ standard deviation (being n_l the number of connections of layer l) we get a desired zero-mean Gaussian distribution in the weight distribution. Biases are initialized to zero. All models are optimized using stochastic gradient descent with Nesterov momentum.

3.4.5 Testing procedure

The network is trained with a data augmented scheme that include rotations. Presumably an ensemble (Zhou, Wu, and Tang, 2002) that includes rotated versions of the original image would perform better than the single original image. Using a trained network with a significant accuracy, different ensemble schemes are tested over the cross validation set to identify the one that maximizes the classification accuracy.

| Testing scheme | Predictions | κ_{CV} |
|--|-------------|---------------|
| Baseline: Original image (crop center) | 1 | 0.669 |
| Original + rot 180° (crop center) | 2 | 0.683 |
| Center, Left top, Left bottom, Right top, Right bottom cropped | 5 | 0.684 |
| Original + Hflip + Vflip + rot 180° | 4 | 0.686 |
| Five 72° rotated (crop center) | 5 | 0.699 |
| All | 14 | 0.701 |

TABLE 3.1: Testing scheme performance results

Table 3.1 shows the accuracy of different testing schemes for a given model. The ensemble that performs the best is the one formed by all the 14 different evaluations. The Five 72° scheme is only 0.002 points under the best tested scheme and reduces significantly the computation time required. Geometric means perform slightly better (average of 0.005 points of κ) than arithmetic means. The testing scheme chosen is the Five 72° with

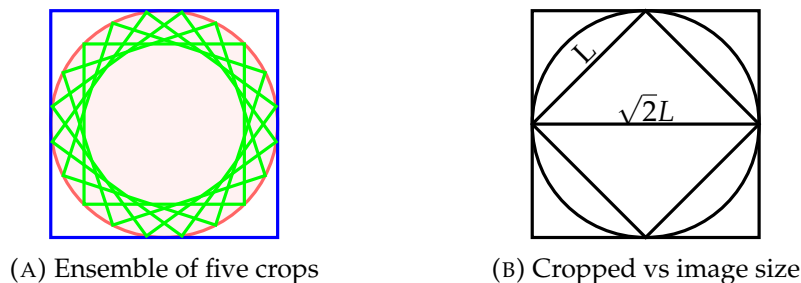


FIGURE 3.2: Testing ensemble used for evaluation

geometric means due to its good compromise between computation costs and performance. In figure 3.2 we show a representation of the scheme. Blue square represents the image size, red circle the retinal image area and the five green squares, the areas of the image that are fed to the neural network at test time. As the diagram show, most of the useful information for the classification is considered by one of the 5 different inputs.

3.4.6 Probabilistic combination of the models of both eyes

DR usually affects both eyes, specially when the illness is in high severity stages. We analyze the frequency of co-occurrence of the five DR categories in the images of our dataset. The dataset is big enough to infer from the frequencies of co-occurrence of the classes, the conditional probabilities of having one class in one eye given another class in the other.

In table 3.2 we show the frequencies of occurrence of all the possible combinations of classes in both eyes. Notice that the larger frequencies are found in the diagonal, indicating that is usual that both eyes have similar levels of severity.

Using the frequentist interpretation of probability that defines an event's probability as the limit of its relative frequency in a large number of trials, we use this frequencies as an estimation for the calculation of the conditional probability. In table 3.3 we show the values of all the calculated conditional probabilities of $P(\text{Left}|\text{Right})$. The same can be done for the matrix $P(\text{Right}|\text{Left})$.

Using the Bayes rule, we can estimate the probability distribution of

3.4. Methodology for retinal image classification

47

| Eyes | C0 | C1 | C2 | C3 | C4 | Sum |
|------|-------|------|------|-----|-----|-------|
| C0 | 12155 | 407 | 295 | 3 | 11 | 12871 |
| C1 | 435 | 600 | 171 | 2 | 4 | 1212 |
| C2 | 336 | 222 | 1998 | 96 | 50 | 2702 |
| C3 | 3 | 1 | 87 | 307 | 27 | 425 |
| C4 | 10 | 1 | 39 | 40 | 263 | 353 |
| Sum | 12939 | 1231 | 2590 | 448 | 355 | 17563 |

TABLE 3.2: Frequencies of combined occurrence of classes in both eyes (left: rows, right: columns)

| Eyes | C0 | C1 | C2 | C3 | C4 |
|------|---------|---------|---------|---------|---------|
| C0 | 0.93940 | 0.33062 | 0.11389 | 0.00669 | 0.03098 |
| C1 | 0.03361 | 0.48740 | 0.06602 | 0.00446 | 0.01126 |
| C2 | 0.02596 | 0.18034 | 0.77142 | 0.21428 | 0.14084 |
| C3 | 0.00023 | 0.00081 | 0.03359 | 0.68526 | 0.07605 |
| C4 | 0.00077 | 0.00081 | 0.01505 | 0.08928 | 0.74084 |

TABLE 3.3: Probability of occurrence of Left eye class (rows) given the occurrence of the Right eye class (columns)

eye A , using the probability distribution of eye B given by our model. Being $P(Left)$ and $P(Right)$, the probability distributions obtained by our predictive model with the left image and the right image, respectively, we can estimate P_L and P_R using Eq. 3.2. To merge the information obtained from our model $P(X)$ with the estimated coming from the other eye we calculate the arithmetic mean. The class with maximum value is the one selected for each eye.

$$\begin{aligned}
 P_L &= P(Left|Right)P(Right) \\
 P_R &= P(Right|Left)P(Left)
 \end{aligned}
 \tag{3.2}$$

3.5 Experiments

Different experiments have been conducted to analyze the quality of the classification with different parameters of the DCNN. First, we perform an study of the best image size. Due to the type of image classification that is done, it is crucial to choose the right size of the input images in order to detect the important features involved in the RD severity detection. As explained before, cropping is part of the data augmentation scheme. The original size is chosen from the NN input size as $\sqrt{2}$ times the input size. In this way, due to the circular nature of the retina, we maximize the useful information of the square cropped from the center of the image (see Fig. 3.2). The input sizes tested are:

- Resizing to 181x181 cropped to 128x128 NN input
- Resizing to 362x362 cropped to 256x256 NN input
- Resizing to 543x543 cropped to 384x384 NN input
- Resizing to 724x724 cropped to 512x512 NN input

Different number of layers have also been studied for each image size. In table 3.4 are presented the higher classification rates obtained from the best models obtained for different input sizes. The number of layers of the best models are also shown.

| Layers | Input size | κ_{test} | FN | FP |
|--------|-------------|-----------------|-------|-------|
| 12 | (3,128,128) | 0.488 | 11.6% | 11.5% |
| 14 | (3,256,256) | 0.636 | 4.4% | 28.7% |
| 16 | (3,384,384) | 0.668 | 7.9% | 14.9% |
| 16 | (3,512,512) | 0.725 | 5.0% | 11.9% |

TABLE 3.4: Best classification results for different input sizes

As the input size and the complexity of the network is increased the results obtained become better. Greater sizes give more definition of the

underlying features in the image and the increased complexity of the network, increasing the number of layers, allows the construction of abstractions in the form of features of features that improves the classification accuracy. In table 3.6 we show the architecture details of the best model, a very deep network of 16 layers. This indicates that the distinction of the severity categories of DR in images is not an easy classification problem. With the 512x512 model we achieve a $\kappa_{test} = 0.725$ using only the information contained in the examined retine image.

Next, we study if the inclusion of the co-occurrence information of both eyes is able to improve the quality of the classifier. Table 3.5 shows the final accuracy obtained combining both eyes for all the sizes. In the 512x512 model the accuracy is increased in about 0.03 κ points, a value that makes our model perform near human level expertise with a final $\kappa_{test} = 0.752$.

| Layers | Input size | κ_{test} | FN | FP |
|--------|-------------|-----------------|-------|-------|
| 12 | (3,128,128) | 0.555 | 11.2% | 12.9% |
| 14 | (3,256,256) | 0.661 | 4.4% | 28.7% |
| 16 | (3,384,384) | 0.722 | 11.2% | 4.0% |
| 16 | (3,512,512) | 0.752 | 6.5% | 7.0% |

TABLE 3.5: Best classification results adding the probabilistic information of both eyes

3.6 Conclusions

In this chapter is shown that deep learning techniques are not only very effective for solving general classification tasks, but also for prediction in medical imaging. For our case study of diabetic retinopathy disease grading, having enough data our method is able to perform near human level expertise.

Work of next chapters will be centered on testing the newer schemes, the use of alternative cost functions that encode the prior information of the ordering of the classes and other more elaborated methods for combining the information coming from both eyes.

| Layer | Type | Characteristics | Output Size |
|-------|-----------------|---|--------------|
| | Input | 3 RGB channels | (3,512,512) |
| 1 | Convolution | 8 filters 3x3 1,1 stride, 1,1 padding | (8,512,512) |
| 2 | Convolution | 16 filters 3x3 1,1 stride, 1,1 padding | (16,512,512) |
| 3 | Convolution | 16 filters 3x3 1,1 stride, 1,1 padding | (16,512,512) |
| - | Max pooling | 2,2 size, 2,2 stride | (16,256,256) |
| 4 | Convolution | 32 filters 3x3 1,1 stride, 1,1 padding | (32,256,256) |
| 5 | Convolution | 32 filters 3x3 1,1 stride, 1,1 padding | (32,256,256) |
| - | Max pooling | 2,2 size, 2,2 stride | (32,128,128) |
| 6 | Convolution | 64 filters 3x3 1,1 stride, 1,1 padding | (64,128,128) |
| 7 | Convolution | 64 filters 3x3 1,1 stride, 1,1 padding | (64,128,128) |
| - | Max pooling | 2,2 size, 2,2 stride | (64,64,64) |
| 8 | Convolution | 128 filters 3x3 1,1 stride, 1,1 padding | (128,64,64) |
| 9 | Convolution | 128 filters 3x3 1,1 stride, 1,1 padding | (128,64,64) |
| - | Max pooling | 2,2 size, 2,2 stride | (128,32,32) |
| 10 | Convolution | 128 filters 3x3 1,1 stride, 1,1 padding | (128,32,32) |
| 11 | Convolution | 128 filters 3x3 1,1 stride, 1,1 padding | (128,32,32) |
| - | Max pooling | 2,2 size, 2,2 stride | (128,16,16) |
| 12 | Convolution | 128 filters 3x3 1,1 stride, 1,1 padding | (128,16,16) |
| 13 | Convolution | 128 filters 3x3 1,1 stride, 1,1 padding | (128,16,16) |
| - | Max pooling | 2,2 size, 2,2 stride | (128,8,8) |
| 14 | Convolution | 256 filters 3x3 1,1 stride, 1,1 padding | (256,8,8) |
| 15 | Fully connected | 256 elements | (256) |
| 16 | Softmax | 256 to 5 elements | 5 |

TABLE 3.6: Best performing DCNN architecture

Chapter 4

Kappa a Loss Function for Ordinal Regression

The aim of this work was to study the possibilities of using the Quadratic Weighted Kappa evaluation function as a loss function for optimizing deep neural networks. In this chapter we explore the usage of QWK for ordinal regression using deep learning models. For this purpose 3 case studies of completely different nature are presented, proving an increase of more than 5% in results over traditional log-loss optimization. This method generalize directly to other multi-class classification problems where there is a prior known information about the predefined ordering of the classes. The work presented in this chapter have been published in the paper (Torre, Puig, and Valls, [2018](#)).

4.1 Introduction

Optimization of neural networks for multi-class classification is traditionally done using logarithmic loss. Logarithmic loss has a very robust probabilistic foundation: minimizing it, is the same as minimizing the logarithmic likelihood, that is equivalent to do a Maximum Likelihood Estimation (MLE) or equivalently, to find the Maximum a Posteriori Probability (MAP), given a uniform prior (Murphy, [2012](#)). This loss function is designed to find perpendicular vectors in the output space. This model is suitable when output classes are independent, but it may not be good in

cases where classes are ordered. This is the case of some disease prediction, where an incremental severity scale is present. Normally in those cases a ordinal regression approach is better. In such cases, disease predictor vectors are best modeled as a gradation of some internal properties not always explicitly known, than as independent classes formalized as the perpendicular vectors that logarithmic loss tries to find.

Several quality measures exist in the machine learning and statistics literature (Mehdiyev et al., 2016) for measuring the effectiveness of classification models. Kappa index is a well-known statistic coefficient defined by Cohen (Cohen, 1960) to measure inter-rater agreement on classifying elements into a set of categories (i.e. disjoint classes). Later, Weighted Kappa index was defined for the case of ordered categories (i.e. from best to worst). In this coefficient disagreements are treated differently than in the original Cohen's Kappa (Cohen, 1968).

Weighted Kappa index (κ) is used in many medical diagnosis systems because diseases have different degrees of severity, which are naturally ordered from mild to the most critical cases. If the diagnose is based on image analysis, the classification is even more difficult because in the data image interpretation is normally present some level of subjectivity that sometimes makes the conclusions of different experts to differ (Hripcsak and Heitjan, 2002). Weighted kappa is able to measure the level of discrepancy of a set of diagnosis made by different raters over the same population (Viera and Garrett, 2005). Depending on the index value, the strength of agreement between both raters can be evaluated (see table 4.1).

Examples of the usage of the κ index for measuring inter-rater agreement in medical context are: the measure of reliability in ultrasound scans interpretation (Hintz et al., 2007), evaluation of expert agreement in diagnosis of glaucoma (Varma, Steinmann, and Scott, 1992), evaluation of reliability of radiographic assessment (Günther and Sun, 1999), the inter-observer agreement evaluation in DR detection (Patra et al., 2009), among many others.

κ takes into account the ordering of the classes and penalizes the erroneous predictions in function of the distance between the real and the predicted class. In that way, a failure in a prediction that is close to the real category is considered better than a prediction that is farther. The penalization weights depend on the type of the chosen weighted kappa. In a linear

| κ | Strength of agreement |
|-----------|-----------------------|
| <0.20 | Poor |
| 0.21-0.40 | Fair |
| 0.41-0.60 | Moderate |
| 0.61-0.80 | Good |
| 0.81-1.00 | Very good |

TABLE 4.1: Table for interpretation of Weighted Kappa, after Landis & Koch (1977)

penalization the weight is proportional to the distance, in the quadratic weighted kappa (κ) - the one studied in this chapter - the penalization is proportional to the square of the distance.

In this chapter, we study the direct optimization of the κ index, using it not only as a evaluation function but also as loss function during the training of the model. In the cases where there is some order relation between the output classes, the optimization of the loss function needs to learn this order from the available data to make good predictions. Our hypothesis is that a loss function that encodes such a priori order knowledge can perform better or faster than the usual logarithmic loss function, due to the fact that we are including this additional information known beforehand.

To prove this hypothesis, we use 3 problems of different complexity and with different type of data. Moreover, the neural net model required in each case has an increasing complexity.

The last case that we study, the more complex one, is a DR image classification problem. Diagnosis of DR from eye fundus images has been previously studied and it is considered a hard problem, because the classification into levels of severity is based on indicators that are difficult to detect in the images (Torre, Valls, and Puig, 2016b), (Escorcia-Gutierrez et al., 2016). We check its stability and compare the performance of the results obtained from the use of the standard logarithmic loss against the results obtained from the optimization of κ .

The study is organized as follows: in section 4.2 we present the deep learning standard method of optimization showing the standardized loss function used for classification, in section 4.3 we propose the new cost function for multi-class classification of ordinal data (ordinal regression) with

all the mathematical equations required for the optimization using first order gradient descent algorithms, in section 4.4 we define the experiments, in section 4.5 we present the results obtained and finally in section 4.6 we present the conclusions of the chapter.

4.2 Deep learning method

Supervised deep learning techniques are recently used extensively for many automatic classification tasks. In the case of images, most of the state of the art methods are based on the use of deep convolutional neural networks (DCNN): CIFAR-10 (Graham, 2014), CIFAR-100 (Clevert, Unterthiner, and Hochreiter, 2015), STL10 (Dundar, Jin, and Culurciello, 2015), SVHN (Liao and Carneiro, 2015), ImageNet (Krizhevsky, Sutskever, and Hinton, 2012a), among many others. These techniques are focused on learning multiple levels of representation and abstraction that help to make sense of the hidden information in data such as images. In this way, having a complete set of correctly classified images and without any a priori understanding of the features, the model is able to learn the properties of the image that minimize a defined cost function that is direct or indirectly related with the classification score index to optimize.

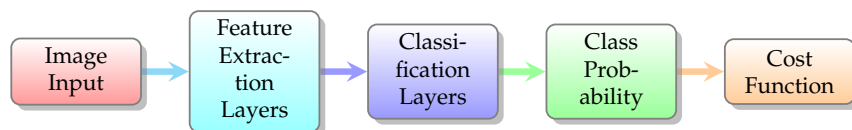


FIGURE 4.1: High level description of a deep learning image classification scheme

As shown in Fig. 4.1 for image classification, several convolutional neural networks are optimized for making a good feature extraction. These layers are followed by one or more classification layers. Finally, the last output layer is formed by as many outputs as classes to predict. In the output layer is usual to have a soft-max function that represents the output probability of every class to predict. Normally, the class assigned to the image is the one with the highest value of probability.

The main parameters to define are: total number of layers, the size of the convolutions with its stride and padding, the activation function to use,

4.2. Deep learning method

the number of convolutional filters for every layer and the type and number of elements of classification layer (fully connected or convolutional).

Moreover, once the architecture of the DCNN has been defined, the neural network has a set of parameters to optimize in order to achieve the most accurate prediction of the data. This is done by optimizing a function of the output variables, called *loss function*. This function depends on the output probabilities given by the model and it is defined in a way that minimizing it, maximizes the probability of the correct class. If the defined function is differentiable with respect to the output variables, then is possible to apply a gradient descent based algorithm to optimize the function (Saad, 1998). In every optimization step the classification derivative of the loss function is calculated and back-propagated through the network. The parameters are updated according to the optimization algorithm rules in order to reduce the discrepancy between the output of the model and the true value given by the known data.

Although binary classification is possible, many real problems distinguish more than 2 classes, so multi-class assignment procedures are usually required. Multi-class classification is addressed mainly by the optimization of the logarithmic loss (log-loss) function (see eq. 4.1). This function is very easy to optimize using first order gradient descent methods due to the simplicity of its derivatives, its numerical stability and experimental tested validity (Goodfellow, Bengio, and Courville, 2016). Additionally, the logarithmic loss has a very robust probabilistic foundation: minimizing it is the same as minimizing the logarithmic likelihood, that is equivalent to do a Maximum Likelihood Estimation (MLE) or equivalently, to find the Maximum a Posteriori Probability (MAP), given a uniform prior (Murphy, 2012). This function does not encode any prior information about the classes thus, it is a general purpose function that performs well in many applications.

$$\mathcal{L} = \frac{1}{N} \sum_{i=1}^N \sum_{c=1}^C t_i \log y_{i,c} \quad (4.1)$$

Where:

N : is the number of samples

t_i : is 1 for the correct class of the i th sample and 0 elsewhere

C: is the number of classes

On the other hand, there are applications where we have a priori information about some properties of the classes to predict. For example, in the case of ordinal regression, the different categories are sorted in a predefined way, representing a gradation of the output classes. When the log-loss is applied for the classification in this type of problems, the model has to learn such ordering from the data in order to obtain enough accuracy of the classification rate. In this case, a specialized loss like weighted kappa could be more appropriate than a general loss like the logarithm. In the rest of this chapter we will study if Weighted Kappa can perform better or even faster, due to the fact that it does not need to learn the order from the available data.

4.3 Weighted kappa as loss function in deep learning

In this section we present our contribution to the optimization of neural networks in general and deep learning in particular using Weighted Kappa index. Weighted Kappa has been normally used as an index to measure the inter-rating agreement between raters in a multi-class classification problem where the categories have an a priori defined ordering, in such a way that the classes to categorize are a high level abstraction of some sort of intrinsic information that we want to extract from data.

Three matrices are involved in the calculation of this index: the matrix of observed scores, O , the matrix of expected scores based on chance agreement, E , and the weight matrix, ω . The Weighted Kappa is defined as eq. 4.2.

$$\kappa = 1 - \frac{\sum_{i,j} \omega_{i,j} O_{i,j}}{\sum_{i,j} \omega_{i,j} E_{i,j}} \quad (4.2)$$

, where:

C: is the number of classes

$$i, j \in \{1, 2, \dots, C\}$$

4.3. Weighted kappa as loss function in deep learning

57

$O_{i,j}$: the number of observations classified in the i -th category by the prediction model and they are in the j -th category in the correct classification (i.e. "true value").

$E_{i,j}$: outer product between the two classification histogram vectors (prediction and "true value"), normalized such that E and O have the same sum.

$\omega_{i,j}$: weight penalization for every pair i, j . Generally, $\omega_{i,j} = \frac{(i-j)^n}{(C-1)^n}$. For linear penalization $n = 1$. For quadratic penalization (more commonly used and the studied in this chapter): $n = 2$.

This index establishes a penalization when there is a discrepancy between the classifiers that depends on the distance between both predictions. In the case of the κ the penalization of the discrepancy grows quadratically with the distance between the two ratings (i.e. ordered classifications). If the predicted classes of both raters is the same, we say that there is an *absolute* concordance between both raters and no penalization is applied. When the predicted classes are different, we say that there is *relative* concordance between both raters and there is a penalization in the calculation of the inter-rating index that is proportional - in the case of quadratic κ - to the square of the distance between both predictions.

In the numerator of eq. 4.2 we take into account the discrepancies between the observed classification of the prediction model and the true assignments. These discrepancies are calculated for all the N items. This penalizing term is normalized dividing their value by the expected discrepancy, obtaining as a result a value between -1 and 1. A value of 1 of the index indicates a perfect agreement between both raters, -1 a perfect symmetric disagreement between the classes and 0 indicates that a random assignment method is used (i.e. no agreement at all).

4.3.1 Mathematical foundation

In Deep Convolutional Neural Networks and in neural networks in general, the optimization problem to solve during the training of the model is based on finding the values of the parameters for the model that maximize the probability of a correct classification. Thus, if the evaluation index of

the correctness of the classification is κ , the optimization problem can be formulated as presented in equation 4.3.

$$\text{maximize } \kappa = 1 - \frac{\sum_{i,j} \omega_{i,j} O_{i,j}}{\sum_{i,j} \omega_{i,j} E_{i,j}}, \text{ where } \kappa \in [-1, 1] \quad (4.3)$$

However, optimization of the loss function (\mathcal{L}) is normally presented as a minimization problem, therefore in equation 4.4 we present the same problem converted to minimization. Notice that in this case, we propose to take the logarithm of the index, in order to increase the penalization of incorrect assignments.

$$\text{minimize } \mathcal{L} = \log(1 - \kappa) \text{ where } \mathcal{L} \in (-\infty, \log 2] \quad (4.4)$$

In neural networks for multi-class classification the model constructed does not give a unique predicted class as output, but a probability distribution over the set of possible classes. Consequently, we need to rewrite κ in terms of probability distributions. Having $\kappa = 1 - \mathcal{N}/\mathcal{D}$, in eq. 4.5 we show the expression of the numerator \mathcal{N} in terms of the probabilities of the prediction. In eq. 4.6 we also show the redefinition of the denominator \mathcal{D} in order to take into account the probabilities given by the model.

$$\mathcal{N} = \sum_{i,j} \omega_{i,j} O_{i,j} = \sum_{k=1}^N \sum_{c=1}^C \omega_{t_k,c} P_c(X_k) \quad (4.5)$$

$$\mathcal{D} = \sum_{i,j} \omega_{i,j} E_{i,j} = \sum_{i=1}^C \hat{N}_i \sum_{j=1}^C \left(\omega_{i,j} \sum_{k=1}^N P_j(X_k) \right) \quad (4.6)$$

, where:

X_k : input data of the k-th sample

$$E_{i,j} = \frac{N_i \sum_{k=1}^N P_j(X_k)}{N} = \hat{N}_i \sum_{k=1}^N P_j(X_k)$$

N : number of samples

N_i : number of samples of the i-th class

$$\hat{N}_i = \frac{N_i}{N}$$

4.3. Weighted kappa as loss function in deep learning

59

t_k : correct class number for sample k

$P_c(X_k)$: conditional probability that the k -th sample belongs to class c given that the true class is t_k

4.3.2 Partial derivatives of the weighted kappa loss function

For solving this optimization problem using any gradient descent based algorithm, we need to derive the partial derivatives of the loss function with respect to the output variables of the network.

For the case minimizing the loss function $\mathcal{L} = \log \frac{\mathcal{N}}{\mathcal{D}}$, the derivative takes the next form:

$$\frac{\partial \mathcal{L}}{\partial y_m} = \frac{1}{\mathcal{N}} \frac{\partial \mathcal{N}}{\partial y_m} - \frac{1}{\mathcal{D}} \frac{\partial \mathcal{D}}{\partial y_m} \quad (4.7)$$

And $\frac{\partial \mathcal{N}}{\partial y_m}$ and $\frac{\partial \mathcal{D}}{\partial y_m}$ can be calculated with the next expressions:

$$\frac{\partial \mathcal{N}}{\partial y_m(X_k)} = \omega_{t_k m} \quad (4.8)$$

$$\frac{\partial \mathcal{D}}{\partial y_m(X_k)} = \sum_{i=1}^C \hat{N}_i \omega_{i,m} \quad (4.9)$$

Where: $m \in \{1, 2, \dots, C\}$

In array form it can be rewritten as:

$$\frac{\partial \mathcal{N}}{\partial y_m} = \begin{pmatrix} \omega_{t_1,1} & \omega_{t_1,2} & \dots & \dots & \omega_{t_1,C} \\ \omega_{t_2,1} & \omega_{t_2,2} & \dots & \dots & \omega_{t_2,C} \\ \dots & \dots & \dots & \dots & \dots \\ \omega_{t_N,1} & \omega_{t_N,2} & \dots & \dots & \omega_{t_N,C} \end{pmatrix} \quad (4.10)$$

$$\frac{\partial \mathcal{D}}{\partial y_m} = \begin{pmatrix} \sum_{i=1}^C \hat{N}_i \omega_{1,i} & \dots & \dots & \dots & \sum_{i=1}^C \hat{N}_i \omega_{C,i} \\ \sum_{i=1}^C \hat{N}_i \omega_{1,i} & \dots & \dots & \dots & \sum_{i=1}^C \hat{N}_i \omega_{C,i} \\ \dots & \ddots & \dots & \dots & \dots \\ \sum_{i=1}^C \hat{N}_i \omega_{1,i} & \dots & \dots & \dots & \sum_{i=1}^C \hat{N}_i \omega_{C,i} \end{pmatrix} \quad (4.11)$$

With the definition of the loss function and its derivatives we have all the equations required to apply any first order optimization algorithm on a neural network based learning method.

4.4 Experiments

The aim of the experiments of this chapter is to test the performance of the proposed optimization loss function. Although our main area of interest is medical image analysis, we present two other completely different classification problems in order to prove the generality of the improvement of the performance when optimizing the qwk-loss function for solving ordinal regression problems. Three real case studies are solved, which are presented in order of increasing model complexity. In *Case 1* the relevance of the results provided by eCommerce search engines is estimated using a linear classifier; in *Case 2* the level of expectancy of contracting a life insurance is predicted using a fully connected 3-layer perceptron; finally, in *Case 3*, the most complex, a deep convolutional neural network is trained to solve a DR image classification problem. All three are real-world problems that are proposed as challenges in different competitions hosted in the Kaggle Platform¹. These problems were chosen because in all three the index used for evaluation in the Kaggle challenge is κ . It is worth to note that the neural network models presented here may not necessarily be the best ones for solving the concrete case studies. In some cases it is better another approach, however we study and present the neural network model because the contribution of this chapter is for this learning method.

4.4.1 Case 1. Search results relevance

Problem definition

Many electronic commerce sites have a search engine that helps the user to find the most suitable products. Search algorithms are developed ad-hoc for each site. Sometimes, the user experience with the results provided by these systems is discouraging, which may lead to a poor use of the online shop. Currently, small online businesses have no good way of evaluating

¹<https://www.kaggle.com/competitions>

the performance of their search algorithms, making it difficult for them to provide a good customer experience. The objective of this problem is to measure the relevance of the results reported by a search engine. Given the queries entered by customers and the resulting product descriptions reported by the search engine, the model has to predict the relevance that customers will give to the results obtained from the search engine. Such relevance is classified in four different categories sorted from not relevant (1) to very relevant (4).

Data

The dataset was created using query-result pairings from the CrowdFlower platform. The training data set includes 41,327 records with the next fields: product identification, query, product description, median relevance reported by three different raters as a value between 1 and 4 and the relevance variance of the scores given by the raters. The test data set includes 256,735 records with the next fields: product identification, user query and a product description. The dataset comes from the *Crowdflower Search Results Relevance* competition hosted in the Kaggle Platform.

Procedure

The training set has been split into two random subsets: 85% of the data is used for training and 15% is used for validation. As a pre-processing step, TF-IDF algorithm (Ramos, 2003) is applied to the query and product fields of the training set in order to make a first feature extraction. A singular value decomposition (SVD) of the features is applied and truncated to the first 400 components. After centering and scaling, the 400 components are feeded to a linear classifier that is trained using the Adam optimizer (Kingma and Ba, 2014) either with the log-loss or the qwk-loss function.

4.4.2 Case 2. Life insurance assessment

Problem definition

The goal of this classification problem is to rate the customers of an insurance company in eight categories in function of the expectancy for the

customer of contracting a life insurance, from low expectancy (class 1) to high expectancy (class 8). The USA company Prudential helps people of all ages and backgrounds grow and protect their wealth through a variety of products and services, including life insurance. The dataset includes the personal, medical and commercial information that this company has gathered from they customers.

Data

A database with 128 categorical, discrete and continuous variables is available with personal information, contracted products, medical history and family history of customers. The training set consist of 59,381 records. The test set consist of a total of 19,765 records. Some of the variables are missing. For every training record a class label is reported. The dataset comes from the Prudential Life Insurance Assessment competition hosted in the Kaggle Platform.

Procedure

Training set has been split into two random subsets: 85% of the data is used for training and 15% is used for validation. As a preprocessing step, all the categorical variables are converted to dummy variables. The empty values are filled with the mean value and finally all the dataset is normalized and scaled to have zero mean and unit standard deviation. After this, the initial 128 input variables are converted into 1,078 variables. These new variables are the input of a 3-layer fully connected multilayer perceptron. The first hidden layer has 128 units, the second one 64 and the output one 8. The two hidden layers use a ReLU activation function and are preceded by a batch-normalization layer. The model is trained using the Adam optimizer either with the log-loss or the qwk-loss functions.

4.4.3 Case 3. Diabetic retinopathy detection

Problem definition

DR is a leading disabling chronic disease and one of the main causes of blindness and visual impairment in developed countries for diabetic patients. Studies reported that 90% of the cases can be prevented through early detection and treatment (Romero-Aroca et al., 2006). Eye screening through retinal images is used by physicians to detect the lesions related with this disease. Due to the increasing number of diabetic people, the amount of images to be manually analyzed is becoming unaffordable. Moreover, training new personnel for this type of image-based diagnosis is long, because it requires to acquire expertise by daily practice.

In 2003 the medical community established a standardized classification based on four severity stages ((Wilkinson et al., 2003)) determined by the type and number of lesions (as micro-aneurysms, hemorrhages and exudates): class 0 referring to no apparent retinopathy, class 1 as a Mild Non-Proliferative Diabetic Retinopathy (NPDR), class 2 as Moderate NPDR, class 3 as a Severe NPDR and class 4 as a Proliferative DR.

The problem consists on optimizing a deep convolutional neural network to maximize the classification rate with a test set of images never seen before. The generalization capability will be scored against the quadratic weighted kappa over the test set.

Data

The dataset used in this work consists of two independent high resolution image sets (train and test). For every patient right and left eye images are reported. All the images are classified by ophthalmologists according to the standard severity scale presented before in (Wilkinson et al., 2003). The images are taken in variable conditions: by different cameras, illumination conditions and resolutions.

The training set contains a total of 35,126 images; 25,810 of class 0, 2,443 of class 1, 5,292 of class 3, 873 of class 3 and 708 of class 4. The test set contains a total of 53,576 images; 39,533 of class 0, 3,762 of class 1, 7,861 of class 2, 1,214 of class 3 and 1,206 of class 4.

The images come from the EyePACS dataset used in a Diabetic Retinopathy Detection competition hosted on the internet Kaggle Platform.

The models

Four different models have been used, one for every different image size. The idea was to first design small models based on restricted image sizes in order to have a small training time that could allow to run the maximum amount of experiments. This big set of previous experiments would allow to restrict the hyper-parameter space. Bigger models, slow to train, would then be trained with the best selection of hyper-parameters. For image sizes will be used: 128x128, 256x256, 384x384 and 512x512. The high resolution images of the dataset are resized to this values prior the training.

All models follow the scheme defined in fig. 4.1. The feature extraction layers use all 3x3 convolutions with padding of 1 and stride of 1, followed by a batch normalization (Ioffe and Szegedy, 2015) and a ReLU activation function (Dahl, Sainath, and Hinton, 2013). Every two feature layers, a 2x2 max-pooling layer of stride 2 is applied for dimensionality reduction. The number of feature layers vary depending on the image size. All models use a unique classification layer followed by the final output soft-max layer. The number of layers and the total number of parameters of each model are summarized in table 4.5.

The model used for the 128x128 image case has 1.16 million parameters, 10 feature layers of 32/32, 64/64, 128/128, 128/128 filters in every convolution (/ separate the filters for every map size, the commas indicate a 2x2 max-pooling operation) and a 4x4 convolution of 128 filters as a classification layer. The model used for the 256x256 image case has 1.44 million parameters, 12 feature layers of 32/32, 64/64, 128/128, 128/128, 128/128 filters in every convolution and a 4x4 convolution of 128 filters as a classification layer. The model used for the 384x384 image case has 1.77 million parameters, 12 feature layers of 32/32, 64/64, 128/128, 128/128, 128/128 filters in every convolution and a 6x6 convolution of 128 filters as a classification layer. Finally, the model used for the 512x512 image case has 11.3 million parameters, 12 feature layers of 16/16, 32/32, 64/64, 128/128, 256/256, 512/512 filters in every convolution, a 5x5 convolution of 512 filters as classification layer, followed by a 4x4 average pooling and a dropout

layer (ratio = 0.3) previous to the final soft-max output layer.

Procedure

The original training set is split into two random subsets: one with 90% of the data and other with 10%. The last one is used as a validation set for hyper-parameter selection.

Notice that the image set is highly imbalanced. In order facilitate the learning, the training set is artificially equalized using data augmentation techniques (Krizhevsky, Sutskever, and Hinton, 2012b) based on 0-180 degrees random rotation, X and Y mirroring and contrast and brightness random sampling.

A random initialization based in the Kaiming&He approach (He et al., 2015) is used for all the networks. All models are optimized using a batch based first order optimization algorithm called Adam (Kingma and Ba, 2014). We study different learning rates in order to find the optimal one for each loss function.

As qwk-loss function uses a normalization term in the denominator, we will use a batch-based gradient calculation. Presumably this loss function will be more sensible to small batches that the log-loss, this is the reason for considering the batch size (BS) an important hyper-parameter to study.

For every batch, the images are chosen randomly from the training set, with repetition. Data augmentation techniques are applied to augment the diversity of the classes (random rotations and brightness and contrast modifications). The epoch size is set to maintain fixed the total number of images per epoch to 100,000. This value is approximately the number of sample images required to ensure that all of them have been selected every epoch. Additionally, the number of updates per epoch of the parameters of the neural network is changed for different batch sizes. In the case of small batch sizes the number of updates per epoch is greater than the case of bigger batch sizes. Studying different batch sizes we would also explore different number of parameter updates. In all experiments training were run for 100 epochs.

4.5 Results

In this section we present the results of the experiments. For each case, we present a table with the detailed experiments done training the model with the two loss functions with different parameters. Additionally, a figure is presented with the results obtained in the best model achieved in the training stage, for every batch size and loss function.

4.5.1 Case 1. Search results relevance

For the selection of the best hyper-parameters a grid search is done over the learning rate (LR) and the batch size (BS) of the model. In table 4.2 we show all the experiments. In every row of the table we show the results obtained from training the model either with the log-loss and with the qwk-loss functions.

In figure 4.2 we show the best results achieved for every batch size with the validation set for the best hyper-parameter selection. As we can see, the models trained with qwk-loss function perform consistently better in all the configurations.

The κ_{val} indicator is always higher for the model that optimizes qwk-loss function. This indicates that the class order information has been correctly introduced into the model. Therefore, the classification mistakes are done within neighbor categories and not within separated categories (which is highly penalized with the quadratic weighted kappa index).

After the study, we check the performance of the best model trained with qwk-loss and log-loss, using the test set (i.e. against never seen before records) consisting on 256,735 records. The test of the best model trained with qwk-loss reports a $\kappa_{test} = 0.500 \pm 0.043$ (95% confidence). The best model trained with log-loss achieves a kappa in the test set of $\kappa_{test} = 0.468 \pm 0.050$ (95% confidence). The difference between the two models is about a 6% increase of the value of κ_{test} (see fig. 4.6).

4.5.2 Case 2. Life insurance assessment

In figure 4.3, the best results achieved on the training stage for every batch size and learning rate are shown. For each batch size, 5 LR values are

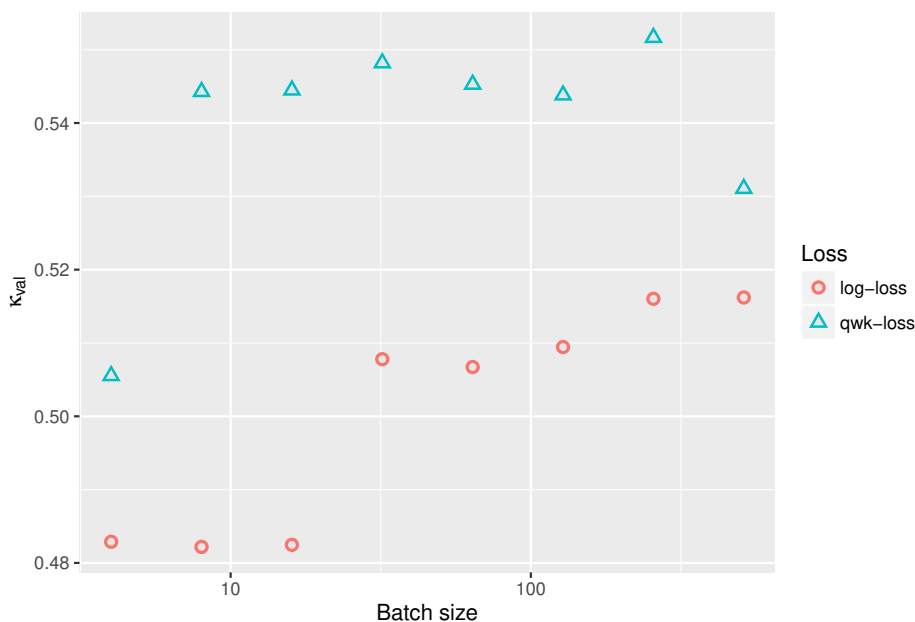


FIGURE 4.2: κ_{val} of the best model for every batch size (case 1: search results relevance)

tested. In bold we have the best κ_{val} of each batch size. This are graphically displayed in fig. 4.3. Next, the best parameters are chosen for the two models and the performance is evaluated using the test set, consisting on 19,765 records. The test of the best model trained with qwk-loss reports a $\kappa_{test} = 0.618 \pm 0.016$ (95% confidence). In the case of the best model trained with log-loss the value of kappa in the test set is $\kappa_{test} = 0.562 \pm 0.018$ (95% confidence). A significant difference between the two best models in the test set is found, with about a 10% increase of the value of κ_{test} (see fig. 4.6).

4.5.3 Case 3. Diabetic retinopathy detection

Table 4.4 shows the collection of all the conducted experiments where *input* represents the size of the input layer, *BS* the batch size used in the experiment, *LR* the learning rate, κ_{train} the maximum value of κ achieved during training over the training set, κ_{val} the maximum value of κ achieved during

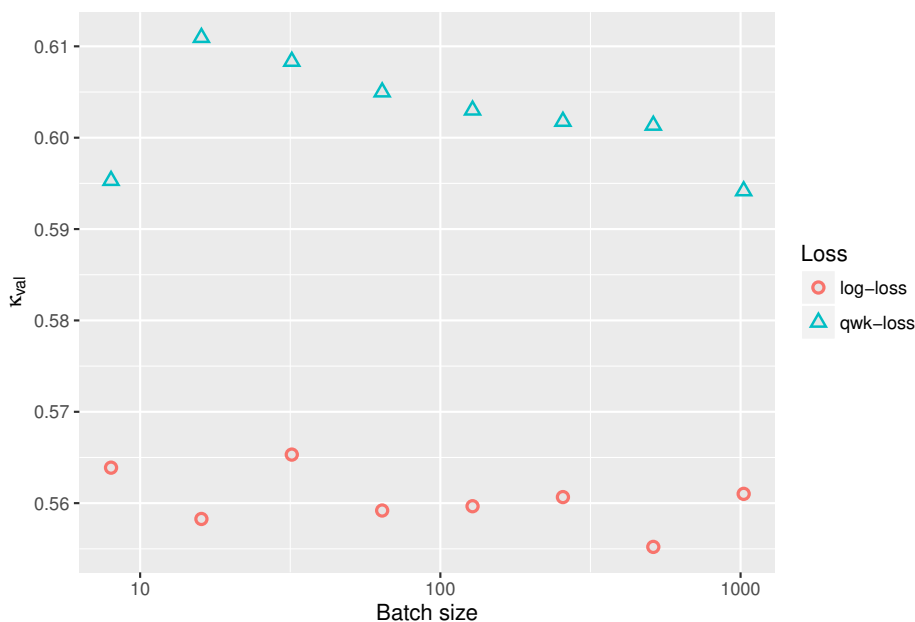


FIGURE 4.3: κ_{val} of the best model for every batch size (case 2: life insurance assessment)

training over the validation set, gap the difference between κ_{train} and κ_{val} , $epoch$ the epoch where the maximum value of κ_{val} is achieved and finally $updates$ the number of parameters updates required to achieve the maximum value of κ_{val} .

We can see that for every input size the maximum value achieved over the training set optimizing qwk-loss is always higher than the maximum value achieved optimizing log-loss (bold values). The gaps between both training and validation are also lower in the case of qwk-loss indicating a lower overfitting of the training data. We see that qwk-loss consistently reports better results than log-loss except for very low values of BS. In those cases, the qwk-loss performs worse than log-loss, but even in those cases the maximum value achieved by log-loss is lower than the best value of qwk-loss for the same model over the whole set of experiments.

In figure 4.4 we show a graphical representation of the maximum value of κ_{val} for the different configurations. We can see that directly optimizing

qwk-loss gives consistently better results than optimizing log-loss. Only in the case of very small batch sizes (for this application case, $BS = 5$) log-loss performs better than qwk-loss. This is probably due to the fact that qwk-loss uses a normalization term in the denominator that with not big enough batch sizes could cause instabilities in the gradient that affect the performance. In any case, even in those cases the results obtained with the log-loss are worse than the best achieved using the qwk-loss configuration.

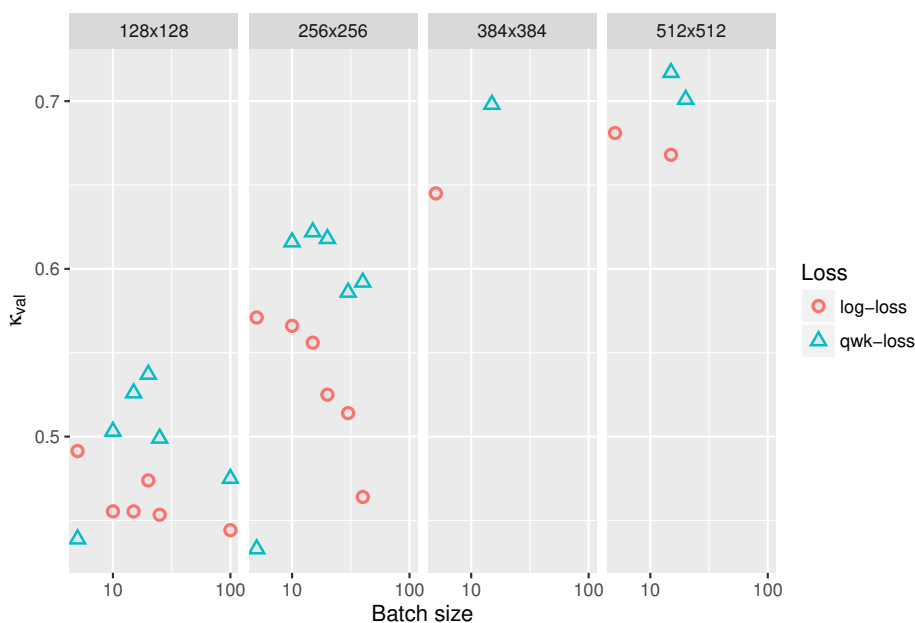


FIGURE 4.4: κ_{val} achieved for the DR detection use case in every experiment in function of the batch size and the loss function used

The optimal batch size for solving this DR classification is of 5 in the case of using the log-loss and 15 in the case of the qwk-loss. For greater values of this hyper-parameter, the increase in precision of the calculation of the gradient does not report any advantage in the optimization. In the case of the log-loss a lower precision in the calculation of the gradient works better. It could probably be due to the fact that this imprecision in the calculation increases the stochasticity of the optimization and due to the fact that we are not optimizing directly the metrics index. This makes possible

to explore adjacent zones that could work better for improving the metrics index than the ones that specifically improve the log-loss. Additionally, although smaller batch sizes give worse approximations of the gradient, the number of updates per epoch of the parameters of the model is greater. This seems to be an advantage in this case.

After all this study, we check the performance of the best model trained with qwk and log losses against the *never seen before* 53,576 image test set. The test of the best model trained with qwk-loss reports a $\kappa_{test} = 0.740 \pm 0.006$ (95% confidence). In the case of the same model trained with log-loss the value of $\kappa_{test} = 0.686 \pm 0.008$ (95% confidence). The difference between the two best models in the test set is of more than a 7% increase of the value of κ . (see case 3 in fig. 4.6)

Fig. 4.5 helps to understand the difference between the performance of the optimized loss functions. This figure displays the histograms of the predicted classes for every true class. It can be seen how the predicted histograms of the log-loss trained model are more scattered than the ones of the qwk-loss trained model. In those cases where there is a discrepancy between the real value and the predicted one, the model trained with the qwk-loss assigns a category that is closer to the true category than the ones predicted by the log-loss trained model. This can be seen specially in the central category T2, where the distribution of the qwk-loss model is concentrated in categories 1, 2 and 3 (with around 30% each), while in the log-loss model, there are 25% observations classified into class 0 as well as 10% into class 4. This is of great importance when the classification is related with medical diagnosis. For a patient having severe retinopathy (class 4) it is better to be classified having a moderate or a proliferative one (closer classes) than to be classified as having a mild or as not having any retinopathy at all.

4.5.4 Overall discussion on the performance improvement

In this section, the quality of the classification with the testing datasets is analyzed, although a brief comment has been made before on each case study. Figure 4.6 shows the κ index obtained on the testing data for the three case studies with the best model of every loss function. With this

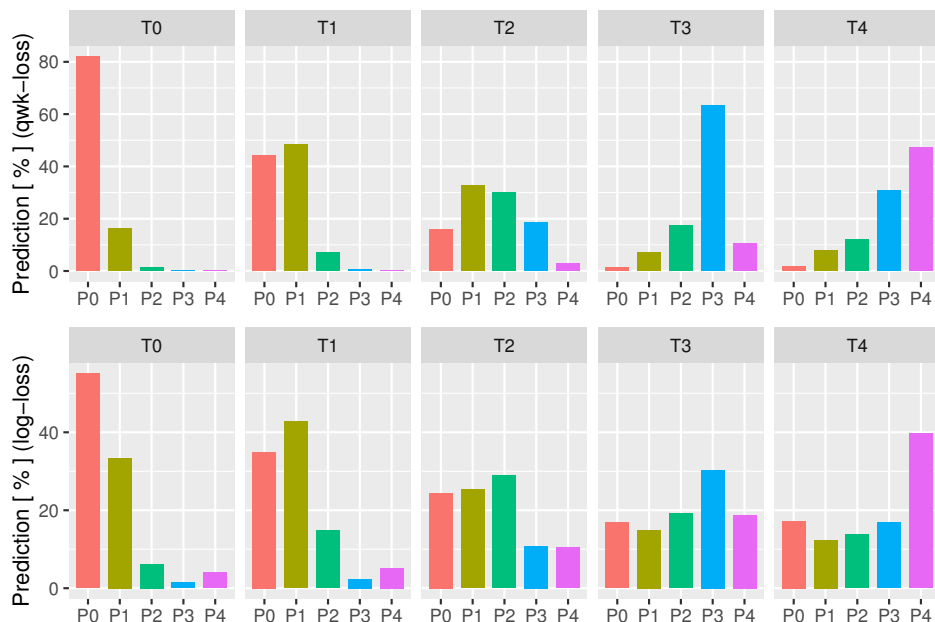


FIGURE 4.5: Histograms of the predicted classes for every real class over the test set for the best qwk-loss (above) and log-loss (below) trained models in the DR multi-class classification use case

figure we can check if the difference between the two optimization techniques is statistically significant or not. Improvement is clear for Case 2 and Case 3. Case 1 also has almost non-overlapping boxplots but the κ_{test} value achieved is more similar in the two models. However, in this case study the neural network used was the simplest one, thus the influence of the loss function in the final model is less. Improvement achieved with qwk-loss optimization is, thus, clear and supports the initial hypothesis of this research work.

4.6 Conclusions

We presented a new loss function for training deep learning models in ordinal classification problems based on the optimization of the weighted

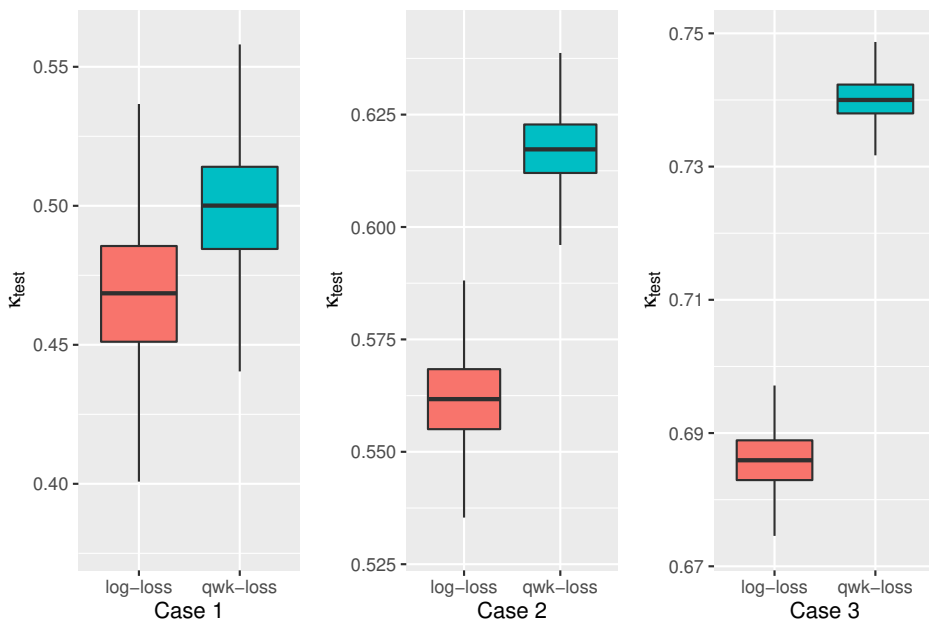


FIGURE 4.6: QWK confidence intervals for the log and qwk best models for the three studied cases

kappa index. In contrast to the logarithmic loss that uses a uniform prior over the set of classes, this new loss function defines a penalization over the discrepancy that is proportional to a power of the distance (quadratically in the case of κ) that allows to encode the prior known information about the predefined ordering of the classes.

We checked the performance of this new loss function with three different real-world case studies with diverse types of input data: textual in the first, categorical and numerical in the second and images in the third. Moreover, each case study was solved using decision models of increasing level of complexity: a linear classifier in the first, a multilayer perceptron in the second and a deep convolutional neural network in the third.

The results presented in this chapter show that with the direct optimization of the κ index consistently better generalization results can be achieved than with the standard use of the logarithmic loss. Log-loss has to learn the predefined ordering of the classes from data and this seems to

be a disadvantage. Results showed that, depending on the use case, between 6-10% of improvement of κ scores can be obtained from the direct optimization of the function.

This is a significant improvement that may be worth in many domains, such as the one of medical diagnosis, since an accurate detection of the level of severity of a disease usually has great influence on the treatment prescription and the possibility of minimizing bad consequences of the illness.

One minor drawback of the new loss is its low performance with very small batch sizes in the image classification study. The experiments show that for the retinopathy classification problem with batch sizes of 5, the performance of the function is lower than using the logarithmic loss. This parameter is for sure problem dependent and has to be taken into account as an important parameter to check in other image classification tasks that use a deep neural network.

| ID | BS | LR | $\kappa_{val}^{qwk-loss} 10^3$ | $Epoch_{best}^{qwk-loss}$ | $\kappa_{val}^{log-loss} 10^3$ | $Epoch_{best}^{log-loss}$ |
|----|-----|-------|--------------------------------|---------------------------|--------------------------------|---------------------------|
| 1 | | 1e-02 | 405 | 10 | 439 | 9 |
| 2 | | 1e-03 | 485 | 6 | 476 | 6 |
| 3 | 4 | 5e-04 | 506 | 15 | 483 | 14 |
| 4 | | 1e-04 | 503 | 19 | 467 | 3 |
| 5 | | 1e-05 | 461 | 99 | 455 | 50 |
| 6 | | 1e-02 | 450 | 13 | 444 | 6 |
| 7 | | 1e-03 | 544 | 6 | 482 | 0 |
| 8 | 8 | 5e-04 | 524 | 9 | 475 | 18 |
| 9 | | 1e-04 | 535 | 31 | 482 | 10 |
| 10 | | 1e-05 | 445 | 99 | 479 | 50 |
| 11 | | 1e-02 | 504 | 18 | 425 | 3 |
| 12 | | 1e-03 | 535 | 10 | 480 | 1 |
| 13 | 16 | 5e-04 | 543 | 11 | 480 | 1 |
| 14 | | 1e-04 | 545 | 50 | 483 | 9 |
| 15 | | 1e-05 | 395 | 99 | 479 | 86 |
| 16 | | 1e-02 | 515 | 12 | 436 | 2 |
| 17 | | 1e-03 | 548 | 16 | 494 | 1 |
| 18 | 32 | 5e-04 | 548 | 17 | 508 | 4 |
| 19 | | 1e-04 | 519 | 60 | 501 | 17 |
| 20 | | 1e-05 | 385 | 99 | 485 | 99 |
| 21 | | 1e-02 | 520 | 10 | 473 | 8 |
| 22 | | 1e-03 | 531 | 12 | 488 | 4 |
| 23 | 64 | 5e-04 | 545 | 37 | 506 | 9 |
| 24 | | 1e-04 | 514 | 61 | 507 | 25 |
| 25 | | 1e-05 | 377 | 99 | 400 | 99 |
| 26 | | 1e-02 | 513 | 4 | 479 | 5 |
| 27 | | 1e-03 | 544 | 23 | 497 | 6 |
| 28 | 128 | 5e-04 | 527 | 31 | 499 | 8 |
| 29 | | 1e-04 | 503 | 72 | 509 | 55 |
| 30 | | 1e-05 | 317 | 99 | 0 | 0 |
| 31 | | 1e-02 | 510 | 8 | 490 | 1 |
| 32 | | 1e-03 | 552 | 32 | 516 | 14 |
| 33 | 256 | 5e-04 | 490 | 21 | 507 | 24 |
| 34 | | 1e-04 | 421 | 45 | 469 | 48 |
| 35 | | 1e-05 | 189 | 99 | 61 | 34 |
| 36 | | 1e-02 | 512 | 18 | 488 | 7 |
| 37 | | 1e-03 | 531 | 38 | 516 | 24 |
| 38 | 512 | 5e-04 | 509 | 64 | 493 | 27 |
| 39 | | 1e-04 | 443 | 99 | 450 | 86 |
| 40 | | 1e-05 | 15 | 4 | 41 | 43 |

TABLE 4.2: List of all experiments for Case 1: Search results relevance

4.6. Conclusions

75

| ID | BS | LR | $\kappa_{val}^{qwk-loss} 10^3$ | $Epoch_{best}^{qwk-loss}$ | $\kappa_{val}^{log-loss} 10^3$ | $Epoch_{best}^{log-loss}$ |
|----|------|-------|--------------------------------|---------------------------|--------------------------------|---------------------------|
| 1 | 8 | 1e-02 | 412 | 0 | 564 | 5 |
| 2 | | 1e-03 | 593 | 3 | 550 | 4 |
| 3 | | 5e-04 | 592 | 8 | 556 | 2 |
| 4 | | 1e-04 | 595 | 11 | 560 | 4 |
| 5 | | 1e-05 | 588 | 20 | 556 | 27 |
| 6 | 16 | 1e-02 | 570 | 1 | 555 | 8 |
| 7 | | 1e-03 | 605 | 5 | 550 | 4 |
| 8 | | 5e-04 | 611 | 7 | 558 | 2 |
| 9 | | 1e-04 | 605 | 7 | 558 | 9 |
| 10 | | 1e-05 | 596 | 14 | 554 | 28 |
| 11 | 32 | 1e-02 | 587 | 0 | 560 | 1 |
| 12 | | 1e-03 | 604 | 2 | 565 | 3 |
| 13 | | 5e-04 | 608 | 2 | 552 | 4 |
| 14 | | 1e-04 | 603 | 11 | 562 | 11 |
| 15 | | 1e-05 | 598 | 24 | 545 | 44 |
| 16 | 64 | 1e-02 | 587 | 0 | 547 | 7 |
| 17 | | 1e-03 | 605 | 3 | 557 | 5 |
| 18 | | 5e-04 | 603 | 4 | 559 | 4 |
| 19 | | 1e-04 | 600 | 5 | 557 | 8 |
| 20 | | 1e-05 | 595 | 38 | 542 | 30 |
| 21 | 128 | 1e-02 | 592 | 2 | 554 | 4 |
| 22 | | 1e-03 | 602 | 5 | 560 | 2 |
| 23 | | 5e-04 | 603 | 4 | 556 | 8 |
| 24 | | 1e-04 | 599 | 7 | 558 | 18 |
| 25 | | 1e-05 | 567 | 48 | 537 | 45 |
| 26 | 256 | 1e-02 | 589 | 6 | 555 | 1 |
| 27 | | 1e-03 | 602 | 3 | 555 | 2 |
| 28 | | 5e-04 | 598 | 6 | 555 | 1 |
| 29 | | 1e-04 | 592 | 6 | 561 | 20 |
| 30 | | 1e-05 | 589 | 49 | 515 | 26 |
| 31 | 512 | 1e-02 | 601 | 16 | 555 | 1 |
| 32 | | 1e-03 | 601 | 5 | 548 | 5 |
| 33 | | 5e-04 | 598 | 3 | 554 | 9 |
| 34 | | 1e-04 | 598 | 15 | 548 | 19 |
| 35 | | 1e-05 | 563 | 49 | 523 | 48 |
| 36 | 1024 | 1e-02 | 594 | 4 | 549 | 3 |
| 37 | | 1e-03 | 592 | 5 | 561 | 7 |
| 38 | | 5e-04 | 594 | 5 | 554 | 12 |
| 39 | | 1e-04 | 593 | 21 | 547 | 22 |
| 40 | | 1e-05 | 472 | 49 | 470 | 49 |

TABLE 4.3: List of experiments for Case 2: Life insurance assessment

| Input | BS | Loss | LR | $\kappa_{train}10^3$ | $\kappa_{val}10^3$ | Gap | Epoch | Updates 10^{-3} | |
|-----------|-----|-----------|--------------------|----------------------|--------------------|------------|-------|-------------------|-----|
| 128 | 5 | log | 10^{-5} | 771 | 418 | 353 | 78 | 1560 | |
| | | | 10^{-4} | 851 | 491 | 360 | 73 | 1460 | |
| | | | 10^{-3} | 676 | 418 | 258 | 29 | 580 | |
| | | qwk | 5×10^{-5} | 545 | 402 | 143 | 50 | 1000 | |
| | | | 10^{-5} | 646 | 439 | 207 | 70 | 1400 | |
| | | | 10^{-4} | 497 | 326 | 171 | 31 | 620 | |
| | 10 | log | 10^{-5} | 797 | 397 | 400 | 82 | 820 | |
| | | | 10^{-4} | 874 | 455 | 419 | 81 | 810 | |
| | | | 10^{-3} | 514 | 336 | 178 | 57 | 570 | |
| | | qwk | 10^{-5} | 774 | 476 | 298 | 82 | 820 | |
| | | | 10^{-4} | 755 | 503 | 252 | 84 | 840 | |
| | | | 10^{-3} | 596 | 289 | 307 | 95 | 950 | |
| | 15 | log | 10^{-5} | 803 | 368 | 435 | 79 | 527 | |
| | | | 10^{-4} | 899 | 458 | 441 | 95 | 633 | |
| | | | 10^{-3} | 868 | 447 | 421 | 80 | 533 | |
| | | qwk | 5×10^{-5} | 715 | 491 | 224 | 77 | 513 | |
| | | | 10^{-4} | 800 | 526 | 274 | 77 | 513 | |
| | | | 5×10^{-4} | 823 | 523 | 300 | 72 | 480 | |
| | 20 | log | 10^{-4} | 896 | 474 | 422 | 79 | 395 | |
| | | qwk | 10^{-4} | 835 | 537 | 298 | 93 | 465 | |
| | 25 | log | 10^{-5} | 821 | 315 | 506 | 96 | 384 | |
| | | | 10^{-4} | 913 | 453 | 460 | 93 | 372 | |
| | | | 10^{-3} | 849 | 382 | 467 | 70 | 280 | |
| | | qwk | 10^{-5} | 808 | 423 | 385 | 95 | 380 | |
| 10^{-4} | | | 824 | 499 | 325 | 65 | 260 | | |
| 10^{-3} | | | 655 | 447 | 208 | 80 | 320 | | |
| 100 | log | 10^{-4} | 929 | 377 | 552 | 98 | 98 | | |
| | | 10^{-3} | 947 | 444 | 503 | 99 | 99 | | |
| | | 10^{-2} | 842 | 412 | 430 | 67 | 67 | | |
| | qwk | 10^{-4} | 879 | 450 | 429 | 93 | 93 | | |
| | | 10^{-3} | 798 | 455 | 343 | 71 | 713 | | |
| | | 10^{-2} | - | - | - | - | - | | |
| 256 | 5 | log | 10^{-4} | 871 | 571 | 300 | 52 | 1040 | |
| | | qwk | 10^{-4} | 605 | 433 | 172 | 15 | 300 | |
| | 10 | log | 10^{-4} | 903 | 566 | 337 | 75 | 750 | |
| | | qwk | 10^{-4} | 832 | 616 | 216 | 70 | 700 | |
| | 15 | log | 10^{-4} | 925 | 556 | 369 | 98 | 653 | |
| | | qwk | 10^{-4} | 878 | 622 | 256 | 93 | 620 | |
| | 20 | log | 10^{-4} | 923 | 525 | 398 | 97 | 485 | |
| | | qwk | 10^{-4} | 891 | 618 | 273 | 97 | 485 | |
| | 30 | log | 10^{-4} | 925 | 514 | 411 | 93 | 310 | |
| | | qwk | 10^{-4} | 900 | 586 | 314 | 98 | 327 | |
| | 40 | log | 10^{-4} | 922 | 464 | 458 | 93 | 233 | |
| | | qwk | 10^{-4} | 894 | 592 | 302 | 78 | 195 | |
| | 384 | 5 | log | 10^{-4} | 863 | 641 | 222 | 38 | 760 |
| | | 15 | qwk | 10^{-4} | 889 | 698 | 191 | 93 | 620 |
| 512 | 5 | log | 10^{-4} | 980 | 681 | 299 | 88 | 1760 | |
| | 15 | log | 10^{-4} | 978 | 668 | 310 | 94 | 626 | |
| | | qwk | 10^{-4} | 884 | 717 | 167 | 86 | 573 | |
| 20 | qwk | 10^{-4} | 903 | 701 | 202 | 89 | 445 | | |

TABLE 4.4: List of experiments for Case 3: DR detection

| Input | Total Layers | Feature Layers | Classific. Layers | Params 10^{-6} | $\kappa_{val}^{qwk-loss}$ | $\kappa_{val}^{log-loss}$ | Δ |
|---------|--------------|----------------|-------------------|------------------|---------------------------|---------------------------|----------|
| 128x128 | 12 | 10 | 1 | 1.16 | 0.537 | 0.491 | 9.3 % |
| 256x256 | 14 | 12 | 1 | 1.44 | 0.622 | 0.571 | 8.9 % |
| 384x384 | 14 | 12 | 1 | 1.77 | 0.698 | 0.663 | 5.3 % |
| 512x512 | 14 | 12 | 1 | 11.3 | 0.717 | 0.681 | 5.3 % |

TABLE 4.5: Summary of the difference in performance between qwk-loss and log-loss trained models in function of input size for the DR detection case

UNIVERSITAT ROVIRA I VIRGILI

DIABETIC RETINOPATHY CLASSIFICATION AND INTERPRETATION USING DEEP LEARNING TECHNIQUES

Jordi De la Torre Gallart

Chapter 5

Enhanced Models

In this chapter we present a part of the work published in (Torre, Valls, and Puig, 2017). Concretely, the optimized classification model for DR disease grading. The model presented here has a statistically proven ophthalmologist level performance, reaching a inter-rating agreement in never-seen-before Messidor dataset of $QWK = 0.83$, with a unique evaluation and no ensembling.

5.1 Introduction

Deep Learning (DL) methods (Lecun, Bengio, and Hinton, 2015), (Schmidhuber, 2015) have been extensively used in the last years for many automatic classification tasks. For the case of image classification, the usual procedure consists on extracting the important features using a set of convolutional layers and, after that, make a final classification with these features using a set of fully connected layers. At the end, a soft-max output layer gives the predicted output probabilities of belonging to the classes predefined in the model. During training, model parameters are changed using a gradient-based optimization algorithm, which minimizes a predefined loss function.(Goodfellow, Bengio, and Courville, 2016)

Once the classifier has been trained (i.e. model layer parameters have been fixed), the quality of the classification output is compared against the correct "true" values stored on a labeled dataset. This data is considered as the gold standard, ideally coming from the consensus of the knowledge of a committee of human experts.

This mapping allows the classification of multi-dimensional objects into a small number of categories. The model is composed by many neurons that are organized in layers and blocks of layers, piled together in a hierarchical way. Every neuron receives the input from a predefined set of neurons. In addition, every connection has a parameter that corresponds to the weight of the relation.

The function of every neuron is to make a transformation of the received inputs into a calculated output value. For each incoming connection, a weight is multiplied by the input value and the aggregation over all inputs is fed to an activation function that calculates the neuron output. Parameters are usually optimized using a stochastic gradient descent algorithm that minimizes a predefined loss function. Network parameters are updated after back-propagating the loss function gradients through the network. These hierarchical models are able to learn multiple levels of representation that correspond to different levels of abstraction, which enables the representation of complex concepts in a compressed way (Bengio, Courville, and Vincent, 2013), (Bengio, 2009).

The first successful convolutional neural network (CNN) published (LeCun et al., 1998) was designed for hand-written digit recognition. This early CNN implementation used a combination of convolution, pooling and non-linearity that has been the key feature of DL until now. It used convolutions for extracting spatial features, sub-sampling for reducing maps size, a non-linearity in the form of tanh or sigmoids, and a fully connected multi-layer neural network as final classifier. Network parameters were all learned using an end-to-end optimization algorithm using stochastic gradient descent. One of the first successful implementations using GPUs was published in (Cireşan et al., 2010) where they successfully trained a neural network with 9 layers, also for handwritten digit recognition. The DL breakthrough took place with the publication of (Krizhevsky, Sutskever, and Hinton, 2012a) where, for the first time, a CNN won the Imagenet (Deng et al., 2009) classification competition by a large margin. The network, named AlexNet, introduced a set of innovative techniques like data augmentation, the use of rectified linear units (ReLUs) as non-linearities, the use of dropout for avoiding overfitting, overlapping max-pooling avoiding the averaging effects of avg-pooling and the use of GPUs for speeding up the training time. This paper proved experimentally that CNNs were able

to solve complex tasks. From the publication of this paper many improvements were published, like (Sermanet et al., 2014) with the introduction of Overfeat, a network derivation of AlexNet where they proposed learning bounding boxes, which later gave rise to many other papers on the same topic. In (Simonyan and Zisserman, 2015), VGG networks were presented. It was the first time that small 3x3 convolution filters were used and combined as a sequence of convolutions. The previous big filters of 9x9 and 11x11 present in AlexNet started to become smaller. The great advantage of VGG network was the insight of stacking 3x3 convolutions as a substitution of large filters. These ideas were used in the design of posterior networks like ResNet and Inception. GoogleNet (Szegedy et al., 2015) and Inception (Szegedy et al., 2016) were the first attempts to reduce the size of big networks. DL was becoming very useful for categorization of images and video frames, but its main concern was its low efficiency in size and computation. Inception module used a parallel calculation of 1x1, 3x3 and 5x5 convolutions significantly reducing the number of operations required by networks like AlexNet and VGG. Bottleneck layers (1x1 convolutions) were used before the calculation of bigger size convolutions for reducing the number of input filters, reducing in this way the computational costs without losing generality. So, 1x1 convolutions have been proven to achieve state-of-the-art results in Imagenet classification tasks. The reason of this success is that input features are correlated, being removed by combining them appropriately with the 1x1 convolutions. Then, after convolution with a smaller number of features, they can be expanded again into a meaningful combination for the next layer. Another revolution came with the introduction of residual networks in (He et al., 2016). These networks used a combination of 3x3 convolutional layers with a by-pass of the input every two layers that was summed up to the output. The introduction of such bypass improved the gradient propagation through the network allowing the use of deeper networks and improving the classification capabilities. In (Szegedy et al., 2017), a modified version of Inception networks called InceptionResNet was published to introduce this idea to such networks. Residual blocks allowed the reduction of training time, not improving significantly the classification performance.

DL models have been also successfully applied in many medical classification tasks. In (Esteva et al., 2017) a DL classifier was designed achieving dermatologist-level accuracy for skin cancer detection. In (Zhu et al.,

2018) a 3D CNN for automated pulmonary nodule detection and classification was built. In (Wang et al., 2018) a CNN Alzheimer's disease classifier with high performance was also described. In (Gulshan, Peng, and Coram, 2016) the authors presented a DR classifier with better performance than human experts in the detection of the most severe cases of the disease.

5.2 Related work

Many deep learning classifiers for DR have been published in the last years. In (Torre, Puig, and Valls, 2018) a DL classifier was published for the prediction of the different disease grades. This model was trained using the public available EyePACS dataset. The training set had 35,126 images and the test set 53,576. The quadratic weighted kappa (QWK) evaluation metric (Cohen, 1968) was close to the reported by human experts in the test set using a unique DL model without ensembling.

In (Gulshan, Peng, and Coram, 2016) a binary DL classifier was published for the detection of the most severe cases of DR (grouping classes 0 and 1 of DR on one side, and classes 2, 3 and 4 on another). This model was trained using an extended version of the EyePACS dataset mentioned before with a total of 128,175 images and improving the proper tagging of the images using a set of 3 to 7 experts chosen from a panel of 54 US expert ophthalmologists. This model surpassed the human expert capabilities, reaching approximately a performance of 97% in sensitivity and 93.5% in specificity in test sets of about 10,000 images. The strength of this model was its ability to predict the more severe cases with a sensitivity and specificity greater than human experts. The drawback, as many DL based models, is its lack of interpretability. The model acts like a *intuition machine* with a highly statistical confidence but lacking an interpretation of the rationale behind the decisions, making difficult to the experts to have clues to improve the diagnostics.

5.3 Classification model for DR

5.3.1 Data

We use the EyePACS dataset presented in chapter 2. The dataset is split into two disjoint sets containing eye images of different patients, one for training and the other for testing.

The training set contains a total of 75,650 images; 55,796 of class 0, 5,259 of class 1, 11,192 of class 2, 1,805 of class 3 and 1,598 of class 4. The validation set used for hyper-parameter optimization has 3,000 images; 2,150 of class 0, 209 of class 1, 490 of class 2, 61 of class 3 and 90 of class 4.

The test set contains a total of 10,000 images of patients not present in training set; 7,363 of class 0, 731 of class 1, 1,461 of class 2, 220 of class 3 and 225 of class 4.

This dataset is not so rich and well tagged as the used in (Gulshan, Peng, and Coram, 2016) but allows to train models near human expertise that are useful to show the purposes of our work, which is not only a good performance of the classification results but mainly to provide tools for interpretability of the final classification of each patient.

5.3.2 Construction of the classifier

The model calculates the probability $P(\mathcal{C}|\mathcal{I})$, being \mathcal{C} one of the possible output classes and \mathcal{I} the retina image. Using as a last layer a *SoftMax* function over the values after the last linear combination of features. This probability is calculated as $P(\mathcal{C}|\mathcal{I}) = \frac{e^{S_C}}{\sum_{j=1}^C e^{S_j}}$. Let us call S_C the score of class C , being S_C the final value of each output neuron before applying the *Softmax*. *Softmax* function is required for calculating the probability of every class, but in case of being interested only on $\text{argmax}(\text{Softmax})$, we do not need evaluate *Softmax* because $\text{argmax}(S_i) = \text{argmax}(\text{Softmax}(S_i))$. Thus, we skip *Softmax* from the interpretation analysis.

Design guidelines for DR classification

Up to now, the design of deep neural network models is mainly driven by experience. Nowadays it is still more an art than a science and lacks a systematic way for designing the best architecture for solving a problem. In previous works (see (Torre, Valls, and Puig, 2016a) and (Torre, Puig, and Valls, 2018)), we have tested different kinds of architectures for DR classification. Using the previous experience in such works we report here a set of guidelines that have been used to build the proposed classification model for DR. These design principles for DR classification can be summarized into: use an optimal image resolution, use all the image information available, use a fully CNN, use small convolutions, adapt the combination of convolution sizes and number of layers to have a final RF as similar as possible to the image size, use ReLU as activation function, use batch normalization in every layer, use QWK as a loss function, use an efficient number of features and use a linear classifier as the last layer.

Use an optimal image resolution On the one hand, image input size has a great importance in the classification results. For this problem, other papers like (Torre, Valls, and Puig, 2016a) have shown that better results can be achieved with retina diameters of 512 pixels than with 384, 256 or 128 pixels. Some tests done using densities larger than 512 pixel/diameter seem to not improve significantly the classification rates. On the other hand, the hardware of calculation devices fix a limitation on the available resources. Input image size has a great impact on the memory and calculation time required for the training and test of the deep neural network models. For this present work, we tested models of 128, 256, 384, 512, 640, 724, 768 and 892 pixels of retina diameter. With this dataset, diameters greater than 640 does not seem to report better results. The optimal size is a retina diameter equal to 640 pixels. This is the one used for the results shown in this chapter.

Use all the available image information In previous studies published in (Torre, Valls, and Puig, 2016a), due to hardware limitations, the classification models were designed using limited input information, using only part of the available input, requiring ensembling solutions to combine the

results from evaluating different parts of the same retina. A 512x512 input image model was used with a random selection of a rotated square (diagonal equal to the retina diameter). In this way only a 64% of the retina information available was used in the classification prediction. On test time, five rotated versions of the input were averaged in order to get a better evaluation result. In this chapter, we use a network that receives all the input information available not requiring ensembling on test time. Only background located further from the diameter is removed.

Use a fully convolutional neural network CNNs are computationally more efficient than fully connected ones. CNNs are ideal for exploiting the typical high local pixel correlations present in images.

Use small size convolutions Spatial convolutions are very expensive in memory and time requirements, growing both quadratically with kernel size. Papers (Simonyan and Zisserman, 2015), (He et al., 2016), (Szegedy et al., 2016) proved experimentally that stacking small convolution layers and increasing depth is possible to obtain better results than using convolutions of bigger size with less depth. In (Eldan and Shamir, 2016) and (Cohen, Sharir, and Shashua, 2016) theoretical studies proved also that model expressiveness grows exponentially with depth. In our chapter, we follow a similar approach to the one used in (Simonyan and Zisserman, 2015) using exclusively 3x3 convolutions in every feature layer. Even convolution sizes are discarded due to its asymmetry when used with zero padding.

Adapt convolution sizes and number of layers to get a RF as similar as possible to the image size One important aspect of CNNs is the RF size. RF defines the theoretical space covered by a convolution in the input-space. The ideal case is having a RF in the last layer equal to the image size, because in such a way we are sure that all the information available is used. RFs greater than image size are inefficient, for this reason sometimes can be necessary to slightly modify the convolution sizes of some layer to get the desired one. Figure 5.1 shows the RF growth of our model.

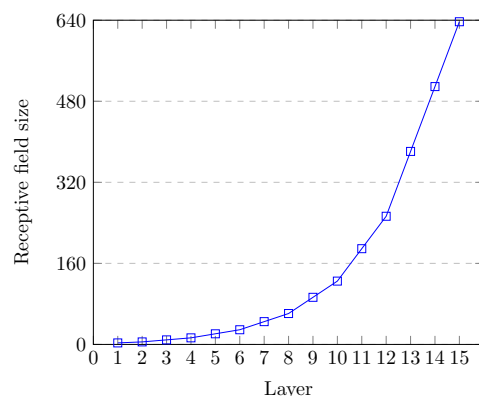


FIGURE 5.1: Model RF growth

Use rectified linear unit (ReLU) as activation function ReLU is a computationally efficient activation function that is very suitable to be used with very deep CNNs (Dahl, Sainath, and Hinton, 2013). We have tested other activation functions such as LeakyReLU, ELU and SeLU reporting similar and even worse results, introducing complexity to the model without adding any significant advantage to the final result.

Use batch normalization in every layer Batch normalization (Ioffe and Szegedy, 2015) stabilize the training and accelerates convergence. In this application there is a great difference between using batch normalization or not. To the point that not using it makes very difficult or even impossible the training.

Use QWK as a loss function For multi-class classification the standardized loss function to use is the logarithmic loss (Goodfellow, Bengio, and Courville, 2016). In (Torre, Puig, and Valls, 2018) it is shown that for ordinal regression problems, where not only a multi-class classification is taking place but also it is possible to establish a sorting of the classes based on some hidden underlying causes, QWK-loss can also be used with better results. The properties of this function as a loss function have been widely studied in (Torre, Puig, and Valls, 2018). The difference in performance of

the final results is very high. Optimizing directly QWK allows achieving better classification results.

Use a linear classifier as a last layer For simplicity and interpretability, we expect the model to disentangle completely the features required for the classification. Final classification is required to be done using a linear combination of last layer features.

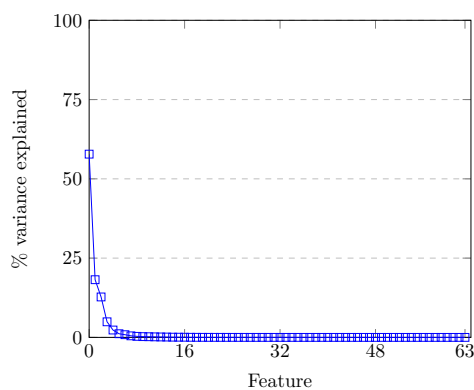


FIGURE 5.2: Feature space cumulative PCA variance of training set

Use a efficient number of features With infinitely number of resources we can use a big network. In our project we have limited device resources. In addition, we would like to be able to implement the result in devices with low resources too. Having this in mind, we tested networks of different sizes. In order to check the redundancy of information, we made a principal component analysis (PCA) in the feature space of the last layer, arriving to the conclusion that about 32 of the features explain 98.3 % and 48 features, 99.997% of the total variance. We studied different configurations using different number of features from 512 to 32. Values of 32 showed a reduction in performance that increased when using 64 features. Higher number of features did not improve the results. In figure 5.2 we show the variance explained by the 64 feature vector space.

Classification model description

Following the given guidelines, our model uses a $3 \times 640 \times 640$ input image obtained from a minimal preprocessing step, where only the external background borders are trimmed and later resized to the required input size. Figure 5.3 shows a block diagram of the model. It is a CNN with 391,325 parameters, divided in 17 layers. Layers are divided into two groups: the feature extractor and the classifier. The feature extraction has 7 blocks of 2 layers. Every layer is a stack of a 3×3 convolution with stride 1×1 and padding 1×1 followed by a batch normalization and a ReLU activation function. Between every block a 2×2 max-pooling operation of stride 2×2 is applied. After the 7 blocks of feature extraction, the RF of the network has grown till reaching 637×637 , that is approximately equal to the input size 640×640 (see fig 5.1 to see the RF of every layer). Afterwards, the classification phase takes place using a 2×2 convolution. A 4×4 average-pooling reduces the dimensionality to get a final 64 feature vector that are linearly combined to obtain the output scores of every class. A soft-max function allows the conversion of scores to probabilities to feed the values to the proper cost function during the optimization process. The feature extractor has 16 filters in the first block, 32 in the second and 64 in all the other.

5.3.3 Training procedure

As presented in section 5.3.1, the training set training set has 75,650 images and the validation set used for hyper-parameter selection 3,000. Notice that the image set is highly imbalanced. In order to facilitate the learning, the training set is artificially equalized using data augmentation techniques (Krizhevsky, Sutskever, and Hinton, 2012b) based on $0 - 180^\circ$ random rotation, X and Y mirroring and contrast&brightness random sampling.

A random initialization based in the Kaiming&He approach (He et al., 2015) is used. All models are optimized using a batch based first order optimization algorithm called Adam (Kingma and Ba, 2014). The loss function used for optimizing the model is the QWK-loss function, with a batch size of 15 and a learning rate of 3×10^{-4} (Torre, Puig, and Valls, 2018). For every batch, the images are chosen randomly from the training set, with repetition.

After network training, a linear classifier formed by the combination of the 128 features of the two eyes of the patient is trained. In this way is possible to increase further the prediction performance of the model using all the information available of the patient.

5.4 Results

The model is trained for 300 epochs, reaching a QWK value of 0.814 on the validation set. The value achieved in the testing set (with images not used in the training) of 10,000 images is of 0.801. Using a linear classifier for combining the features of both eyes QWK_{test} , we can reach a QWK value of 0.844. Expert ophthalmologist report QWK inter-rating agreement values close to 0.80.

If we consider a binary classification with two categories, one for severe cases of DR (grouping classes 2, 3 and 4) and another for non-sever cases (classes 0 and 1), we can calculate the usual classification evaluation metrics. Over EyePACS test set we obtain the following values for different measures¹: N=10,000, TP=1,727, TN=6,859, FP=1,235, FN=179, Sensitivity=0.906 (95% CI: 0.893 to 0.919), Specificity=0.847 (95% CI: 0.840-0.855), PPV=0.583, NPV=0.975, Accuracy=0.857, F_1 =0.710 and MCC=0.648.

For comparison purposes with other works, we tested also our model against the standardised Messidor-2 dataset (Decenci re et al., 2014). We achieve a QWK of 0.832 for this dataset. Binary classification statistics for prediction of the most severe cases of DR (grouping classes 2, 3 and macular edema) are: N=1200, TP=465, TN=627, FP=61, FN=47, Sensitivity=0.908 (95% CI: 0.883 to 0.933), Specificity=0.911 (95% CI: 0.890-0.933), PPV=0.884, NPV=0.930, Accuracy=0.910, F_1 =0.896 and MCC=0.817.

We can see that the results obtained with the Messidor-2 dataset are better because of the improved quality of images in the dataset and a also a better labelling of the examples.

In order to compare our model with state-of-the-art (Gulshan, Peng, and Coram, 2016), table 5.1 show statistics for prediction of the most severe

¹ Notation: N: sample size, TP: true positives, TN: true negatives, FP: false positives, FN: false negatives, CI: confidence interval, PPV: positive predictive value, NPV: negative predictive value, F_1 : F1 score and MCC: Matthews correlation coefficient

cases of DR (classes 2, 3 or macular edema) for Messidor-2 Dataset. We see that with a two orders of magnitude smaller model, it is possible to obtain good enough values of sensitivity and specificity. Our model is designed to be simple enough to be run in low resources devices, like mobile phones, with good performance. Furthermore, model simplicity eases the score calculations required for generating explanations.

| Reference | Parameters | Depth | Sensitivity | Specificity |
|------------------------|------------|-------|-------------|-------------|
| (Gulshan et al., 2016) | 23,851,784 | 159 | 96.1 % | 93.9 % |
| Our work | 391,325 | 17 | 91.1 % | 90.8 % |

TABLE 5.1: Prediction performance & model complexity comparison of our proposal vs the state-of-the-art model (Messidor-2 data set)

Building a multi-class classification model needs to account for the encoding of required features for distinguishing between the different disease severity levels. This is more difficult than a binary classifier, since it has to differentiate between more levels of DR severity. Thus, training the model for an aggregated detection (grouping the positive classes) increases the accuracy of the classifier, at the prize of missing the coding of important features that separate positive classes (1 to 4).

In our case, ophthalmologists want to distinguish all levels of severity since the treatment can be then personalized to each patient with more detail. Therefore, our goal is to make the model learn such differences in order to visualize them in the explanation model. For this reason, it is better to use all the information available about the gradation of disease (intermediate classes) in order to force the model to encode the required features that allow to separate the intermediate classes, even at the prize of reducing accuracy in the correct predictions. In this way after back-propagating the explanations, we could get the scores that the model report in the evaluation of the different classes for the same image, allowing the expert to get more knowledge about the image detection of DR signs.

5.5 Conclusions

We designed a model for DR classification, reaching more than 90% of sensitivity and specificity for the detection of the more severe cases of DR, not far from the state-of-the-art solution with two orders of magnitude less parameters. The designed model is also able to differentiate between the five standardized levels of disease severity, achieving in the test set of the EyePACS dataset a quadratic weighted kappa of 0.80 with the information of one eye and of 0.844 using the information coming from both eyes. In the Messidor-2 dataset the value of QWK achieved is of 0.83 using only the information of one eye. In all cases, the achieved performance is similar or even better than the reported by experts ophthalmologists, that is also near 0.80.

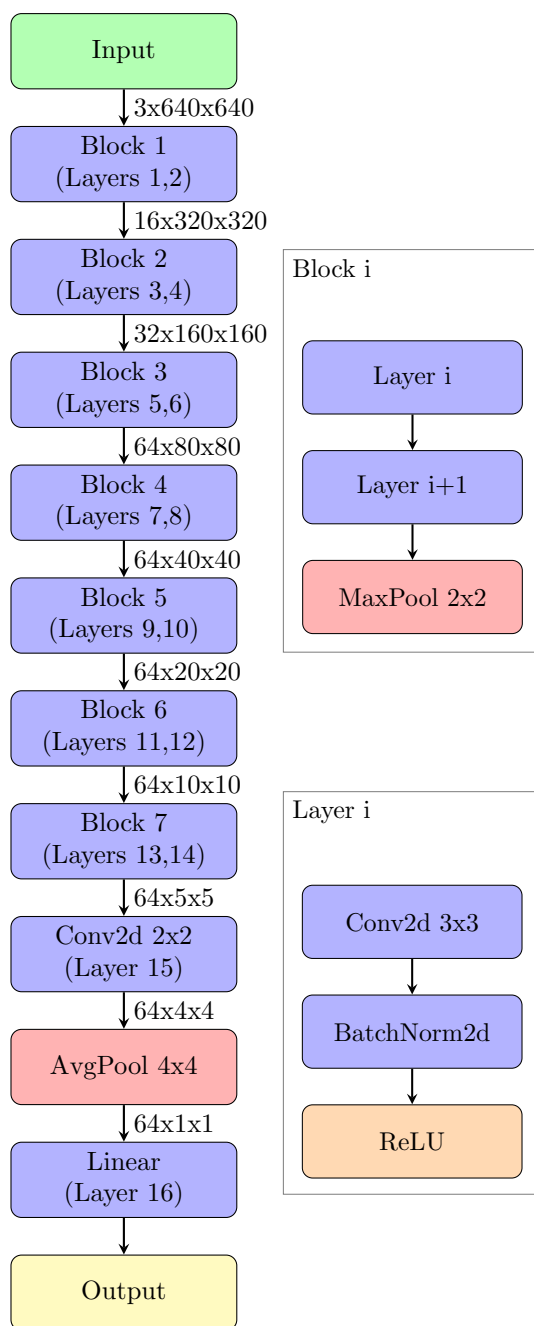


FIGURE 5.3: Prediction model of 391,325 trainable parameters (located in blue blocks).

Chapter 6

Classification Stability

In this chapter we present a stability study done using our best performance algorithm. Deep learning models act many times as black box prediction machines that are trained using, many times, a large but finite training set. The purpose of the analysis presented in this chapter is study how the prediction capabilities of the model are affected by changes in the properties of input images. Learning about this behavior gives a better understanding of the robustness and limitations of the designed model.

6.1 Introduction

Deep learning models are trained using an end-to-end automatic process that allows to learn the best internal representation (ie. the features and the optimal classifier) minimizing a predefined loss function. As a result, an optimal parameterized model is obtained. Such models typically have hundreds of thousands or millions of parameters, being difficult to interpret. The model validity is tested using a test data set hopefully coming from the same data distribution that the training set. Using a big enough test set of never seen before data, it is possible to corroborate the statistical validity of the results reported by the model. Such type of test gives us a overall understanding about the statistical performance, however it does not give us any information about the model behavior under variation of typical input image parameters like rotation, lightness, hue, saturation, zoom, etc.

The purpose of this chapter is the study of results variability under

typical changes in the input image parameters. This study allows a better understanding of the nature of trained models in order to increase its robustness and to know the intrinsic limitations of the trained models.

6.2 Methods

First of all, the method used for testing model robustness consists on defining set of parameters that are considered important to test. For all the set of parameters an interval of variation is defined. For a set of images, representative of the population of study, new images are generated with the new parameters defined. Classification scores are calculated for every new image generated and a graphical representation of classification scores versus parameter values are also generated. With such plots it is possible to determine the stability of model results under typical variations of the input properties.

The image parameters that are studied in this chapter are: rotation, lightness, hue and saturation.

Rotation: The model of study have been trained using data augmentation techniques that included random rotation. Therefore, the model should be robust to changes in image input rotation. Testing against such property will help us decide if multiple evaluations using different input rotated versions are required and also if results are seriously affected to changes of this variable or not. For each image, 360 evaluations have been done using different rotated versions of the same image, each one separated by 1 degree of rotation.

Hue, Lightness and Saturation: The model uses as input a 3 channels red, green, blue (RGB) representation of the retina image. From a conceptual perspective, color space is sometimes better to be considered using another type of representation, ie. hue, lightness and saturation (HLS) color space (see figure 6.1). HLS aligns better with the way human vision perceives color-making attributes. Lightness representing the brightness relative to the brightness of a similarly illuminated white; hue referring to the attribute of a visual sensation according to which an area appears to be

similar to one of the perceived colors: red, yellow, green, and blue, or to a combination of two of them; and saturation showing the colorfulness of a stimulus relative to its own brightness (Fairchild, 2013). Changes in each one of the variables HLS are done maintaining constant the others. For each variable 600 evaluations of the same image are done. Lightness and saturation varying linearly from 25% to 175% of the original image, and hue varying from -180 to +180 degrees of the original hue angle value.

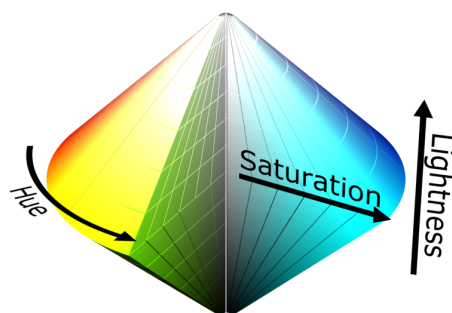


FIGURE 6.1: Hue-Lightness-Saturation color space cone
(source: commons.wikimedia.org)

6.3 Results

The model used for the stability study is the one trained in chapter 5. In the following subsections, stability results of the studied variables are reported. A random selection of images from the public Messidor Dataset (Decencière et al., 2014) have been chosen. Fig. 6.2 show the class 0 images selected for this study, fig. 6.3 the class 1, fig. 6.4 the class 2 and finally, fig. 6.5 the class 3 images.

6.3.1 Rotation

In the four class 0 analyzed samples (fig. 6.6), no change is observed in the value of predicted class when rotation is applied to the input image. All four images are correctly classified as class 0 for all orientations.

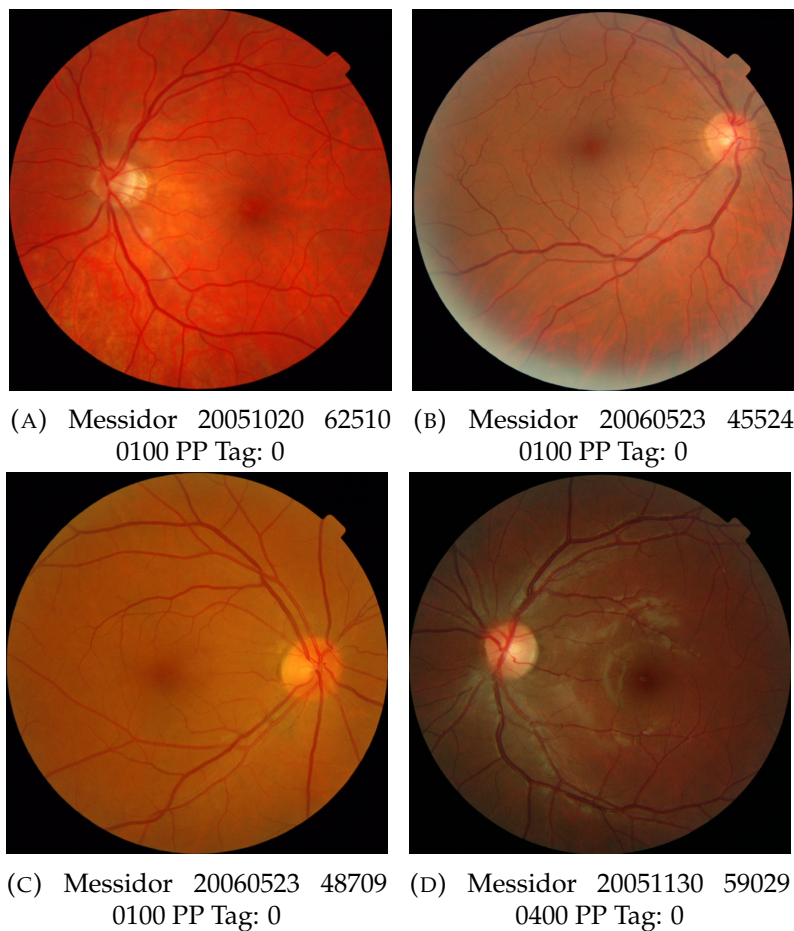


FIGURE 6.2: Images used for testing model robustness (Tag: 0)

For class 1 (fig. 6.7), no change is observed in 3 of the 4 analyzed images, predicting the correct class in all of them for all orientations. In the fourth image a change in the score of predicted class is observed, changing between 0 and 1 class. The network arrive to different conclusions depending on orientation. In any case, the discrepancy is only of one class (between 0 and 1). The model predicts class 0 in 193 of the 360 rotations and class 1 in 167.

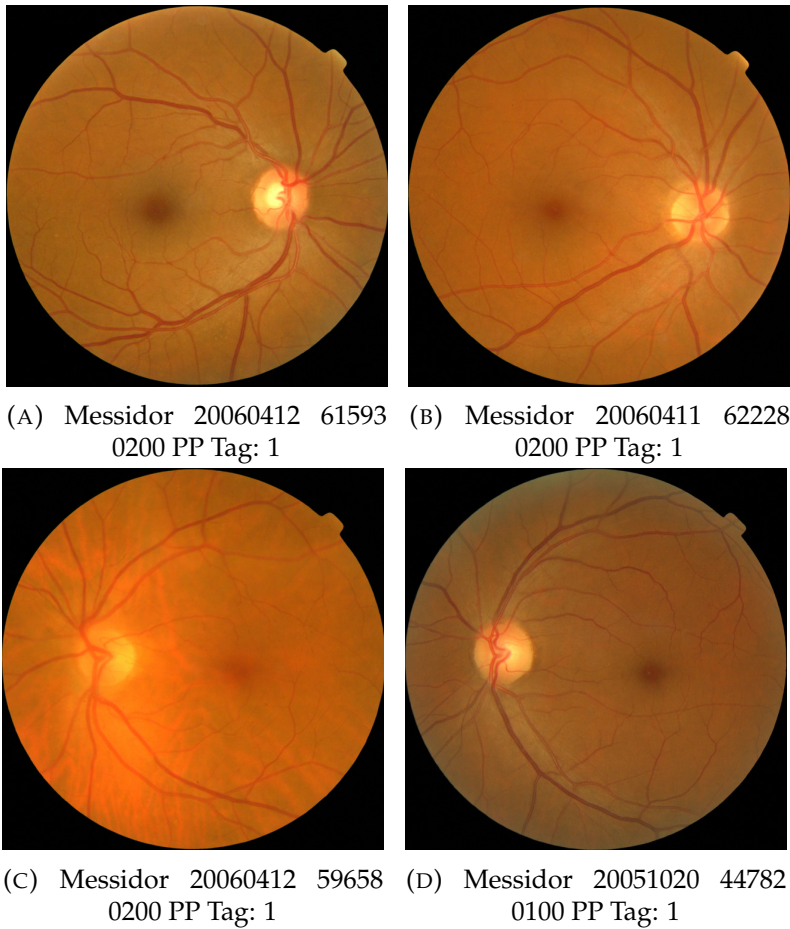


FIGURE 6.3: Images used for testing model robustness (Tag: 1)

For class 2 (fig. 6.8), there is a discrepancy of one class distance between the tag and the predicted value in the first two images. The model predicts class 1 in the first image for all orientations, and for the second image predicts class 1 in 356 of the orientations and class 0 in 4 orientations. For the third and fourth images class 2 is correctly predicted for all the 360 rotated versions.

For class 3 (fig. 6.9), class 3 is correctly predicted in 3 of the 4 images,

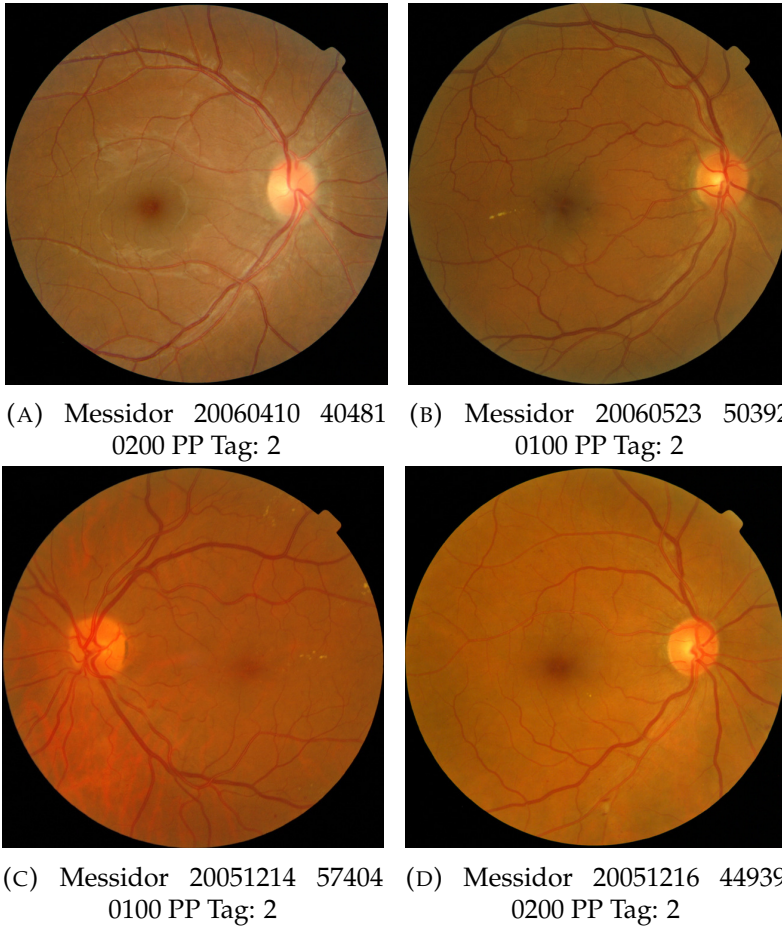


FIGURE 6.4: Images used for testing model robustness (Tag: 2)

having a discrepancy of one class in the second image, predicted globally as class 2. Concretely, for the first image class 3 is predicted in 307 of the orientations and class 2 in 53. For the second, class 2 is predicted in 348 of the orientations and class 1 in 12. For the third, class 3 is predicted in all orientations. Finally in the fourth image, class 3 is predicted in 236 of the orientations and class 2 in 124.

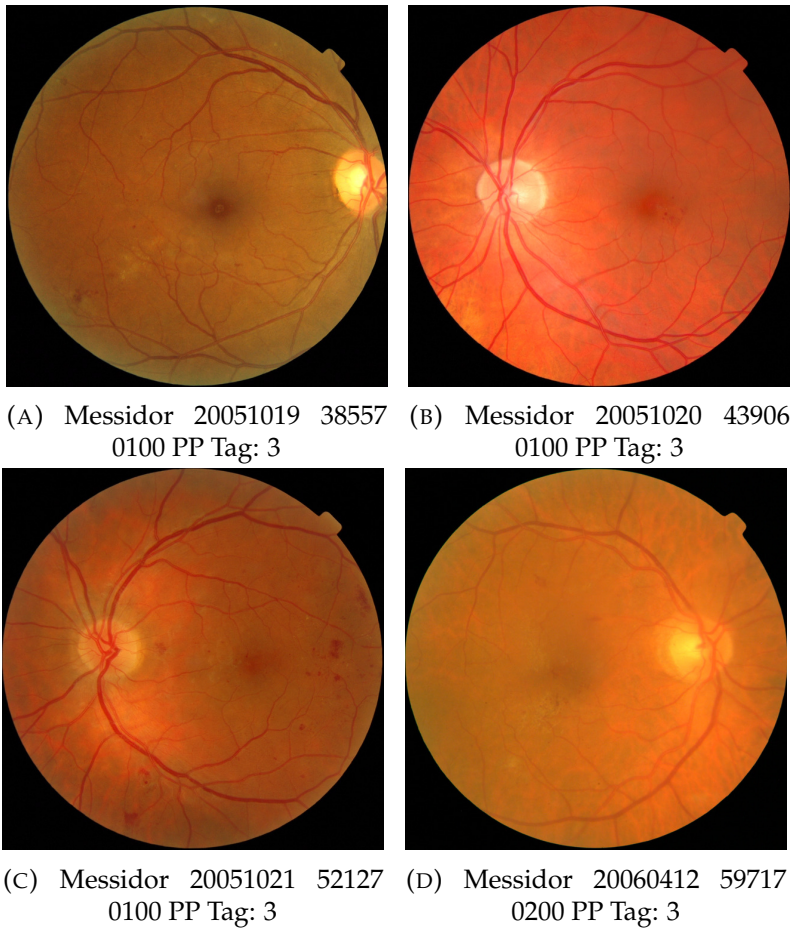


FIGURE 6.5: Images used for testing model robustness (Tag: 3)

6.3.2 Lightness

For all retina images a change in image lightness is applied maintaining constant hue and saturation. A broad change in lightness is studied going from 25% of the original value of lightness to a 75% more lightness. This variation helps to study the effect of light in the image in the predicted classes.

Figure 6.10 shows the results for class 0 studied classes. For all four images a similar effect in score values of each class is observed for all the studied range of lightness following a parallel behavior under changes of lightness.

Figure 6.11 shows the results for class 1 images. All score classes follow a similar change in the curves, being parallel between each other, except class 0 curve that consistently show higher values of its score relative to all other classes in both extremes of the lightness spectrum. Either for dark or for too clear images, class 0 score increases respect all the other classes increasing the probability of false negatives in both extremes. The values of lightness under and above which class 0 score becomes the highest are 43 and 125 for first image, 30 and 125 for the second, 38 for the third and 70 and 105 for the fourth. For all four images the predicted value under initial conditions is 1.

Figure 6.12 shows the results for class 2 images. The effect of lightness is similar to the observed in previous cases, that is class 0 increasing in both extremes of the curve with one difference: the score signaling of class 2 and 3 are above the increase in value of class 0 scores. That's why only in the first case, that is predicted as class 1, a important reduction of lightness causes a false negative (under 40). In all other cases, the prediction is equal to the tag (class 2) showing a good stability under a high range of lightness.

Figure 6.13 shows the results of class 3 images. Similar effects to the previous cases are observed that is, an increase of class 0 and 1 scores in the low and high lightness extremes, not being important under mild changes of lightness.

6.3.3 Saturation

For all retina images a change in image saturation is applied maintaining constant hue and lightness. A broad change in saturation is studied going from 25% less from original value to 75% more saturation. This variation helps to study the effect of color saturation in the image in the predicted classes.

Figure 6.14 shows the changes in predicted scores under different saturation degrees. No modification in predicted class is observed for the first

three images. A change predicted class is observed in the last case for values of saturation under 90s.

Figures 6.15, 6.16 and 6.17, show the scores for class 1, 2 and 3 images respectively. No significant changes are observed in the behavior of predicted classes, being the score maps flat in most of the cases.

6.3.4 Hue

Hue is the studied variable having the most important influence on class prediction. This is an expected result due to its nature. Hue angle represents color, being such property the most important characteristic used for differentiating lesions, thus the model is expected to use color information for score determination. Extreme hue values far from true values give the higher score to class 0. Only in a narrow range between the original values the model is able to find the correct classification. Figures 6.18, 6.19, 6.20 and 6.21 show the score representations for changes in hue. The pattern observed is the same for all images of all classes.

6.4 Conclusions

The objective of this chapter was to study the capabilities and limitations of the classification model designed in chapter 5. For this purpose a test of the robustness of its results has been done applying different changes to the inputs, in order to determine the important elements that have to be taken into account in inference time. The chosen properties of study have been: rotation, lightness, saturation and hue. A set of four random images of each class have been selected and modified according to the properties of study. A graphical representation of each variable versus scores have been generated in order to study the influence of each one of such variables in predicted classes.

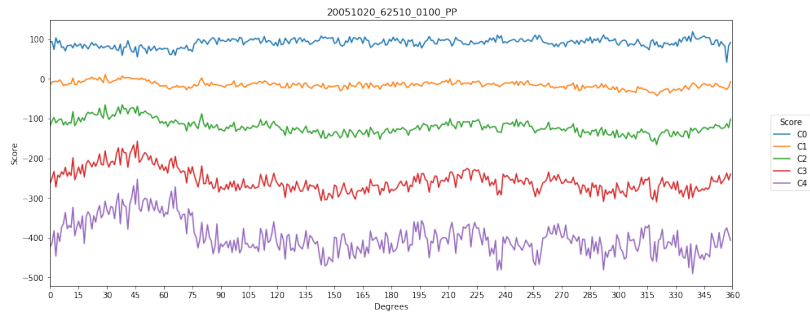
From this analysis we have made several observations:

- A) The model shows a high robustness to changes in rotation. One evaluation is enough in most of the cases, allowing only a slight improvement in statistical results when more than one evaluation is used.

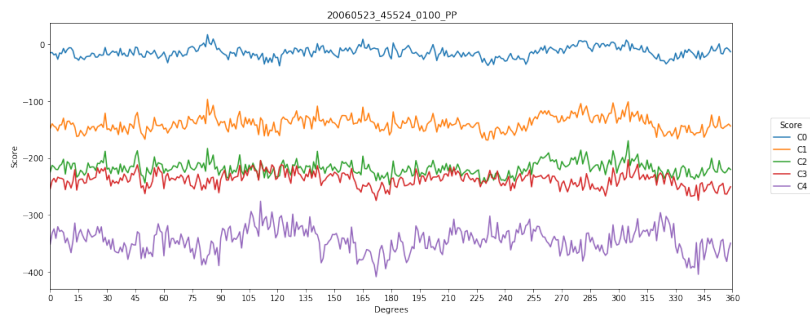
This means that is not necessary to rotate the image in order to improve the classification results. It also means that if the photo is taken in different rotations, the classifier works also correctly.

- B) Lightness extremes cause an increase in class 0 scores that could produce false negatives. Such effect is less important when predicting images of classes greater than 1, because the signals produced by the positive detection is higher than the increase in class 0 scores, produced by lightness extreme values. These results show that model is highly robust to changes in image illumination. This study also produced a range on lightness variation that could be used to decide if an image has the proper illumination condition to be used for inferring a classification or if must be discarded.
- C) Saturation does not seem to have an important effect on predicted scores. Most of the generated maps are flat. We can conclude then that model is robust to changes in input image saturation.
- D) Hue is critical for the model. The model only work well under certain intervals. This result is consistent with experts use of color information to differentiate between aneurysms, exudates, and other disease related lesions. The color of such lesions is also related to vessels color and the eye fundus color (as well as macula). Therefore, altering hue has a great impact on the features used by the model for lesion identification. However, hue variations are a change difficult to have with well calibrated cameras.

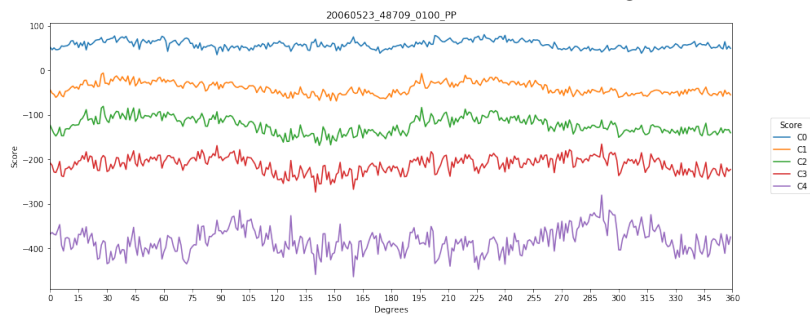
This type of studies allows the identification of strengths and weaknesses of the models. Other variables could also be studied, like for example zoom, original image resolution, etc. to have a prior knowledge about model behavior under certain input conditions that may occur in inference time. However, we have not considered such studies because, due to the nature of our problem, we can assure to have a fixed resolution and zoom in our input images.



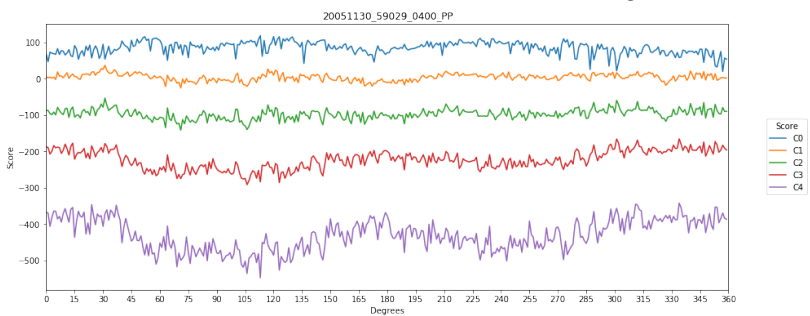
(A) Messidor 20051020 62510 0100 PP Tag: 0



(B) Messidor 20060523 45524 0100 PP Tag: 0

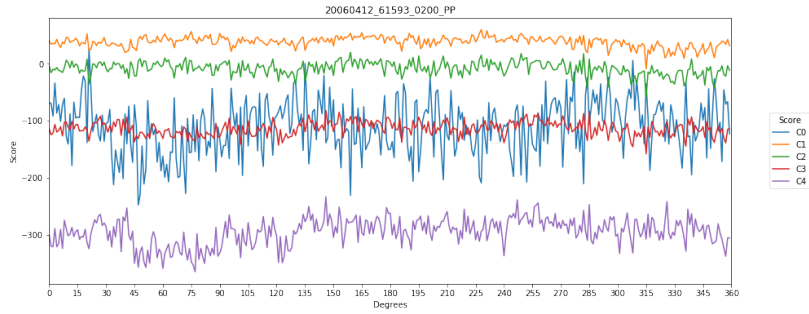


(C) Messidor 20060523 48709 0100 PP Tag: 0

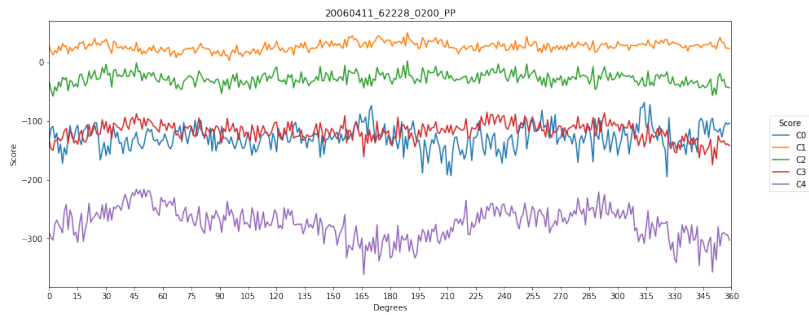


(D) Messidor 20051130 59029 0400 PP Tag: 0

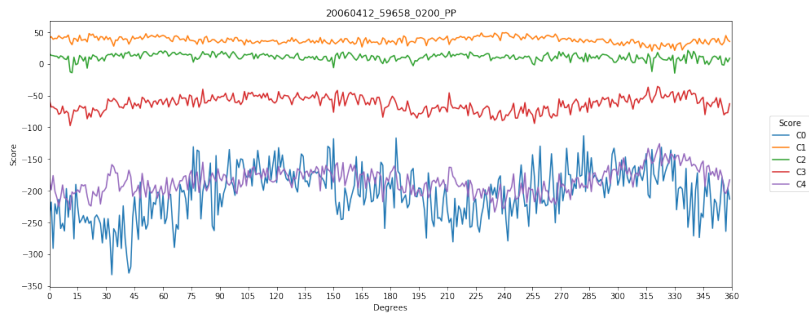
FIGURE 6.6: Class Score vs Input Rotation (Tag: 0)



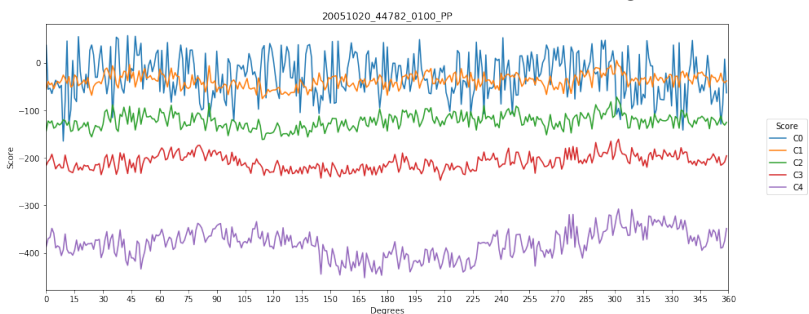
(A) Messidor 20060412 61593 0200 PP Tag: 1



(B) Messidor 20060411 62228 0200 PP Tag: 1

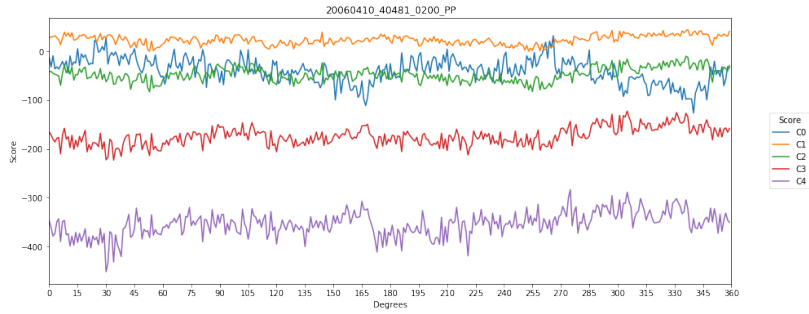


(C) Messidor 20060412 59658 0200 PP Tag: 1

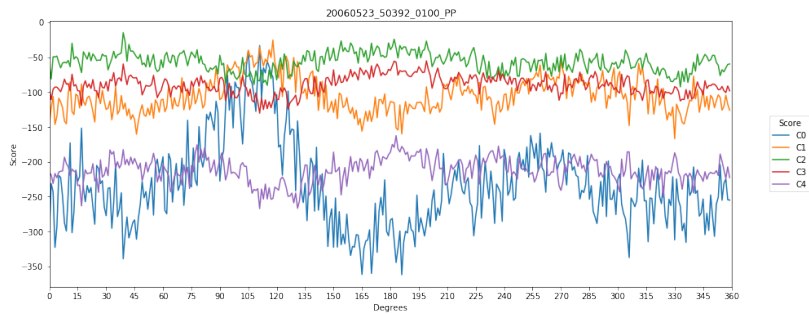


(D) Messidor 20051020 44782 0100 PP Tag: 1

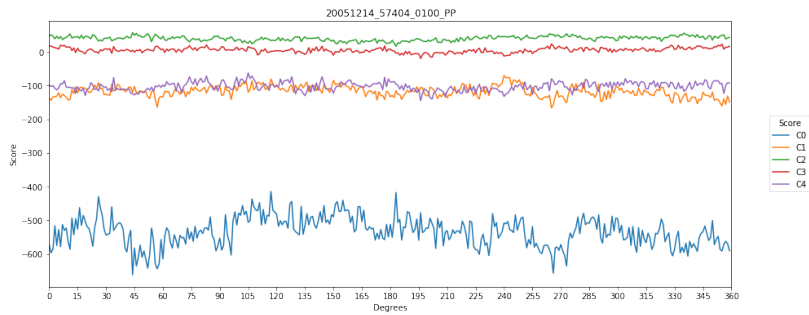
FIGURE 6.7: Class Score vs Input Rotation (Tag: 1)



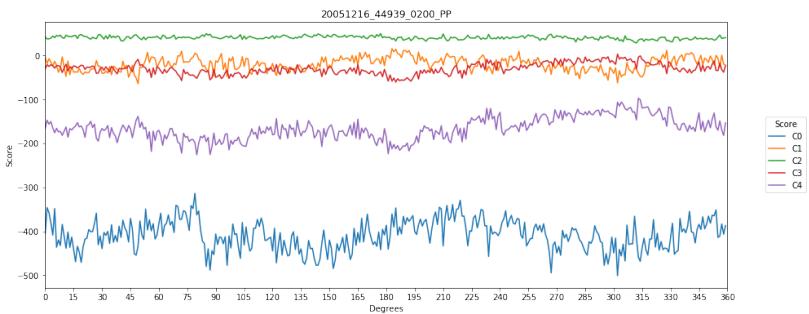
(A) Messidor 20060410 40481 0200 PP Tag: 2



(B) Messidor 20060523 50392 0100 PP Tag: 2

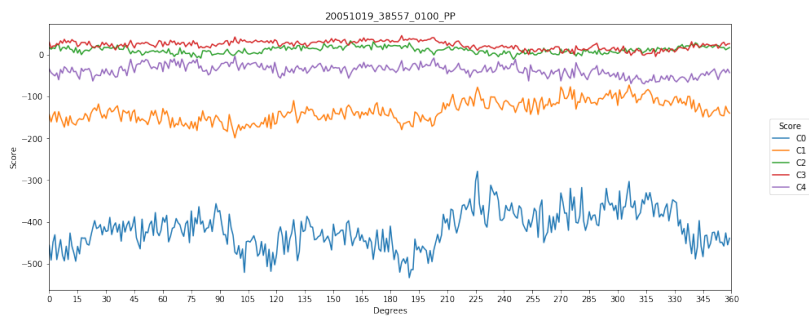


(C) Messidor 20051214 57404 0100 PP Tag: 2

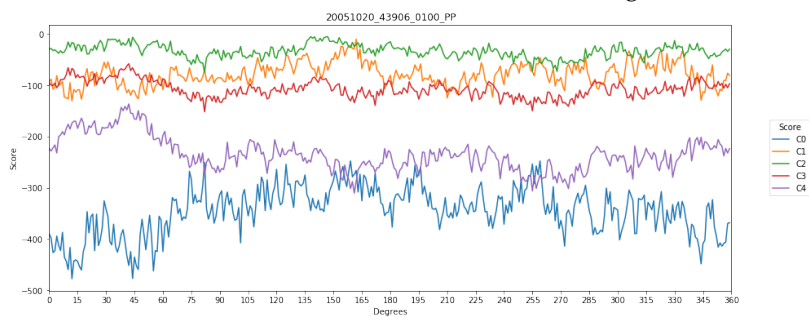


(D) Messidor 20051216 44939 0200 PP Tag: 2

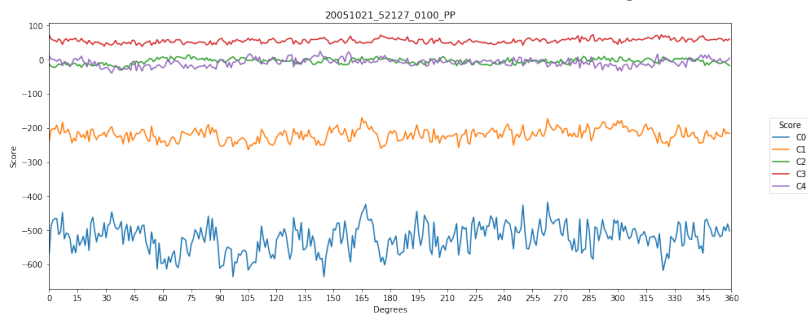
FIGURE 6.8: Class Score vs Input Rotation (Tag: 2)



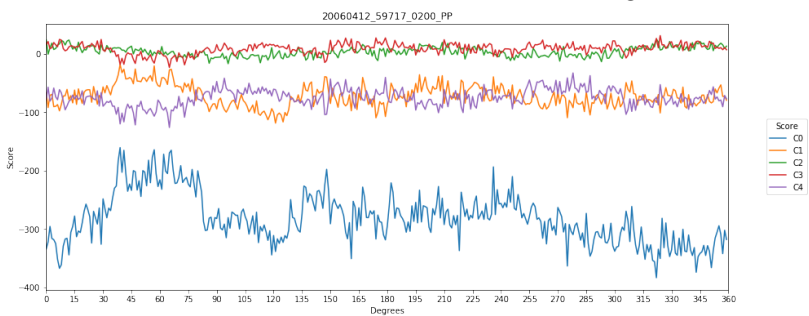
(A) Messidor 20051019 38557 0100 PP Tag: 3



(B) Messidor 20051020 43906 0100 PP Tag: 3



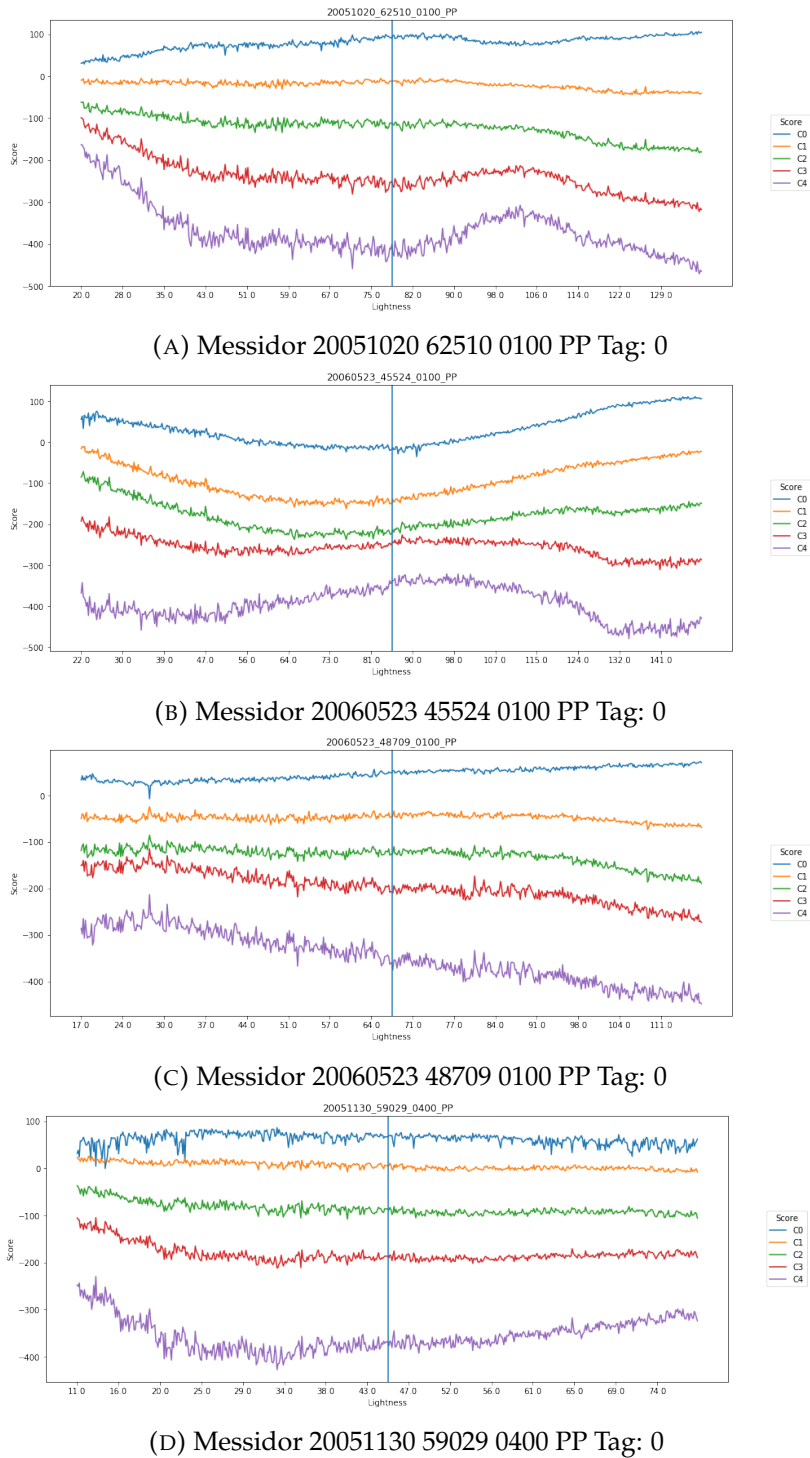
(C) Messidor 20051021 52127 0100 PP Tag: 3

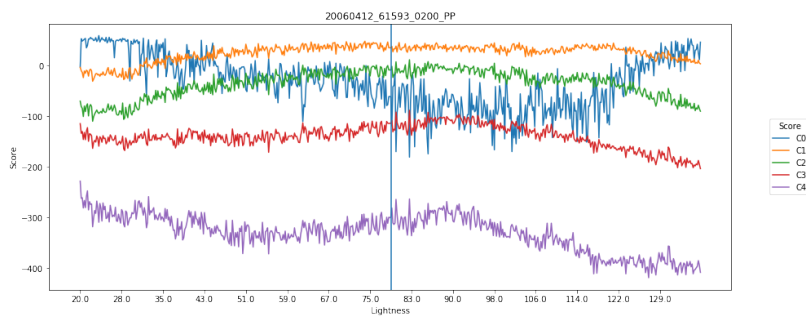


(D) Messidor 20060412 59717 0200 PP Tag: 3

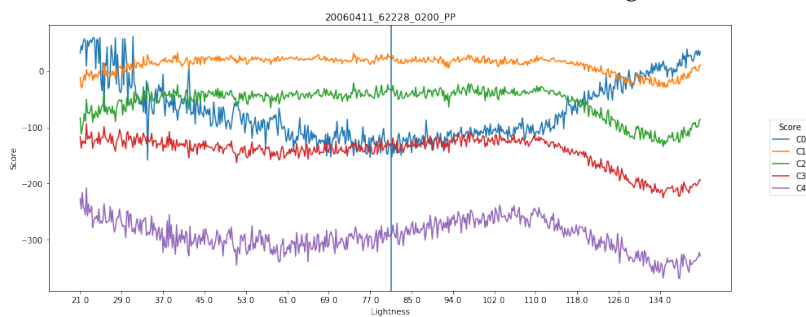
FIGURE 6.9: Class Score vs Input Rotation (Tag: 3)

6.4. Conclusions

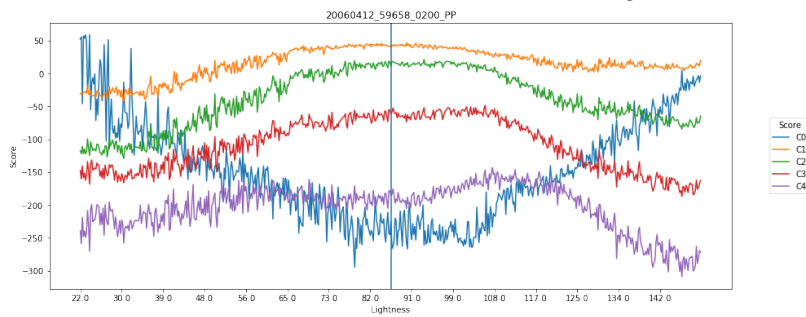




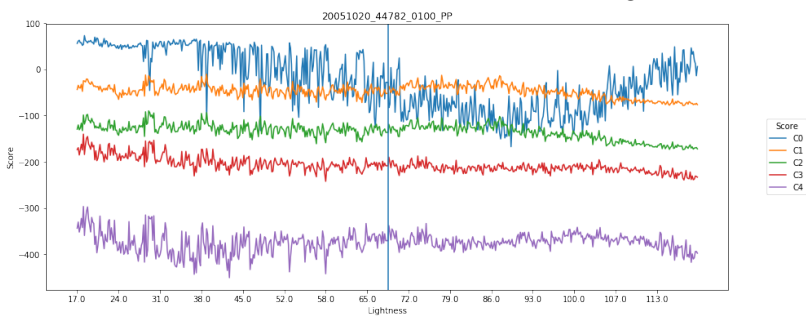
(A) Messidor 20060412 61593 0200 PP Tag: 1



(B) Messidor 20060411 62228 0200 PP Tag: 1



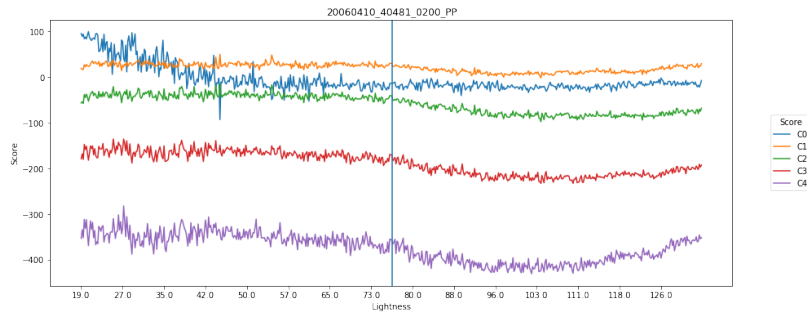
(C) Messidor 20060412 59658 0200 PP Tag: 1



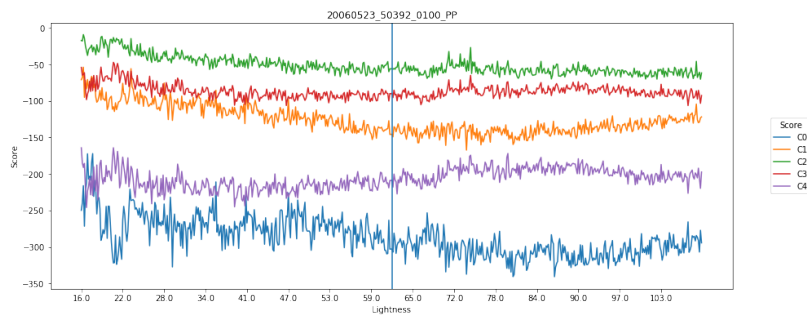
(D) Messidor 20051020 44782 0100 PP Tag: 1

FIGURE 6.11: Class Score vs Input Lightness (Tag: 1)

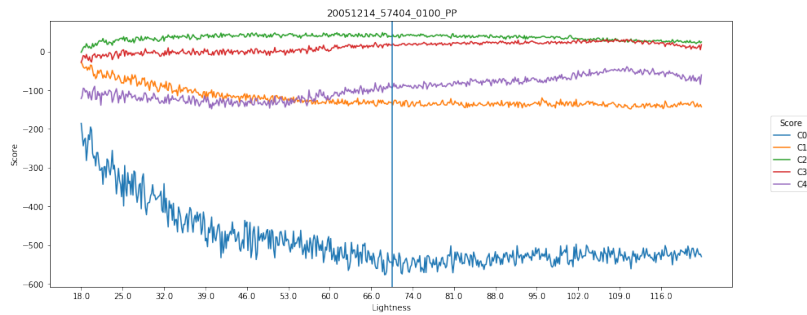
6.4. Conclusions



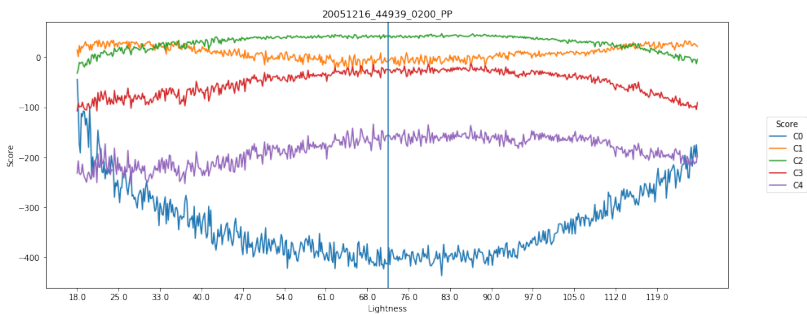
(A) Messidor 20060410 40481 0200 PP Tag: 2



(B) Messidor 20060523 50392 0100 PP Tag: 2

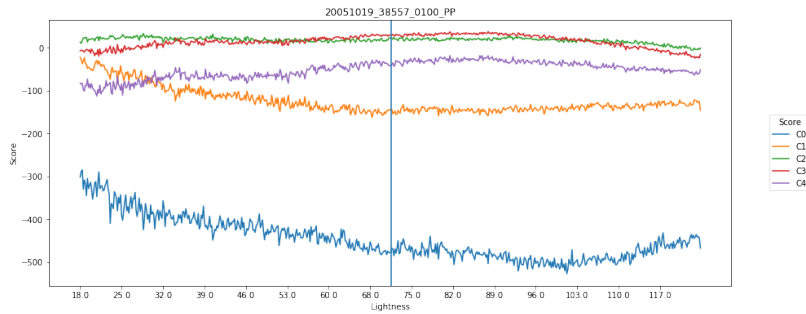


(C) Messidor 20051214 57404 0100 PP Tag: 2

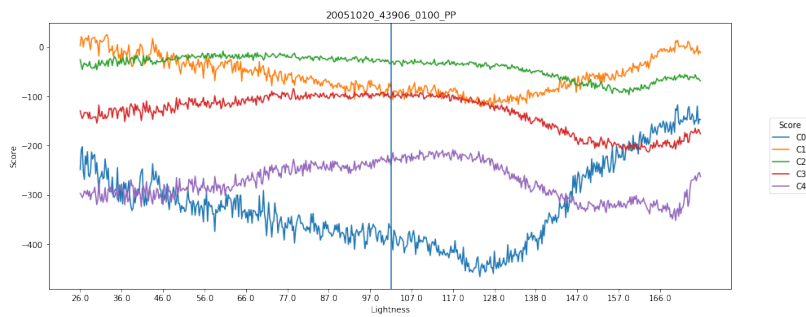


(D) Messidor 20051216 44939 0200 PP Tag: 2

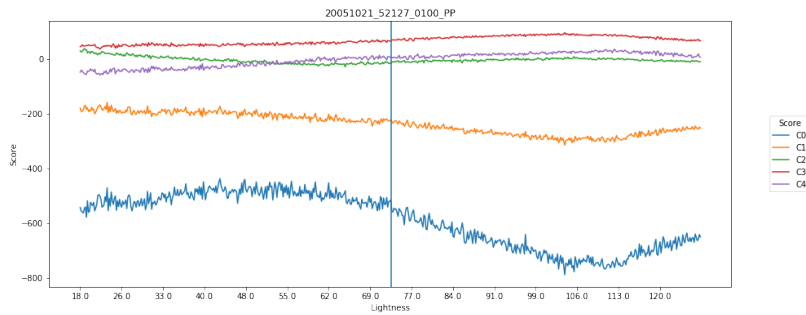
FIGURE 6.12: Class Score vs Input Lightness (Tag: 2)



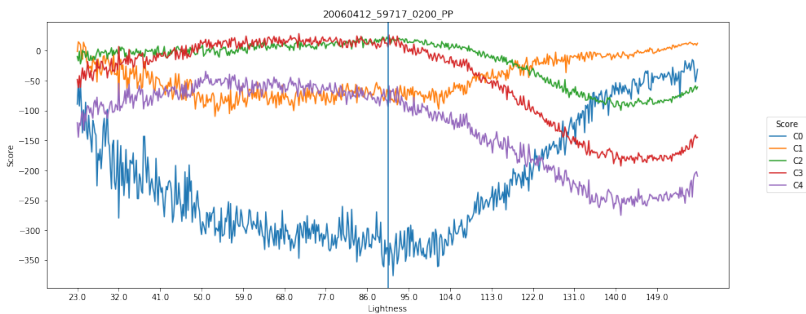
(A) Messidor 20051019 38557 0100 PP Tag: 3



(B) Messidor 20051020 43906 0100 PP Tag: 3



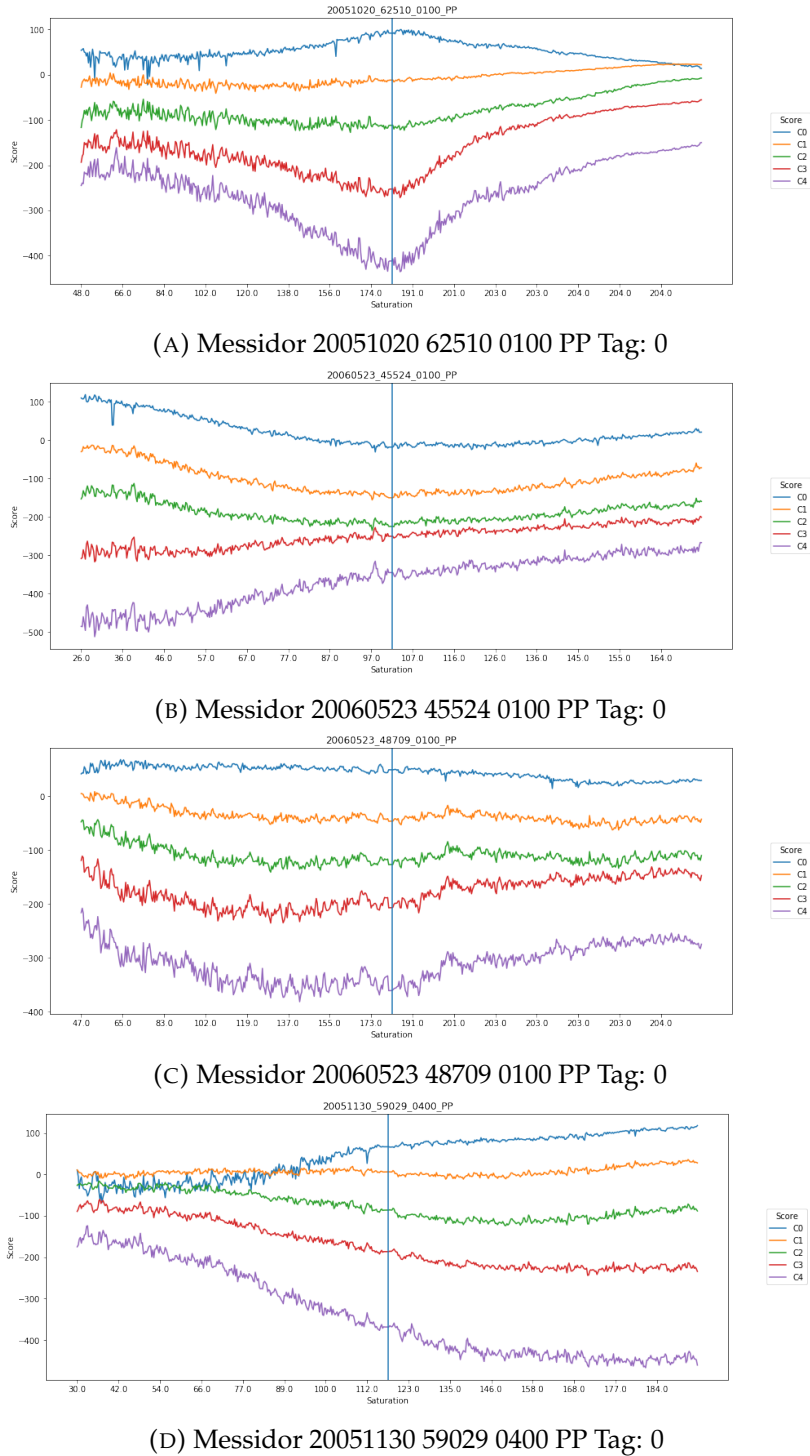
(C) Messidor 20051021 52127 0100 PP Tag: 3

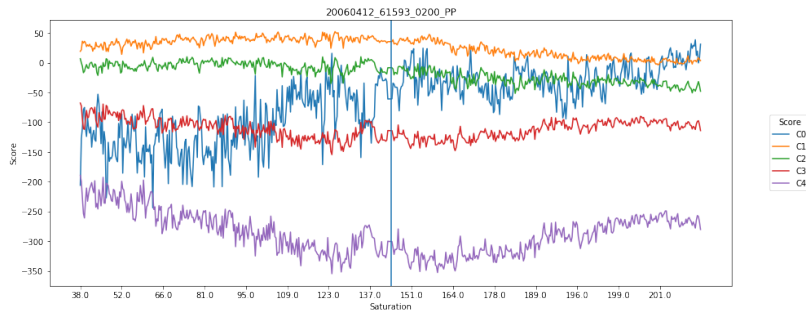


(D) Messidor 20060412 59717 0200 PP Tag: 3

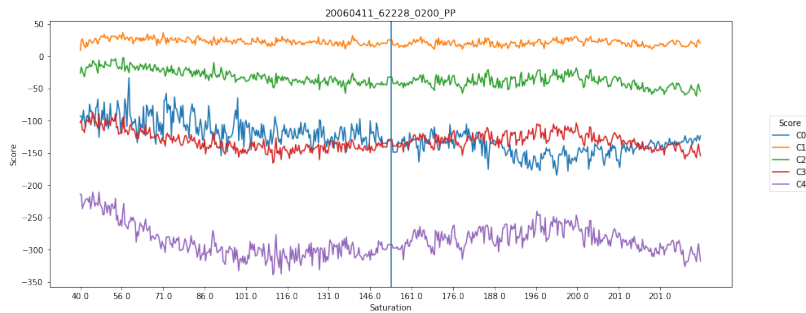
FIGURE 6.13: Class Score vs Input Lightness (Tag: 3)

6.4. Conclusions

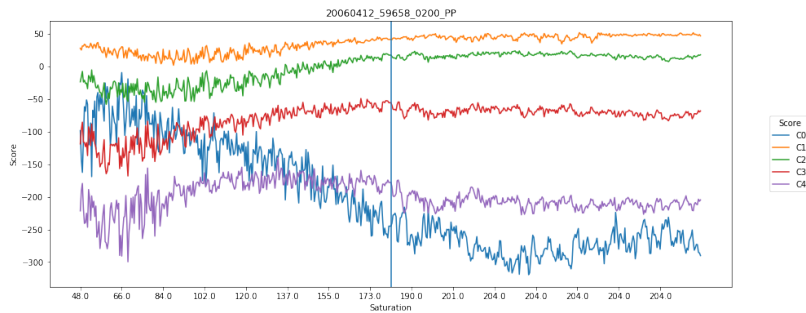




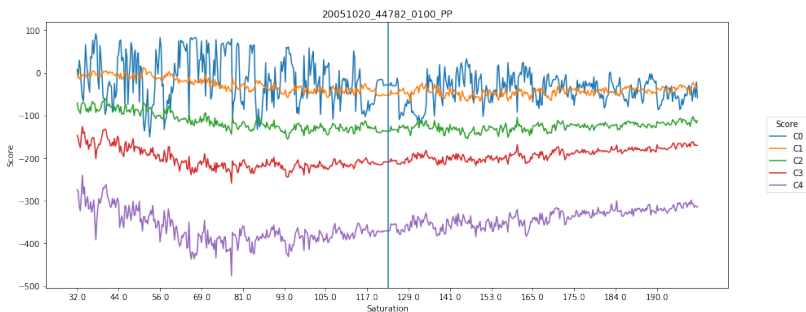
(A) Messidor 20060412 61593 0200 PP Tag: 1



(B) Messidor 20060411 62228 0200 PP Tag: 1

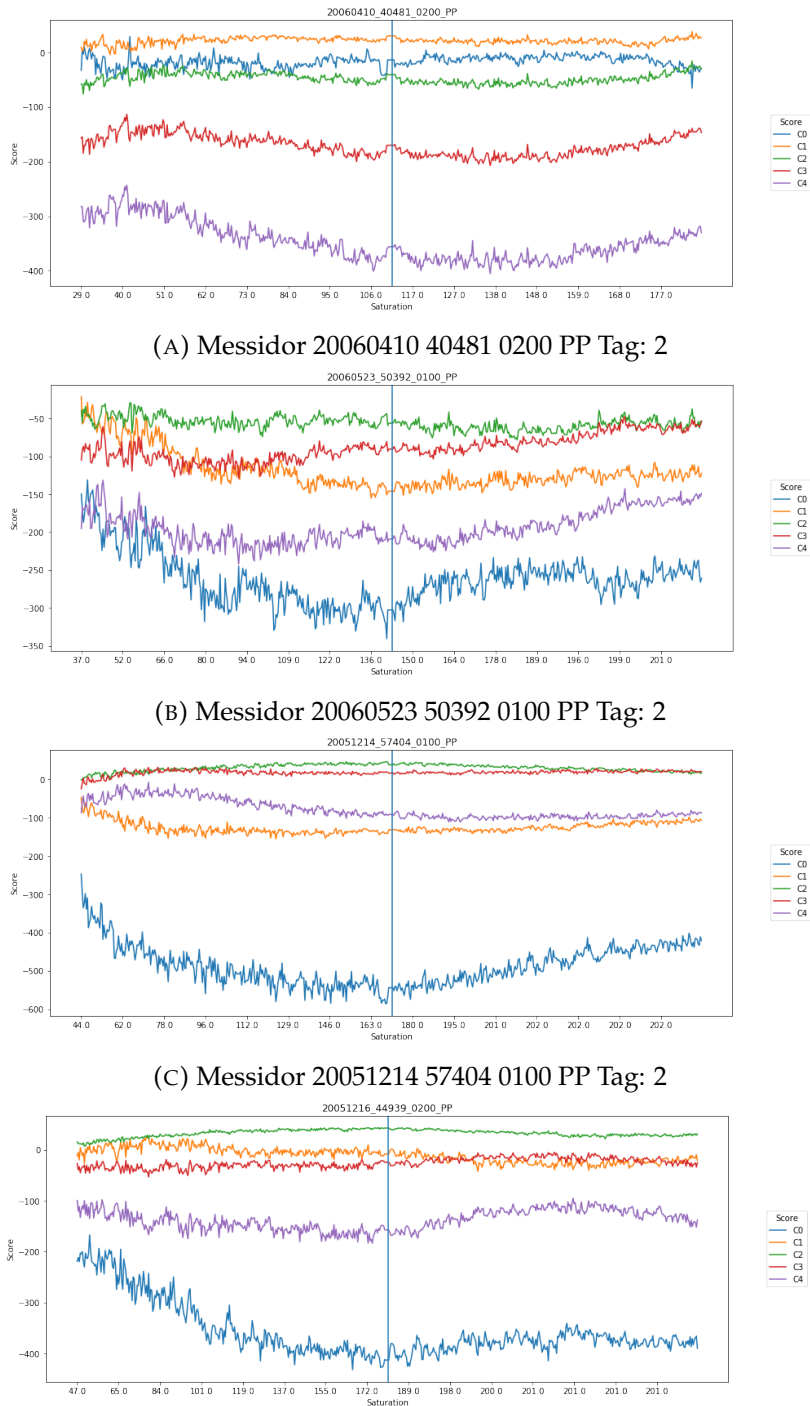


(C) Messidor 20060412 59658 0200 PP Tag: 1

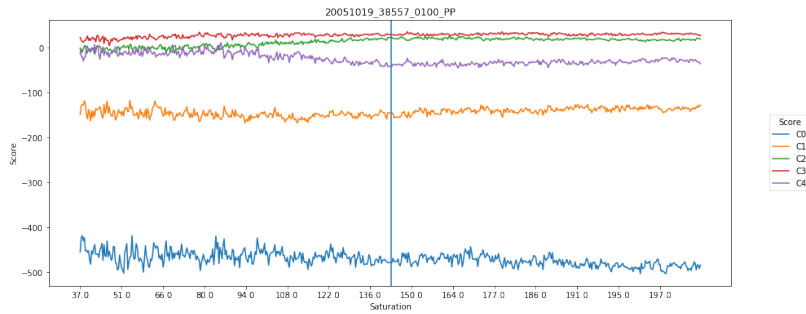


(D) Messidor 20051020 44782 0100 PP Tag: 1

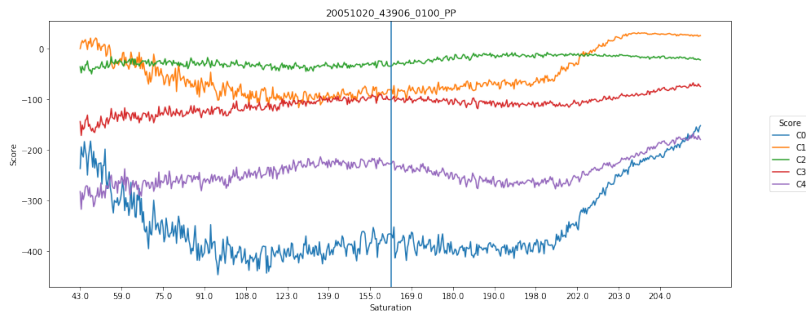
FIGURE 6.15: Class Score vs Input Saturation (Tag: 1)



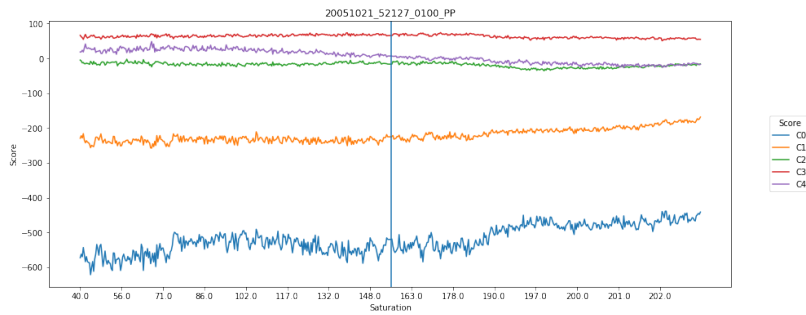
(A) Messidor 20060410 40481 0200 PP Tag: 2
(B) Messidor 20060523 50392 0100 PP Tag: 2
(C) Messidor 20051214 57404 0100 PP Tag: 2
(D) Messidor 20051216 44939 0200 PP Tag: 2
FIGURE 6.16: Class Score vs Input Saturation (Tag: 2)



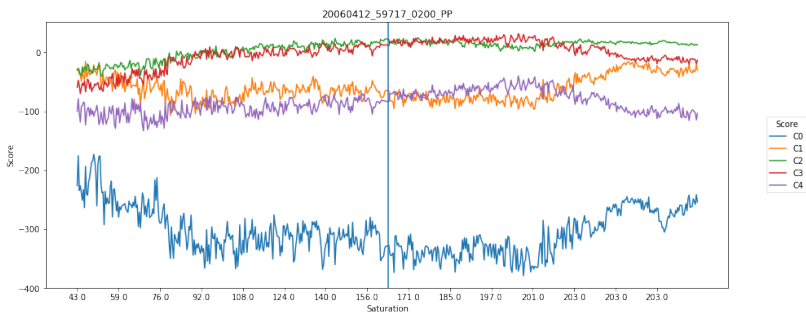
(A) Messidor 20051019 38557 0100 PP Tag: 3



(B) Messidor 20051020 43906 0100 PP Tag: 3



(C) Messidor 20051021 52127 0100 PP Tag: 3



(D) Messidor 20060412 59717 0200 PP Tag: 3

FIGURE 6.17: Class Score vs Input Saturation (Tag: 3)

6.4. Conclusions

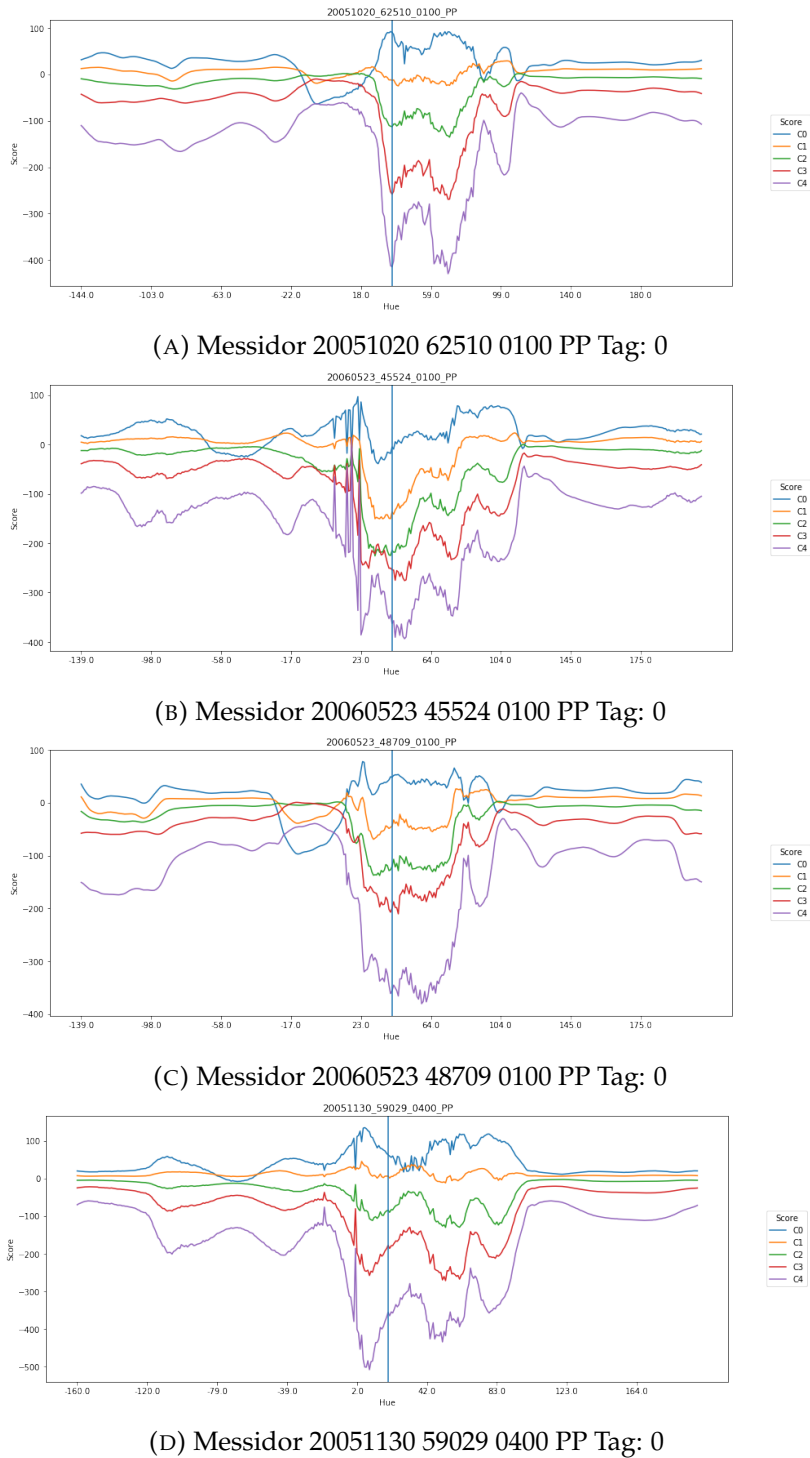
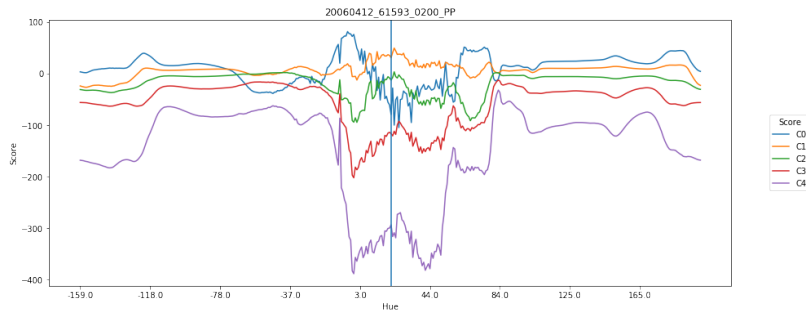
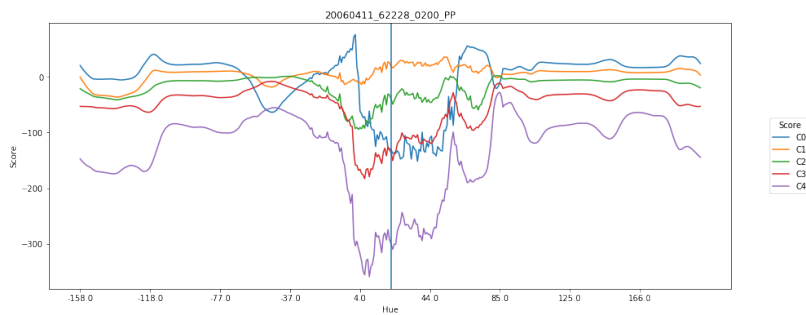


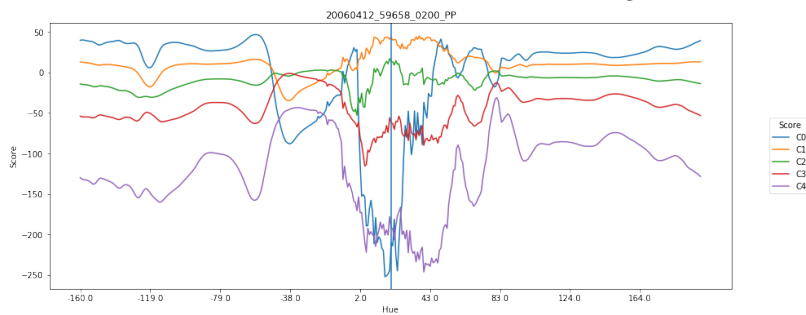
FIGURE 6.18: Class Score vs Input Hue (Tag: 0)



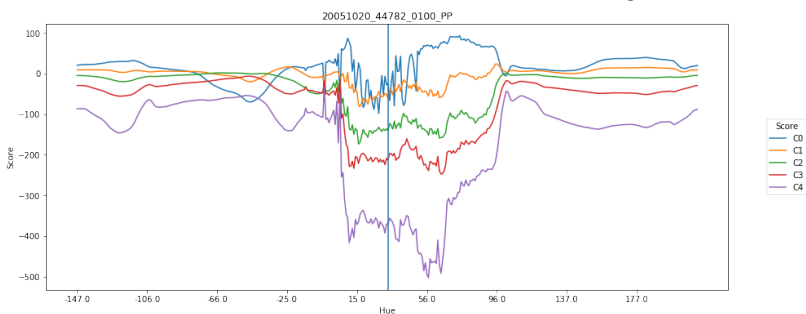
(A) Messidor 20060412 61593 0200 PP Tag: 1



(B) Messidor 20060411 62228 0200 PP Tag: 1



(C) Messidor 20060412 59658 0200 PP Tag: 1



(D) Messidor 20051020 44782 0100 PP Tag: 1

FIGURE 6.19: Class Score vs Input Hue (Tag: 1)

6.4. Conclusions

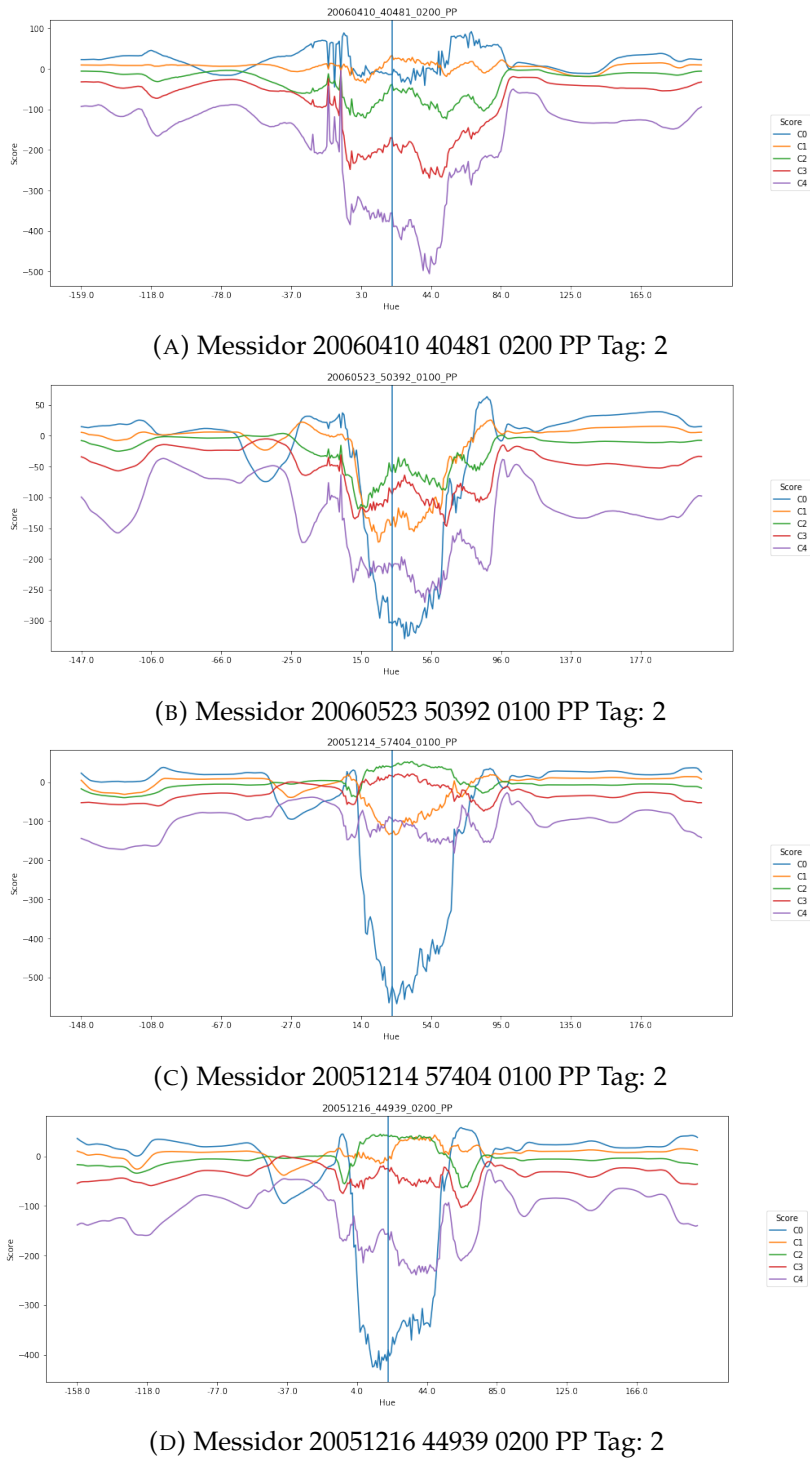
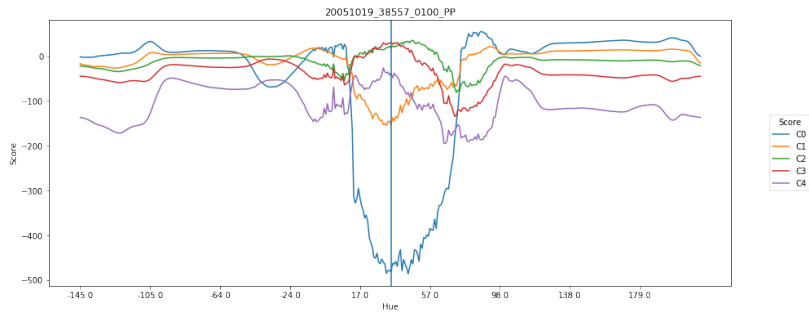
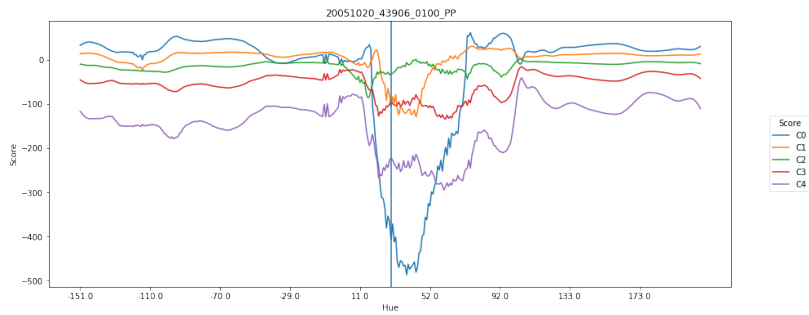


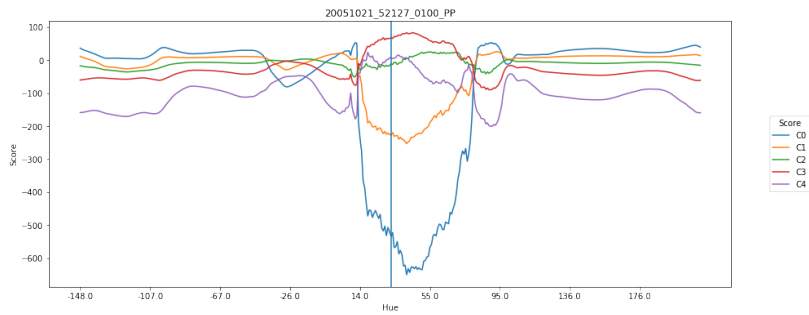
FIGURE 6.20: Class Score vs Input Hue (Tag: 2)



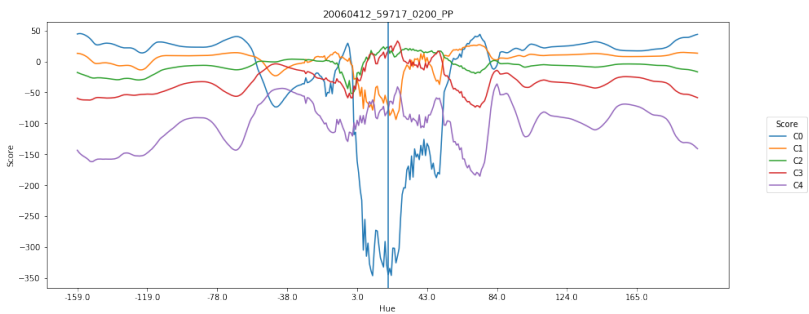
(A) Messidor 20051019 38557 0100 PP Tag: 3



(B) Messidor 20051020 43906 0100 PP Tag: 3



(C) Messidor 20051021 52127 0100 PP Tag: 3



(D) Messidor 20060412 59717 0200 PP Tag: 3

FIGURE 6.21: Class Score vs Input Hue (Tag: 3)

Part II

Interpretation

UNIVERSITAT ROVIRA I VIRGILI

DIABETIC RETINOPATHY CLASSIFICATION AND INTERPRETATION USING DEEP LEARNING TECHNIQUES

Jordi De la Torre Gallart

Chapter 7

Explanation Maps Generation

In this chapter we present work done regarding the interpretation goal of the thesis. In medical diagnosis tasks it is important not only the accuracy of predictions but also the reasons behind decisions. Self-explainable models enable the physicians to contrast the information reported by the model with their own knowledge, increasing the probability of a good diagnostic, which may have a significant influence in patient's treatment. The aim of this work is the elaboration of a general purpose interpretation algorithm, able to generate pixel maps that help in the interpretation of classification results reported by the model. With this model, it is possible to generate automatically very precise lesion maps that are learned indirectly only from general classification information. The model encodes statistical regularities present in data and the model presented in this chapter is able to visualize them. The system is organized using individual building blocks that make it easily transferable to be used with other architectures and in other completely different domains.

7.1 Introduction

Different attempts have been done for interpreting the results reported by neural networks. In (Zeiler and Fergus, 2014) a network propagation technique is used for input-space feature visualization. After this work, (Bach et al., 2015) used a pixel-wise decomposition for classification problems. This decomposition could be done in two ways: considering the network as a global function, disregarding its topology (functional approach) or using the natural properties of the inherent function topology for applying a

message passing technique, propagating back into the pixel space the last layer output values. After this work, in (Montavon et al., 2017) they used a so-named Deep Taylor decomposition technique to replace the inherently intractable standard Taylor decomposition, using a multitude of simpler analytically tractable Taylor decompositions.

In this chapter we follow an approach similar to pixel-wise decomposition taking into account the compositional nature of the topology, as in (Zeiler and Fergus, 2014) and (Bach et al., 2015). The concept of *score* in our chapter is similar to the concept of *relevance* used in the layer-wise relevance propagation method. The novelty of our approach comes from the fact that we assume that there are two factors that contribute to output score: one is the input-space contribution, while the other is a contribution coming from the receptive fields of each layer. This last contribution depends solely on the parameters of each layer, thus being independent from the input-space. The second factor is not an attribute of the individual pixels that has to be propagated back, but a contribution of the receptive field (RF) that represents the layer as an individual entity. Therefore, we only propagate back the score part that depends on the precedent input in each layer. In the proposed explanation model, we consider the constant part as a property of the RF of each layer. This approach allows us to do an exact propagation of the scores using a de-convolutional approach. Differing also from (Zeiler and Fergus, 2014), our method allows the integration of batch normalization and of other typical neural network block constituents into the score propagation. A full set of score propagation blocks with the more typical DL functional constituents is derived in the chapter, in order to facilitate the portability of this new explanatory method to other networks and applications.

This interpretation model is tested in our application research area: Diabetic Retinopathy for grading the level of disease. This model is able to report the predicted class and also to score the importance of each pixel of the input image in the final classification decision. In such a way, it is possible to determine which pixels in the input image are more important in the final decision and facilitate the human experts an explanation to verify the results reported by the model.

7.2 Related work

In last years, different approximations have been proposed to convert the initial DL black box classifiers into *interpretable classifiers*. In the next sections we introduce the most successful interpretation models existing today: sensitivity maps, layer-wise relevance propagation and Taylor decomposition models.

7.2.1 Sensitivity maps

Sensitivity maps (Simonyan, Vedaldi, and Zisserman, 2013) are pixel-space matrices obtained from the calculation of $\frac{\partial f(I)}{\partial I_{c,i,j}} \quad \forall c, i, j$, where I is the input image and $f(I)$ is the DL function. These matrices are easy to calculate for deep neural networks because they use the same backpropagation rules that are used during training, requiring only one more backpropagation step for reaching the input-space. The problem with this approach is that there is no direct relationship between $f(I)$ and $\nabla f(I)$. The main concern of these models is that being the objective to explain $f(x)$, $\frac{\partial f(I)}{\partial I_{c,i,j}}$ is only giving information about the local change of the function. For high non-linear functions, like deep neural networks, the local variation is pointing to the nearest local optimum, which should not necessarily be in the same direction that the global minimum (Baehrens et al., 2010).

7.2.2 Layer-wise relevance propagation

In (Bach et al., 2015) the authors split the total score of a classification into individual *relevance scores* R_d that act as a positive or negative contributions to the final result.

The method has the next general assumptions: the first one is the nature of the classification function, which has to be decomposable into several layers of computation (like a deep neural network), the second is about the fact that the total relevance must be preserved from one layer to another, which means that the relevance of one layer is equal to the ones of all other layers (eq. 7.1) and, finally, the relevance of each node must be equal to the sum of all the incoming relevance messages of such node and also equal

to the sum of all the outgoing relevance messages from the same node (eq. 7.2).

$$f(x) = \sum_{d \in l+1} R_d^{(l+1)} = \sum_{d \in l} R_d^{(l)} = \dots = \sum_d R_d^{(1)} \quad (7.1)$$

where $R_d^{(l)}$ is the relevance of node d in layer l .

$$R_{i \leftarrow k}^{(l,l+1)} = R_k^{(l+1)} \frac{a_i \omega_{ik}}{\sum_h a_h \omega_{hk}} \quad (7.2)$$

where $R_{i \leftarrow k}^{(l,l+1)}$ is the relevance message passing from node k located in layer $l + 1$ to node i , located in layer l ; a_i is the activation of node i and ω_{ij} is the weight connecting node i and j .

7.2.3 Taylor-type decomposition

Another way for solving the interpretability problem is using the classification function gradient to calculate the next Taylor approximation (Bach et al., 2015):

$$f(I) \approx f(I_0) + \nabla(I_0)[I - I_0] = f(I_0) + \sum_{c=1}^C \sum_{i=1}^H \sum_{j=1}^W \frac{\partial f}{\partial I_{c,i,j}} (I_{c,i,j} - I_{0c,i,j}) \quad (7.3)$$

Being I_0 a free parameter that should be chosen in a way that $f(I_0) = 0$ in the case that $f(I)$ is defined as a function that reports a value greater than one when belongs to the class, and lower than 0 otherwise. Defined in such a way, $f(I) = 0$ express the case of maximum uncertainty about the image. Finding I_0 allows us to express $f(I)$ as:

$$f(I) \approx \nabla(I_0)[I - I_0] = \sum_{c=1}^C \sum_{i=1}^H \sum_{j=1}^W \frac{\partial f}{\partial I_{c,i,j}} (I_{c,i,j} - I_{0c,i,j}) \quad \text{being } f(I_0) = 0 \quad (7.4)$$

Equation 7.4 is per se an explanation of $f(I)$ dependent only of the

7.3. Receptive field score distribution model

125

derivative function and of I_0 . The main concern of this approach is finding a valid root that is close to the analyzed image I using the Euclidean norm. In that way, we are approximating the function with a order 1 Taylor expansion and the residuum is proportional to the Euclidean distance between both points. Different ways for finding I_0 have been proposed. For example, doing a unsupervised search of $f(I)$ over the training set, looking for those images reporting $f(I)$ near 0 and averaging them for finding I_0 .

7.2.4 Deep Taylor decomposition

Deep Taylor decomposition (Montavon et al., 2017) uses an approximation that combines the layer-wise and Taylor type models. Taking advantage of the compositional nature of DL models, this approach assumes also the decomposability of the relevance function, considering the existence for every node of a partial relevance function $R_i(a_i)$ that depends on the activation. It considers this function unknown and applies a Taylor decomposition through a root point. Summing up all the individual contributions, using the relevance conservation property defined in the previous models, makes possible the propagation of intermediate relevance scores until eventually reach the input-space. Then, it generates a heat-map of the total relevance of the prediction in the input image.

7.3 Receptive field score distribution model

In this section we explain the new method proposed in this thesis for distributing the output score into the previous layers in DL models (Torre, Valls, and Puig, 2017). We hypothesize that the output score of a particular classification model is not only due to pixel score contributions but also due to all the contributions of the receptive fields analyzed by the network. In next sections we will prove that, for all typical neural network types of layers, the output score can be expressed as the sum of layer's constants plus a value proportional to the layer's input. Pixel-wise explanation model uses a similar approach for propagating backwards the scores, but with an important difference: pixel-wise (Bach et al., 2015) propagates back not only the input layer contribution, but also constants, such as the bias, etc. Such a way of propagating backwards the scores breaks

the linear transformation. A way of maintaining the linear transformation is propagating backwards only the part that depends on the input, leaving the other part as a contribution of the layer (ie. of the receptive field). As the biases are not propagated, the normalization term used in pixel-wise method is not required anymore. Although neural network design is non-linear, score back-propagation is linear over the activated nodes. Non-linear phase takes place in the forward pass, but the backward part only takes place over the activated nodes. In our formulation, we consider the score entering into a node as the combination of two parts: one that can be transformed into a linear function dependent on the activated inputs and another one that is constant for the considered node. Then, the final score is expressed as the sum of contributions of all nodes belonging to the studied feature space (or pixel space) plus a constant score for the contribution of each node to every following layer. Such node constant scores depend on layer parameters and, in some way, on the output activations of the previous layer. Thus, the propagated score depends solely on the individual activation inputs of the layer. In such a way, we are able not only to find a unique way for mapping the score of every output in the input-space, but also and, most importantly, to find a linear relationship between output scores and image scores. This last property is due to the fact of using exclusively linear transformations in all layers.

Formally, in this work, the following propositions are assumed:

Proposition 1. The score of every activation in the network is proportional to the activation value:

$$S_l = \lambda_l a_l \quad (7.5)$$

being S_l the tensor representative of all the scores of layer l , a_l the activations tensor and λ_l another tensor establishing the required relationship between S_l and a_l for $l \in \{1, \dots, L\}$, being L the total number of layers.

Proposition 2. The score observed as output in one layer can be decomposed into two parts: one dependent on the score of the previous layer S_{l-1} and another one S_{k_l} that is constant because it does not depend on the input activations but only on the model parameters that are used in that layer:

$$S_{l+1} = S_l + S_{k_l} \quad (7.6)$$

7.3. Receptive field score distribution model

127

The propagation model proposed (see fig. 7.1) makes a different treatment of the components S_l and S_{k_l} .

First, S_l is a linear transformation of the layer activation and S_{k_l} is a tensor of the same dimensions independent from the activation that acts shifting the score coming from the previous layer S_{l-1} . In the following subsections we explain how to obtain S_l and S_{k_l} for all the different usual block elements of DL networks.

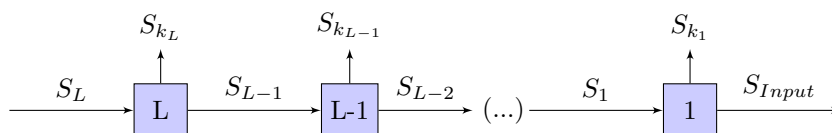


FIGURE 7.1: Score distribution through layers

The output score is expressed as:

$$S_L = \sum_{l=1}^L (\sum S_{k_l}) + (\sum S_{Input}) \quad (7.7)$$

being S_L last layer feature score, S_{k_l} the constant tensors of each layer, $\sum S_{k_l}$ the element-wise sum of scores and $\sum S_{k_l}$ the pixel-wise sum of scores.

Second, if required, S_{k_l} values obtained from each of the layers can also be mapped into the input space using an additional final procedure described in section 7.3.7.

Receptive field pixel maps allow the identification of the parts of the image that the network is considering important. In our case study, DR classification, it is not only important to detect the pixel-size micro lesions but also the clusters of lesions localized in different parts of the image. Taking into account each receptive field contributions apart from the input, facilitates the detection of such clusters and not only the individual contributions of each pixel.

Now, we explain the propagation process for different components of the DL classifier.

7.3.1 Score propagation through an activation function node

In fig. 7.2 we show the activation function node. A input activation a_i is transformed into the output activation as $a_o = \phi(a_i)$. Taking $S_o = \lambda_o a_o$ and substituting a_o , we get $S_o = \lambda_o \phi(a_i)$. According to proposition 1, we have also that $S_i = \lambda_i a_i$. For ReLU family functions ($\phi(x) = \max(0, kx)$), S_i continues verifying the proposition. For other type of activation functions, as we are calculating the score of a particular image, we can consider the network to have parameter-wise activation functions. For a particular image, we can consider the first order Taylor expansion and see the activation function as a linear function of the form $\phi(a_i) = [\phi(a_i^*) + \phi'(a_i^*)(a_i - a_i^*)]$, where a_i^* is a value close enough to a_i to have a good approximation of ϕ . After this transformation, the proposition holds for every type of activation function. Substituting and reordering the expression of S_o we obtain that:

$$S_o = \lambda_o [\phi(a_i^*) - \phi'(a_i^*) a_i^*] + \lambda_o \phi'(a_i^*) a_i \quad (7.8)$$

Now, the output score can be split in two parts: a constant one that is independent of the activation and belongs to the node and another one dependent on the activation. For ReLU, they are $S_o = S_i$ and $S_k = 0$.

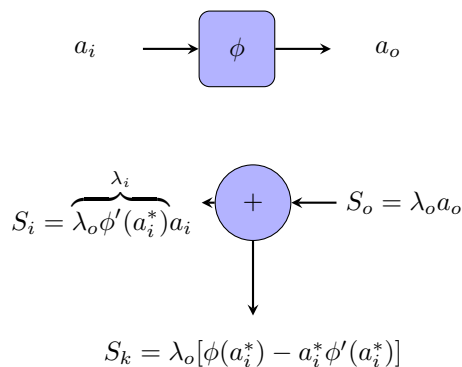


FIGURE 7.2: Score propagation through an activation function node

7.3. Receptive field score distribution model

129

7.3.2 Score propagation through a batch normalization node

The function implemented in a batch normalization node is $a_o = \beta + \gamma\left(\frac{a_i - \mu}{\sigma}\right)$. Having $S_o = \lambda_o a_o$, S_o is also $S_o = \lambda_o\left(\beta + \gamma\left(\frac{a_i - \mu}{\sigma}\right)\right)$. Reordering the expression, we can separate the input independent constants:

$$S_o = \lambda_o\left(\beta - \gamma\frac{\mu}{\sigma}\right) + \lambda_o\frac{\gamma}{\sigma}a_i \quad (7.9)$$

As we see, the output score can be exactly split into a constant value $S_k = \lambda_o\left(\beta - \gamma\frac{\mu}{\sigma}\right)$ that is a inherent property of the node and is completely independent of a_i and into $S_i = \left(\lambda_o\frac{\gamma}{\sigma}\right)a_i = \lambda_i S_i$ following Proposition 2, being $\lambda_i = \lambda_o\frac{\gamma}{\sigma}$ (see fig. 7.3)

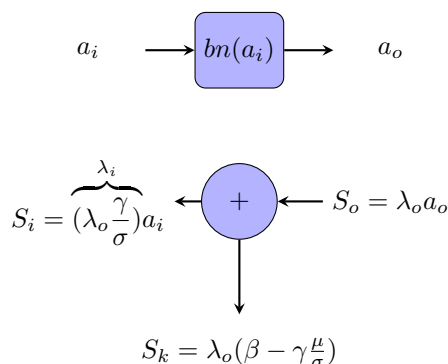


FIGURE 7.3: Score propagation through an batch normalization node

7.3.3 Score propagation through a convolutional layer

In the forward propagation of a two dimensional convolution of an image, the set of all the different feature activations of a predefined locality are linearly combined to get the output a_o (see fig. 7.4). Backpropagating a score in a convolutional layer requires to divide it into all its individual components. Every component can be either positive or negative. There is also a bias part that comes from the inherent nature of the layer and that is not attributable to any of the inputs and that must be treated also as a property of the layer. Due to the nature of the convolution operator, every

input node contributes to the calculation of different outputs. This is the reason why every input receives a contribution of the score of the different outputs that are, then, summed up.

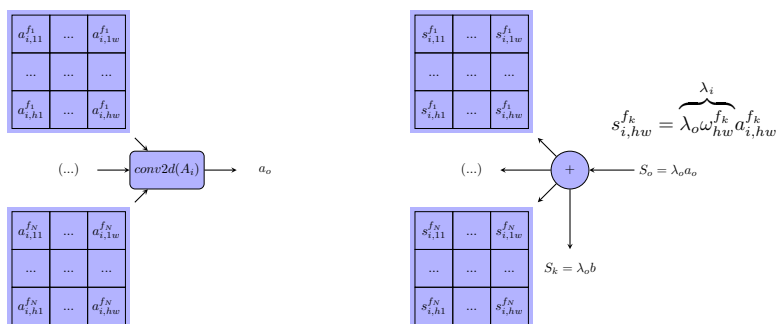


FIGURE 7.4: Convolution score calculation. Score spreads into the different inputs. The bias related part of the score is not backpropagated.

7.3.4 Score propagation through pooling layers

The score propagation through a max-pooling layer is straightforward. The score of output is copied into the input that was selected in the forward pass (see fig. 7.5). For average pooling, it is also straightforward. The score value is split into N equal parts, being N the number of inputs (see fig. 7.5).

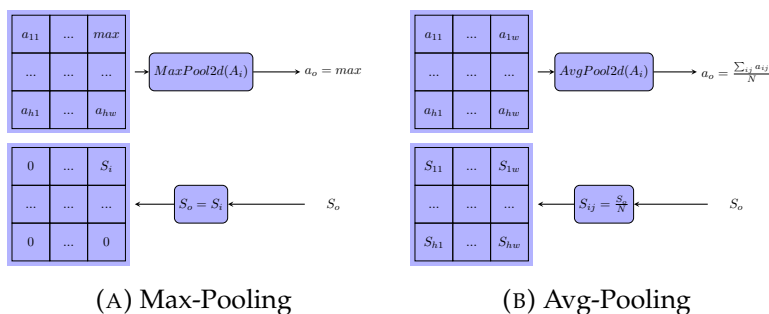


FIGURE 7.5: Score propagation through different pooling layers

7.3.5 Score propagation through a fully connected layer

A fully connected layer is a linear combination of the input activations and their weights. The final score is split into the individual elements, leaving apart the bias that becomes the constant score contribution of the own layer (see fig. 7.6).

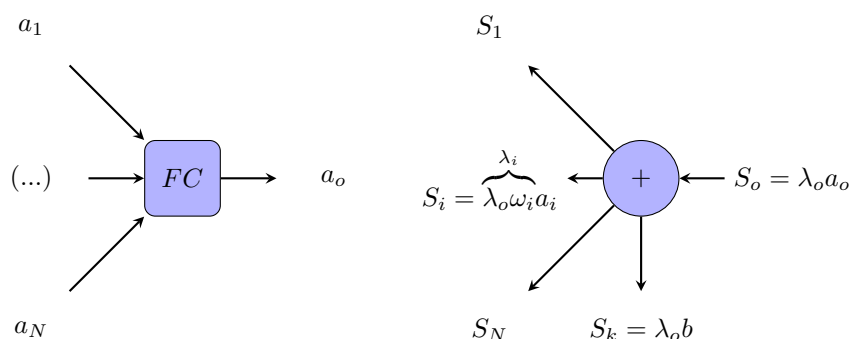


FIGURE 7.6: Score propagation through a fully connected node

7.3.6 Score propagation through a dropout layer

Dropout in evaluation time weights the output to a value proportional to the dropout probability: $a_o = (1 - d)a_i$. Inserting this equation into $S_o = \lambda_o a_o$ and applying the score conservation through the node ($S_o = S_i$ in this case, due to the absence of constant score), we get that the final equation:

$$\lambda_i = \lambda_o(1 - d) \tag{7.10}$$

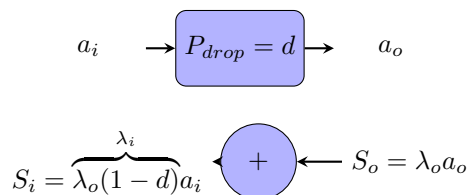


FIGURE 7.7: Score propagation through a dropout node

7.3.7 Mapping the score of hidden layers and S_k into input-space

We know that every node has two score constituents: one input-dependent, that can be easily forwarded, and another one RF-dependent, i.e layer-dependent. At this point, we are going to describe a method to transport backwards also such last values into the input-space. From (Luo et al., 2016), we know that the effective RF is not equal to the theoretical RF. The effective one acts more like a 2D-gaussian function, where the points located in the borders contribute less than the center ones. Using such prior information, it is possible to make an approximate conversion of the full and constant scores in the hidden-space to the input-space using a 2D-gaussian prior. For example, for a 20x20 hidden layer with a RF of 189x189 pixels, we know that each one of such points is a representation value of a 189x189 RF in the input-space. Having a prior information about the statistical distribution of the input-space pixels (in this case gaussian), it is possible to go back. Summing up 20x20 gaussian distributions of mean equal to the hidden-space values and summing up the coincident points, it is possible to map the distribution into input-space. We fixed $RF = 2\sigma$ as an approximate distribution of the scores that seems acceptable (Luo et al., 2016), since 98% of the information of the gaussian is inside the RF. We normalize the function to fit 100% of the information inside the RF.

7.4 Results

The classifier used for application of the interpretation model is the one described in chapter 3. In figure 5.3 can be found the model architecture.

7.4.1 Pixel and receptive field map generation

In this subsection we describe the steps followed in the score calculation of a test set sample. Fig. 7.8 is tagged in the test set as class 4. For this image the model reports the next classification scores (previous to softmax): $C_0 = -451.2$, $C_1 = -229.0$, $C_2 = -53.4$, $C_3 = +37.4$ and $C_4 = +73.2$. Being C_4 the highest value, the image is correctly classified as class 4. In fig. 7.8b we show a black and white version of the image with the distribution of the positive contributions to the class 4 total score in input space. Having the total score map is possible to visualize different versions of it, showing the negative contributions, or the most positive ones, or defining a positive threshold for displaying only the higher scores. In this way is possible to identify the points that contribute the most to a particular classification. There should be a correlation between such points and lesions in the eye if we are studying, as in this sample, a severe disease class.

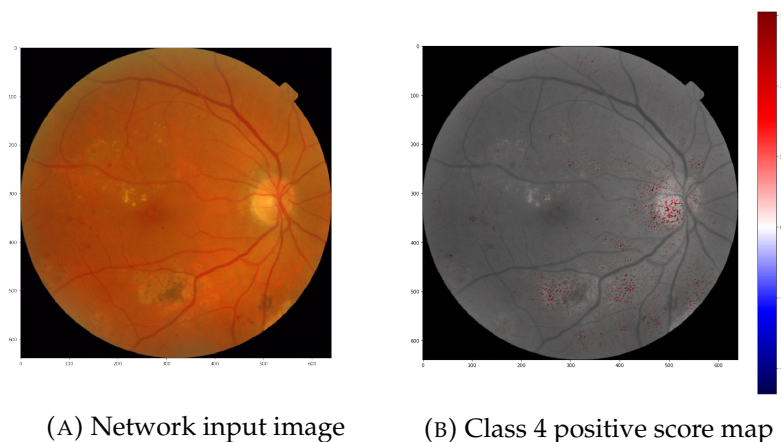


FIGURE 7.8: Class 4 sample image

Figure 7.9 show the aggregated scores for different intermediate layers. For visualization purposes, layer scores are presented considering the layer as a unique block combination of *convolution - batch normalization - ReLU*. The output of this function block can be mathematically expressed as $O = \max(0, \beta + \gamma(\frac{WI+b-\mu}{\sigma}))$, being $S_O = \lambda(\beta + \gamma\frac{b-\mu}{\sigma}) + \lambda\frac{\gamma}{\sigma}WI$. In this way $S_I = \lambda\frac{\gamma}{\sigma}WI$ and $S_k = \lambda(\beta + \gamma\frac{b-\mu}{\sigma})$.

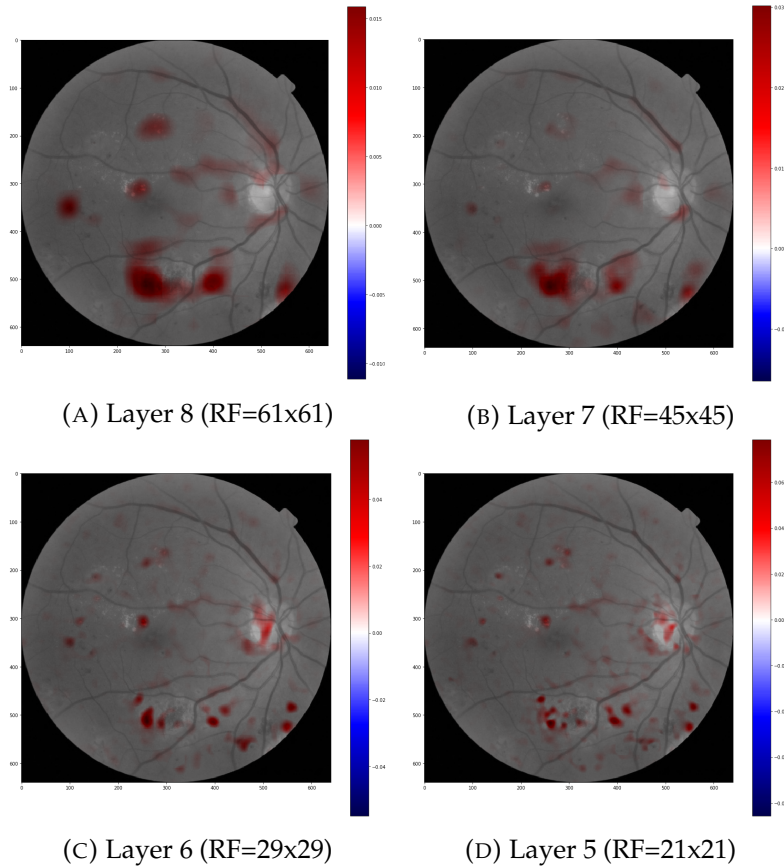


FIGURE 7.9: Some of the class 4 intermediate score maps generated for the sample image

Individual feature scores are first calculated, *receptive field-wise* summed up and mapped into input-space (section 7.3.7). The same is done for $S_k^{(l)} \quad \forall l \in L$. Score inputs can be combined with constant scores to define a unique input score map. The sum of these scores is equal to the last layer inference score and determines the relative importance of every pixel in the final decision. A density plot and a standard deviation can also be calculated. In order to determine the importance of pixels, as noted before, it is possible to restrict the visualization to positive scores or also be even more restrictive and visualize only pixels with a score greater than

a predefined threshold, for example $n\sigma$. These score maps are useful for interpreting the reasons behind a classification, for detecting the cause of non-expected classifications, for example pixels with excessive importance in the final decision, conclusions based only on partial or incorrect information, etc.

In red in figure 7.9 we have the zones that are contributing positively to classify the image as class 4. It is possible to plot also the zones contributing negatively to the classification. In case of being analyzing a class 4, negative score zones(not shown) would be zones without lesions. For clarity purposes only positive values are shown. Regions of red and blue pixels are sequentially fine-grained as the size of the receptive field decreases. Having the possibility to choose the RF size, permits to analyze the areas contributing to image classification at different levels of precision.

Intermediate scores are also very useful for identifying clusters of microlesions and evaluate its combined weight in the final score. They enable the location of lesion clusters and also zones not affected by the disease. For example, in layer 12, with a receptive field of 253x253 the network identifies two zones with high contribution to class 4 score. In layer 11, where the receptive field is smaller (189x189) we see how the detail is increasing, showing more localized zones. In layer 8, 7, 6, 5 and finally input show increasing level of detail dividing big clusters into smaller ones until reaching the input space where individual pixels are identified.

| Map | μ | σ | Max | Min | Sum | Non-null |
|------------|-------|----------|-------|------|-------|----------|
| S_I | 0.0 | 0.17 | +19.6 | -9.1 | +6.7 | 99.97% |
| $\sum S_k$ | 0.0 | 0.06 | +2.7 | -3.7 | +66.5 | 99.90% |
| S_T | 0.0 | 0.19 | +20.2 | -9.6 | +73.2 | 99.97% |

TABLE 7.1: Class 4 score map statistics for the analyzed image

Finally, in figure 7.10 we present the total score map for the analyzed image, plotting not only pixels with positive contribution (red) but also the negative ones (blue). The score input S_I (fig. 7.10a) represents the map obtained from back-propagating the part that linearly depends on inputs. The score constant $\sum S_k$ (fig. 7.10b) is the map obtained from summing up S_k for all layers mapped into input space. Score total S_T (fig. 7.10c)

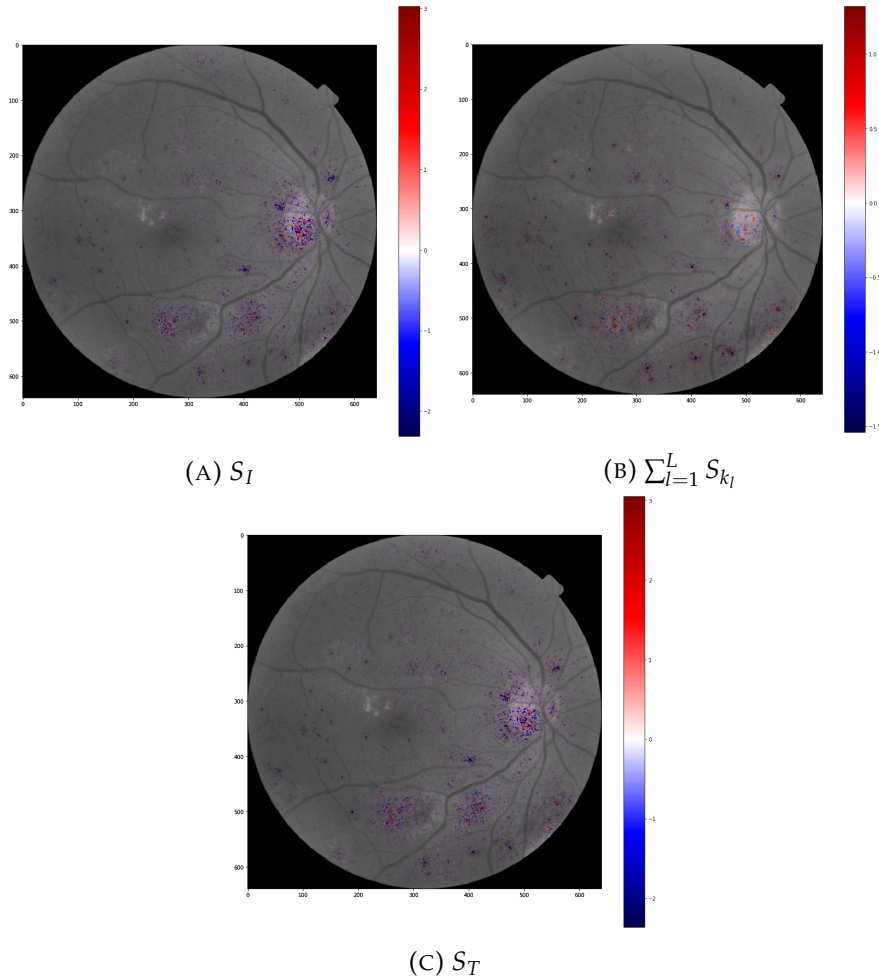


FIGURE 7.10: Total score maps: $S_T = S_I + \sum_{l=1}^L S_{k_l}$

is the sum of the two previous maps and represent the total class 4 score distribution. The sum of all the scores of the pixels is equal to the output score. Table 7.1 shows some statistics of the three score maps. We can see that $\sum S_k$ is the score map contributing the most to final total score. This map is flatter than S_I , so qualitatively S_I and S_T are very similar. It seems that $\sum S_k$ acts more as a mild shifting of each receptive field considered by the network and S_I acts reinforcing the importance of representative

individual pixels.

7.5 Conclusions

In this chapter we proposed a method for generating, for every class, score importance pixel maps, providing ophthalmologists the possibility of both inference and interpretation. The reduced number of model parameters enables the use of these algorithms even in low resources devices, like mobile phones. The score generation is done back-propagating layer-wise only the score part that depends on the inputs and leaving the constant part as a contribution to the score of the considered layer. In this way, this method is able to generate scores in a unique and exact way.

Additionally, we have developed a technique, consisting on applying a 2D-gaussian prior over the RFs, for mapping the constant hidden-space scores to the input. With this technique we can generate a unique score map representative of the class, making possible to distribute the 100% score class information of the output layer.

We concluded also that for a good understanding of the causes behind a classification, not only the pixel-space maps should be considered, but also the intermediate ones. The combination of the micro-information given by the input space maps with the macro-information obtained from intermediate scores is the key for understanding the results and to help the medical personnel to improve the diagnosis processes.

UNIVERSITAT ROVIRA I VIRGILI

DIABETIC RETINOPATHY CLASSIFICATION AND INTERPRETATION USING DEEP LEARNING TECHNIQUES

Jordi De la Torre Gallart

Chapter 8

Feature Space Compression

The motivation of this work is the compression of information present in diabetic retinopathy state-of-the-art models. Neural networks feature spaces are frequently high-dimensional spaces with high correlation values between dimensions, ie. are low dimensional manifolds embedded in high dimensional spaces.

In this chapter a methodology for linear compression of the feature space is presented, allowing the feature space compression from the original 64 dimensions to only 3 with a reduction of performance lower than 2.5%.

8.1 Introduction

In this chapter we study a technique that allows the identification, separation and visualization in the input and hidden space of the independent component (IC) responsible of a particular DR classification decision taken by a DL classifier given a certain eye fundus image. This is done by calculating the minimum number of ICs that are able to encode the maximum information about the particular classification. Identifying such components, we reduce the redundancy of feature space and identify the components that share the minimum mutual information between each other. In that way, under the supposition that the feature extraction phase of the deep learning model has been able to disentangle completely the feature information, we are able to separate the independent elements causing the disease.

Independent Component Analysis (ICA) (Hyvärinen and Oja, 2000) is a statistical method for the separation of a multi-dimensional random signal into a linear combination of components that are statistically as independent from each other as possible. The theoretical foundation of ICA is based on the Central Limit Theorem, which establishes that the distribution of the sum (average or linear combination) of N independent random variables approaches a gaussian as $N \rightarrow \infty$. When ICA method is applied, it is assumed that such separation exist, ie. that is possible to express the signal as a linear combination of independent components. Perfect independence between random variables is achieved when mutual information between them is zero. Mutual information can be expressed as the Kullback-Leibler divergence between the joint distribution and the product of the distributions of each variable. Mutual information can be decomposed, under linear transforms, as the sum of two terms: one term expressing the decorrelation of the components and one expressing their non-Gaussianity (Cardoso, 2003). ICA uses optimization to calculate its components. Two types of optimization objectives can be used: minimize the mutual information or maximize the non-gaussianity of each component.

We use the pixel-wise visualization method to identify in pixel space such independent causes. We use the assessment of experts clinicians for interpreting such ICs.

DL models are organized in layers, being the inputs of each one a combination of the outputs of previous ones. We design the output layer to be a linear combination of last layer feature space components. In this way we are forcing the model to disentangle the important features that, combined in a linear way, allow the achievement of a maximum possible classification score. These components (or other obtained as a linear combination of them, like with ICA analysis), are easy to analyze due to the linear nature of its relationship with the classification scores.

8.2 ICA based interpretation procedure

In this chapter we go a step forward in the interpretation of score maps. Instead of generating directly the pixel maps associated with a particular class, we try to identify and separate independent elements associated with

the disease. Our new contribution comes from the identification, separation and visualization of the IC that explain a particular classification decision. We hypothesize that in order to achieve high performance classification scores, the network has to encode the information required to make the classification. Human experts base its decisions in the number and types of lesions present in the image. That's why in some way, such information has to be present in a disentangled form in last layer feature space, previous to the output layer. Instead of directly visualizing the more important pixels under a classification decision, we split the information of such last feature layer into independent features using a Independent Component Analysis (ICA). A posteriori we use a pixel-wise relevance propagation method to visualize such independent component in input space. In this way, we can, not only generate importance pixel maps, but also differentiate between the underlying independent causes of the disease.

First, we studied the last layer feature space, previous to the output layer linear combination in order to identify its properties and try to isolate the independent elements that are causing a particular classification. For this purpose we used a principal component analysis (PCA) (Pearson, 1901) to appraise the redundancy of this space and a ICA (Hyvärinen and Oja, 2000) using different number of components to identify the minimum of them required to achieve a classification score close enough to the achieved without such a dimensional reduction. ICA allows to find a linear representation of non-Gaussian data so that the components are statistically independent, or as independent as possible. Such a representation seems to capture the essential structure of the data in many applications, including feature extraction (Hyvärinen and Oja, 2000). When the data is not Gaussian, there are higher order statistics beyond variance that are not taken into account by PCA. While PCA captures only uncorrelated components, these uncorrelated components are not necessarily independent for general distributions. ICA minimizes the mutual information (or relative Kullback-Leibler divergence) of non-Gaussian data because two distributions with zero mutual information are statistically independent (Comon, 1994).

For finding the optimal number of IC, we apply ICA to the last layer feature space training set vectors. Using different number of IC and comparing the classification performance of the original model with the obtained using a linear combination of the reduced number of calculated

components, it is possible to find the optimal number of components (n) that does not significantly reduce the classification performance of the original model.

Then, the interpretation model presented in chapter 7 has been modified adding a new layer after the last layer feature space to calculate online the components of every analyzed image. This layer is a linear transformation and acts as a dimensionality reduction layer (see fig. 8.1). The final classification is achieved linearly combining the low dimensional IC layer.

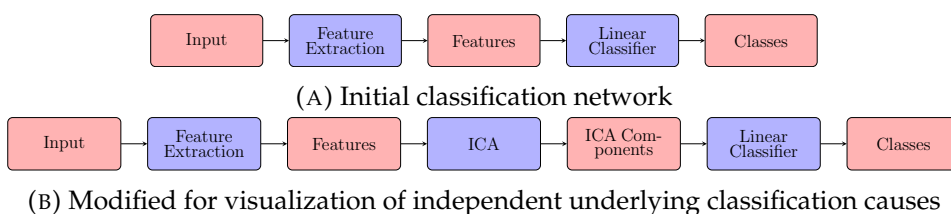


FIGURE 8.1: Model changes done for improving explainability

After identifying the optimal n , we use the receptive field and pixel-wise explanation model presented in chapter 7 to visualize the independent scores in the input space. In this way we are visualizing not only a score map explaining a classification but also differentiating and visualizing the mathematically IC responsible of a particular classification.

8.2.1 Mathematical formalization

Let F_{train} be the set of all feature vectors of training set:

$$F_{train} = \{f^{(i)} : i = 1..T\}, \quad f^{(i)} = (f_1^{(i)}, f_2^{(i)}, \dots, f_m^{(i)}) \quad (8.1)$$

being T the number of elements of the training set, and m the dimension of feature space vector obtained after feature extraction layers of the DCNN.

Let S_{train} the set of IC calculated from F_{train} :

$$S_{train} = \{s^{(i)} : i = 1..T\}, \quad s^{(i)} = (s_1^{(i)}, s_2^{(i)}, \dots, s_n^{(i)}) \quad (8.2)$$

8.2. ICA based interpretation procedure

143

being n the number of IC, $n < m$.

Every $\mathbf{s}^{(i)}$ can be expressed as a linear combination of $\mathbf{f}^{(i)}$:

$$\mathbf{s}^{(i)} = \mathbf{W}\mathbf{f}^{(i)} \quad (8.3)$$

Where \mathbf{W} is calculated using a optimization method, minimizing the mutual information between n IC ($\min_S I(S)$) (Hyvarinen, 1999).

The classification problem solved using F_{train} can be expressed as the maximization of A given that:

$$\max_A [\kappa_{val}(C_{train})] \quad (8.4)$$

being:

$$C_{train} = \{A\mathbf{f}^{(i)}, \forall \mathbf{f}^{(i)} \in F_{train}\} \quad (8.5)$$

being $\mathbf{c}^{(i)} = A\mathbf{f}^{(i)}$ the predicted class vector for feature vector $\mathbf{f}^{(i)}$ and κ_{val} the evaluation function calculated for the validation set.

We want to solve the same problem using a small number of ICA components (feature space compressed version):

$$C'_{train} = \{B\mathbf{s}^{(i)}, \forall \mathbf{s}^{(i)} \in S_{train}\} \quad (8.6)$$

so we find B that $\max_B [\kappa_{val}(C'_{train})]$

being $\mathbf{c}'^{(i)} = B\mathbf{s}^{(i)}$ the predicted class vector using n IC.

The optimal number of IC, ie. the dimension of $\mathbf{s}^{(i)}$ to select is the one that minimizes the difference in performance between both models:

$$\min_n [\kappa_{val}(C'_{train}) - \kappa_{val}(C_{train})] \quad (8.7)$$

8.3 Results

8.3.1 Data

The evaluation of the method has been done using the same EyePACS dataset distribution used in chapter 5.

8.3.2 Baseline model

The model used is also the model described in chapter 5. A schematic representation of the model can be found in figure 5.3.

8.3.3 Model modifications

For all the training set we calculate the last layer feature space, obtaining a 64-dimensional vector as a representation of each image. We observe that this vector is highly redundant. After applying a PCA, with only 10 components it is possible to explain 99% of the variance.

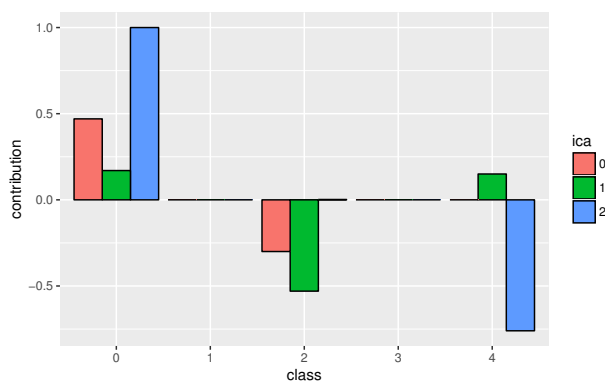


FIGURE 8.2: Contribution of each ICA component in the classification final score

Using the 64-dimensional feature-space vector ($m = 64$) of all the training set, we calculate a set of ICAs using different n values. With each one, we train a linear classifier to calculate the evaluation metric obtained over a validation set (fig. 8.1b). We choose the minimal n that allows achieving

maximum performance. The optimal n for this problem is 3, achieving a $QWK_{val} = 0.790$ not far from the achieved by the original model without dimensionality reduction ($QWK_{val} = 0.800$).

Fig. 8.2 shows the contribution of each component to the score of each class. We can see that ICA values are differentiating between extreme classes 0, 2 and 4. As we are training the network using as a loss function QWK , the optimization takes place as an ordinal regression. We expect the network to find the underlying causes present in the image that produce the predefined sorting of the classes, ie. the types of lesions and the number of them. Class 0 score contributions come from $ICA_0 > 0$, $ICA_1 > 0$ and $ICA_2 > 0$; being the class markers of the presence of disease $ICA_0 < 0$, $ICA_1 < 0$ and $ICA_2 < 0$. Analyzing the pixels with higher negative signals in the three components will give us the points that are contributing the most to the signaling of a possible presence of the disease. Backpropagating the scores of each one of this negative components will give a richer explanation with distinction between three possible independent causes of the final diagnostic given by the model.

We use a two-dimensional t-SNE visualization (Maaten and Hinton, 2008) for qualitative evaluation of the difference between the quality of the separation using the 64 feature vector and of the reduced version with only 3 ICA components. In fig. 8.3 we show the 2D t-SNE visualization for the original feature space and for the ICA reduced space. We can see how for both spaces class 0, 2 and 4 classes are clearly separated. Class 0 and 1 are not properly separated and in the case of 3 and 4, although the separation is not perfect, it is possible to distinguish a different location of both classes for both spaces. As the quantitative index QWK also show, there is not a qualitative separation capability difference between the t-SNE map of the original features and the map of the ICA 3 dimensional compressed feature map. For such 1.25% difference in the classification performance index ($\kappa_{orig} = 0.800$ vs $\kappa_{ICA} = 0.790$) we can conclude that the independent component analysis has been able to find a adequate compressed expression of the information encoded in the network.

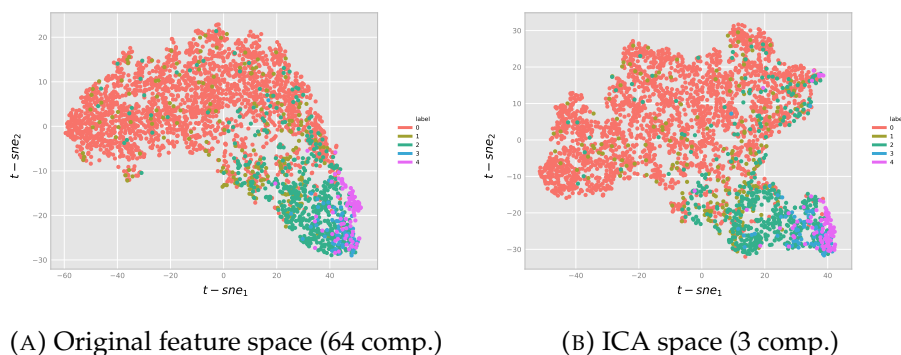
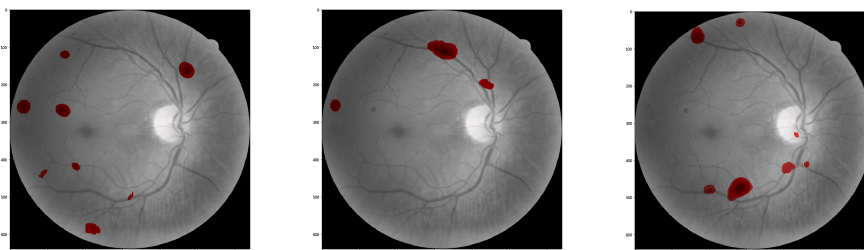


FIGURE 8.3: Comparison between the 2D t-SNE visualization of validation set using the original feature space and the final 3-dimensional ICA space

8.3.4 Score components contribution for a test sample

We use a pixel-wise relevance propagation derived method for visualizing each ICA component independently. In this way, it is possible to visualize the mathematically independent contributions, enhancing the localization of different types of primary elements causing the disease. Figure 8.4 shows the intermediate score maps generated using a RF of 61x61 for an image of class 2. Figure 8.5 shows the same intermediate scores for a class 4 image.



(A) $ICA_0 < -2\sigma$

(B) $ICA_1 < -2\sigma$

(C) $ICA_2 < -2\sigma$

FIGURE 8.4: ICA score maps generated for a class 2 image (predicted also as class 2) using a RF of 61x61

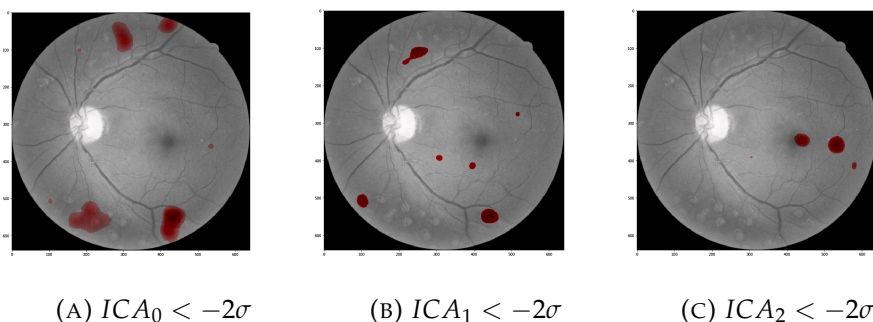


FIGURE 8.5: ICA score maps generated for a class 4 image (predicted also as class 4) using a RF of 61x61

These hidden layer maps are useful when a general map of the lesion locations is enough. Input-space pixel scores are the most suitable when pixel detail is required for detecting the individual lesions causing the disease.

After a validation with ophthalmologist, we can say that ICA_2 score maps have an almost perfect match with real lesions having a very low rate of false positives and false negatives. ICA_0 and ICA_1 include statistical regularities not directly related with relevant lesions. From such interpretation we conclude that ICA acts as a filter separating lesion information present in images from blink artifacts, noise and other statistical regularities present in images.

Figure 8.6 show the input space final scores for ICA_2 . We show the points having contributions higher than a prestablished limit, in this case with values higher than two standard deviations.

8.4 Conclusions

In this paper we studied some of the feature space properties of an already trained DR deep learning classifier of 17 layers described in chapter 5. We saw how, even being a small network, the redundancy of the feature space is very high. We hypothesized that if the network is able to achieve human-level classifications, in some way, it has been able to identify the important

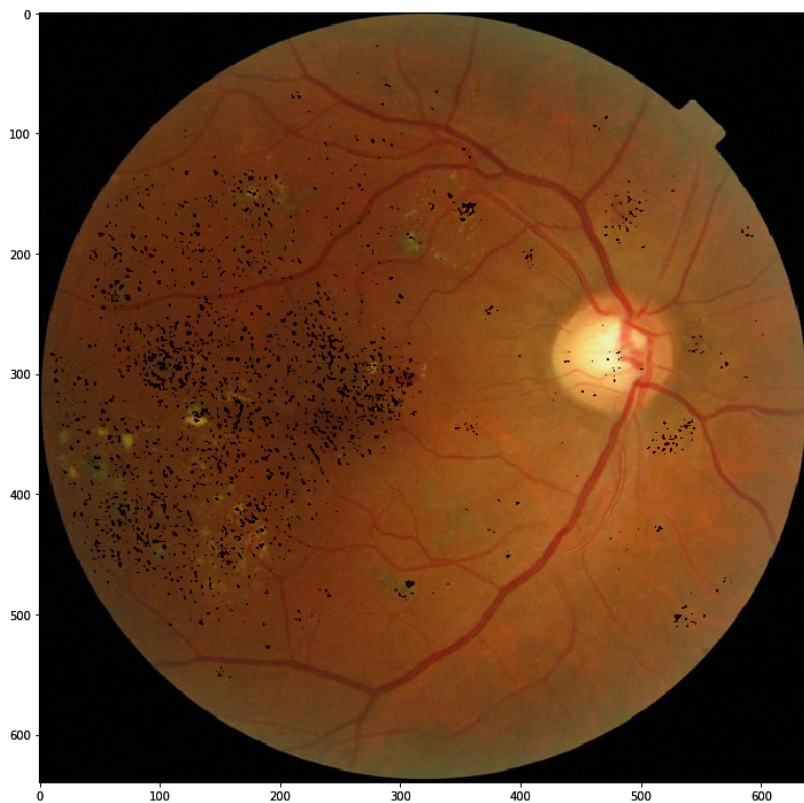


FIGURE 8.6: Visualization of ICA_2 score map for a class 3 image ($-ICA_2 < 2\sigma_2$). The classification model scores are $C_0 = -661.0$, $C_1 = -294.1$, $C_2 = -10.3$, $C_3 = 70.3$, $C_4 = 26.3$; $ICA_0 = 0.0174$, $ICA_1 = -0.0181$, $ICA_2 = -0.0237$

statistical regularities present in the image that are important for the classification. As last layer is a linear classifier, such properties has to be disentangled, ie. expressed in a linear way in such last layer. We applied a independent component analysis over such last layer with the method explained in the paper in order to find the optimal number of components

that maximize the classification capabilities of such compressed version of the features. We experimentally proved that reducing to only 3 components is possible to achieve almost 99% of the evaluation metric. Such value experimentally prove that the ICA compression has been able to extract all the important elements required for the classification. With such elements, we applied a visualization technique for identifying the elements in the image of each one of the components, using a pixel-wise derived visualization technique. We are able to generate three maps for every image each one identifying independent statistical regularities important for the classification.

Our method allows not only the classification of retinographies but also the identification and localization in the image of the independent signs of the disease. The presented ICA score model is of general applicability and can be easily adapted for the usage in other image classification tasks.

UNIVERSITAT ROVIRA I VIRGILI

DIABETIC RETINOPATHY CLASSIFICATION AND INTERPRETATION USING DEEP LEARNING TECHNIQUES

Jordi De la Torre Gallart

Part III

Experimental Application and Conclusions

UNIVERSITAT ROVIRA I VIRGILI

DIABETIC RETINOPATHY CLASSIFICATION AND INTERPRETATION USING DEEP LEARNING TECHNIQUES

Jordi De la Torre Gallart

Chapter 9

Inference using HUSJR data

In this chapter is presented a study done with the collaboration of a team of ophthalmologists of Tarragona province with images collected during 8 years at *Hospital Universitari Sant Joan de Reus (HUSJR)* in the framework of the Spanish project PI15/01150. The results show that the original model trained with EyePACS, after being fine-tuned for the prediction of classes, following the Messidor-2 standard, is able to predict with a high confidence the ophthalmologists' classifications.

9.1 Introduction

Machine Learning paradigm allow computer systems the ability to learn from data. These algorithms permit the identification of the most relevant features and the way of combining them to maximize the performance in a particular classification or regression problem. Identifying such a set of important features enables the generalization of prediction capabilities of the designed models.

After the training process we usually want to use the model for inference over different data. New data can share a priori most of the properties of data used in training, but also it may have distinctive properties not present in the original data that could influence on the classification, ie. the probability distributions of both populations can be similar but also have some differences. Therefore, before applying inference over this new data, it is important to check for the existence of distinctive elements affecting the classification/regression performance. If this happens,

we say that there is a dataset shift between both populations producing a co-variate shift in the model derived features used for prediction by the model (Sugiyama, Lawrence, and Schwaighofer, 2017). Detecting or discarding such a co-variate shift is critical when using models from prediction in similar but different populations.

Exploratory Analysis using Graphical Methods are a very good way of detecting the class separation quality. Feature-space domains are frequently highly correlated spaces that can be compressed into lower dimensional space representations. The shape of the internal representation of the data manifold determines the effectiveness of the dimensionality reduction method. In cases where the manifold holds a linear representation, methods like Principal Components Analysis (PCA) (Pearson, 1901), Multidimensional Scaling (MDS) (Kruskal, 1964) or Independent Components Analysis (ICA) (Hyvarinen, 1999) can be very effective. In cases where the manifold is non-linear or the points are too close to each other, non-linear techniques like Isometric Mapping (ISOMAP) (Tenenbaum, De Silva, and Langford, 2000) or t-distributed Stochastic Neighboring Embedding (t-SNE) (Maaten and Hinton, 2008) are more effective.

For visualization purposes the objective is to find a method that is able to separate diverging points and to cluster those with similar properties in a two-dimensional or three dimensional space. Even in cases where the manifold can be linearly compressed into a smaller representation, if the dimensions are more than three, it does not allow visualization, requiring the usage of non-linear methods to reduce even more the dimensionality to two or three dimensions.

t-SNE is a very effective visualization method that, with the proper selection of parameters, is able to separate effectively the different classes present in the manifold. t-SNE uses an optimization algorithm to minimize the Kullback-Leibler divergence (Kullback and Leibler, 1951) between two probability distributions, one in the original multidimensional space and another one in the visualization space. Variables to optimize are the distance between points in the visualization space.

Therefore, we will use t-SNE for the analysis of the dataset provided by HUSJR. We also have, in this case, the assistance of the ophthalmology team of this hospital. So, we defined a four-step methodology for the testing of the classification model using their dataset. The description of this dataset

can be found in chapter 2.

9.2 Methods

In this section we present the method that is used for adapting the model trained with the EyePACS model to the HUSJR population.

The steps required for model adaptation can be summarized in: model evaluation, standardization of categories, model and dataset adaptations and final evaluation.

9.2.1 Original model evaluation

In this phase disease experts check the model predictions over the test set of the original model. The first thing that has to be checked is the compatibility between class output definition in the original model with the classes defined in the objective data set. If differences in class definition are identified, they must be taken into account because it would require a retraining of the model. This first step allows also the evaluation of the predictions quality and to have a qualitative evaluation on original model test images.

9.2.2 Category standardization

The objective of this part is comparing if the categorization used in original model is the same that is required in the target population. Sometimes, categories can be interpreted in slightly different ways if the definition is more precisely established. This happens in medicine where subjectivity appears. If differences are detected, they require some adaptation either in the target class or in the model class definitions.

9.2.3 Model and dataset adaptations

If evident discrepancies are detected, class re-definitions in original model and target population should be applied, requiring either retraining in model or relabeling in target population. If model classes are redefined, the model must be retrained. If changes are mild, probably a last layer

classification retraining will suffice. If evaluation function results are not optimal, deep changes are required, ie. a full network retraining.

9.2.4 Final evaluation

Finally, the modified dataset is tested with the classification model in order to validate it. Having possible qualitative and quantitative results, the final model can be used for inference in the new objective population.

9.3 Results

In this section we present the results of the four steps proposed for analyzing the HUSJR dataset.

9.3.1 Original model evaluation

The first important difference between model and the new population is the categorization employed. Original model is designed for differentiation of 5 classes. HUSJR population distinguishes between only 4 classes. Expert analysis over images of the original data set indicate that, HUSJR classification groups together class 3 and 4 of the original model.

Two tests are done in order to have a initial evaluation of the performance of the model:

Firstly, an evaluation of all images is done using the original DCNN model. Table 9.1 shows the results obtained of the classification. Calculated QWK index is 0.791 for 4 classes (grouping class 3 and 4). This value is about 1,6% lower than the achieved for the EyePACS test set, ie. $QWK = 0.804$ and a 5% lower than the achieved for Messidor-2 Dataset of the original model ($QWK = 0.831$).

Secondly, t-SNE is used for visualizing the feature-space vector representation of each image. Figure 9.1 shows a two-dimensional t-SNE visualization of the feature space. Each point representing an image and point color representing the tagged class. We can see a gradation separation between classes very similar to the observed in original and in Messidor datasets.

| | Pred 0 | Pred 1 | Pred 2 | Pred 3 | Pred 4 |
|--------|--------|--------|--------|--------|--------|
| True 0 | 15,112 | 2,024 | 159 | 6 | 12 |
| True 1 | 11 | 547 | 326 | 14 | 3 |
| True 2 | 0 | 4 | 439 | 133 | 7 |
| True 3 | 0 | 1 | 20 | 358 | 54 |

TABLE 9.1: Confusion matrix of predicted classes vs classes given by HUSJR with EyePACS trained original model. $QWK = 0.791$ (Grouping together class 3 and 4)

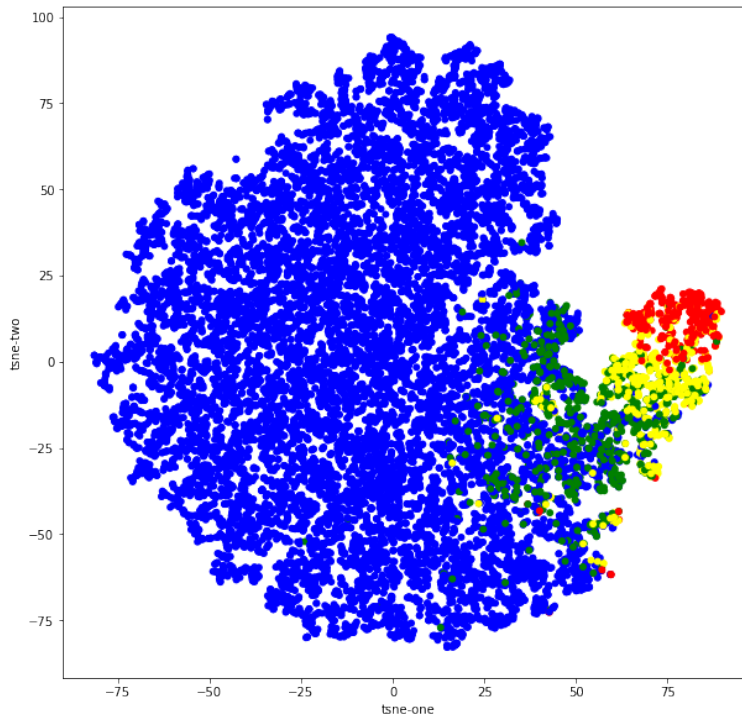


FIGURE 9.1: t-SNE visualization of the feature space representation of samples of HUSJR dataset. Blue points represent class 0 images, green points class 1, yellow points class 2 and red points class 3

9.3.2 Category standardization

Due to the differences observed between the original classification and the new one, HUSJR experts decide to use as a standard classification the defined one in Messidor-2 database (Decencière et al., 2014). In this categorization, only four classes are defined. HUSJR sample is reviewed to adapt the original classification to the new defined standard.

9.3.3 Model adaptation

Original model is designed as a combination of a fully convolutional neural network that acts as a feature extractor. Features are linearly combined for classification. Messidor-2 last layer feature vectors are calculated. A new linear classifier is trained using these features for the prediction of new standardized classes. The combination of original feature extractor with the new last linear layer is used as a new prediction model for calculation of the new predicted classes of the HUSJR sample.

9.3.4 Results re-evaluation

The new confusion matrix obtained for HUSJR is presented in table 9.2.

| | Pred 0 | Pred 1 | Pred 2 | Pred 3 |
|--------|--------|--------|--------|--------|
| True 0 | 15,277 | 1,944 | 83 | 9 |
| True 1 | 5 | 595 | 284 | 17 |
| True 2 | 0 | 2 | 456 | 125 |
| True 3 | 0 | 1 | 6 | 426 |

TABLE 9.2: Confusion matrix of predicted classes vs original classes (HUSJR Dataset) with EyePACS trained original model plus a linear classifier retrained using Messidor Dataset. $QWK = 0.823$

QWK inter-rater agreement evaluation index obtained ($QWK = 0.823$) is similar to the reached between ophthalmologist experts in disease detection.

The indexes obtained for classification of the most severe cases of the disease (considering positive class = 2,3 and negative class = 0,1) are:

- Sensitivity = 0.997
- Specificity = 0.978
- Positive predictive value (PPV) = 0.720
- Negative predictive value (NPV) = 0.9998
- False negative rate (FNR) = 0.003
- False positive rate (FPR) = 0.022
- False discovery rate (FDR) = 0.280
- False omission rate (FOR) = 0.0001
- Accuracy (ACC) = 0.979
- F_1 Score = 0.836
- Matthews correlation coefficient (MCC) = 0.838
- Bookmaker Informedness (BM) = 0.975
- Markedness (MK) = 0.720

Sensitivity obtained is greater than 0.99 and *Specificity* near 0.98 for the detection of the most severe cases of the disease. These and all the other indexes prove experimentally that the model is able to predict with high confidence the correct values of the disease for the new population of study.

9.4 Conclusions

In this chapter, it is studied the applicability of our best model for the prediction of diabetic retinopathy, trained using the EyePACS dataset, for the prediction of diabetic retinopathy in HUSJR. A feature space visualization has been done in order to check its capacity for separating between classes. After checking that the separation was done properly, a first evaluation of the model predictability was done, obtaining good results, but with small

loss in performance. This loss was probably produced to the slight differences in class definitions. After its standardization, the linear classifier of the model was retrained using Messidor-2 Dataset, using as a feature extractor the original model. Performance of the new model was tested again, reaching values of inter-rater agreement similar to the obtained by expert ophthalmologists. Classification indexes for the detection of the most severe cases of the disease are also presented, showing excellent performance also over the new population. Modified model is ready to be used for inference over the new population. Medical team is extremely satisfied with the results. Dr. Pere Romero, head of Ophthalmology Unit at HUSJR confirms that the quality of the classification is good enough to be used in a near future.

Chapter 10

Conclusions

10.1 Summary of contributions

Medical diagnosis is heavily supported by Medical Imaging. The analysis of medical images requires highly specialized expertise that is provided by specialized doctors. The advent of advanced machine learning techniques, like deep learning, is facilitating the design of high performance automatic classifiers in a broad range of applications, also for medical diagnosis. The purpose of this thesis is the exploration of new automatic diagnostic methods for medical diagnosis, concretely for diabetic retinopathy disease grading. As stated before in this work, DR is one of the main causes of blindness in the world. Early detection can reduce disease progression and consequently also the incidence of blindness. The diagnostic of DR is done primarily by retina fundus image analysis, that is done by ophthalmologists specifically trained for this purpose. Automatic diagnostic systems for DR can reduce dramatically not only the costs associated to diagnostic, but also the probability of developing blindness in the general population.

For this purpose we use supervised deep learning techniques. Given a class differentiation based on objective properties present in data, these parameterized models are able to learn the statistical regularities that have to be taken into account to separate the images. In this thesis, convolutional neural networks are used, which are efficient neural networks designed for exploiting local high correlations present in images.

Machine learning methods in general and deep learning in particular are models that learn from data. Thus, a key factor for the success is having

a statistically representative dataset of the population from which we want to predict a concrete property, in this case, a disease class. For this purpose it is required to have a labeled dataset with enough samples (that are of the order of magnitude of thousands elements per class) in order to create models with good generalization. For this purpose, we use a public dataset of EyePACS. This dataset is described in chapter 2.

In chapter 3, we explore the first classification methods. In this case the original images have different high resolution values. Ideally, it is interesting to use images with the highest resolution available, but memory and computation time required make infeasible to use neural network models in such conditions. Furthermore, neural networks architectures are parameterized models that require the usage of constant input size. Additionally, lesions present in images, from which classification is inferred, can be detected with lower resolutions. In this chapter, we explore the usage of different input sizes, data augmentation techniques and optimization strategies, that serve as a basis for selecting the best hyper-parameters. Ensembling techniques, averaging a set of predictions coming from the evaluation of different rotated versions of the same input image, and bayesian analysis, combining predictions of one patient eye with conditional probabilities of having the disease in the other, are also used for improving results. From this preliminary work, a near human-level performance model is obtained. Loss function used in this chapter for neural network parameter optimization is the established standard for multi-class classification, ie. logarithmic loss.

As the evaluation function used for performance measure is quadratic weighted kappa, it is hypothesized that directly optimizing such function could generalize better. In chapter 4 it is presented a way to use quadratic weighted kappa as a loss function for optimization of neural networks. First order derivatives are developed, in order to facilitate its usage with gradient descent derived optimization methods. Different ordinal regression use cases using quadratic weighted kappa as a main evaluation function are studied, proving that in all of them, more than 5% increase in performance can be achieved optimizing directly QWK instead of logarithmic loss.

In chapter 5 the new hardware available enables the usage of higher input resolutions and a faster computation time. This fact combined with

the usage of hyper-parameters selected in chapter 3 and with the design of the new loss function done in chapter 4 permits the design of models with ophthalmologist-level performance. In section 5.3.2 of this chapter, the most important hyper-parameters that have to be taken into account to achieve such results are summarized. This guidelines include parameters like the input size, convolution operators recommended sizes, number of filters per layer, data augmentation strategies, etc.

In chapter 6, model robustness against changes in input images is also studied. Deep learning models are known to be very sensible to changes in input conditions. The objective of this chapter is the study of model robustness to typical changes in input conditions. The studied variables are rotation, hue, saturation and lightness, experimentally proving that the designed model is robust to changes in lightness, saturation and rotation but very sensible, as expected, to hue changes in input images. The hue dependency seems to be due to the fact that network use color information for differentiating lesions from healthy tissue.

At this point, performance standards are achieved, but having the model high statistical confidence, it shares with other deep learning models a major drawback, its lack of interpretability made it behave as a black box intuition machine. For improving medical applicability of such classifiers it is very important not only to have a high confidence statistical classifier but also to have a model that is able to provide an interpretation of the results to physicians.

With the idea of providing interpretation capabilities to our models, in chapter 7, a general purpose pixel-wise explanation model is designed. Such interpretation model backpropagates last layer classification scores until reaching input space generating the so called pixel score maps, that are maps with the distribution of the final score for each input pixel. The pixels having higher scores are identified as the most important for a particular classification. Such model propagates scores through the network in two different ways: scores that depend on layer input are directly propagated to previous layer and constant scores of the layer, ie. related to biases, are transferred directly to the corresponding receptive field using a gaussian prior. Such interpretation model is designed in a modular manner, making it usable for any model architecture and in any application. In this thesis, its validity for predicting lesions (that explain classifications for the

diabetic retinopathy disease grading) is tested, achieving high correlation between predicted and real lesions.

In chapter 8, another way of improving interpretability is explored, that is feature space data compression. Feature space deep learning models tend to be high correlated, high dimensional spaces. In this chapter, a method for compression of such space is proposed. In cases where classification layer is designed as a linear feature combinations we assume that the model is able to disentangle the important features required for the classification, making its dependency linear. For such models, a method is proposed for compressing the feature space based on Independent Component Analysis. A method for the selection of optimal number of components is proposed. The proposed method is of general applicability and its validity is tested using our diabetic retinopathy disease grading model. The original vector space of 64 dimensions is compressed to only three features, achieving 99% of performance of the original model without compression. Furthermore, such independent components can independently visualized in the input space using the method designed in chapter 7.

Finally, in chapter 9 designed models are adapted to be used in a potentially different population coming from Hospital de Reus patients. Feature visualization techniques were used in order to check that the class separation capabilities showed in the original model are compatible with the new population, arriving to a positive conclusion. Compatibility of class definitions is also tested, detecting some discrepancies between the standards defined in EyePACS and the HUSJR requirements. A retraining of the classification layer using Messidor-2 dataset was enough to achieve ophthalmologist level accuracy in the new dataset.

After the work done in this thesis, we can conclude that designed models can be used successfully as a high confidence diagnostic tool that can help to reduce costs in diagnostic and also to reduce the incidence of the DR disease in the general population.

10.2 Future research lines

After the work done in this PhD thesis and the knowledge we have got from deep learning models as well as from diabetic retinopathy disease, some other study lines can be derived.

Future research lines can be focused on the next different directions, that we explain below:

1. *Increase the number of classes to predict*: One of the lines to explore is increasing the number of properties to predict of the original model. Instead of only predicting diabetic retinopathy class, other classes can also be included. Gradability class for example, can add information about image quality, ie. if its enough to be used as a proof of disease. Macular Edema prediction can also be added, incrementing the disease diagnostic information given by the automatic classifier. Furthermore, other diseases not directly related with diabetic retinopathy can also be detected, broadening the spectra of diagnostic. We hypothesize that using the same network for diagnostic of different diseases can help to increase the network performance, due to the increase the number of images available and to the added diversity for the detection of different diseases.
2. *Transfer learning*: Successful networks in challenging tasks like ImageNet, can be good candidates to perform well in specialized medical imaging tasks like ours. Transferring knowledge from trained networks to other completely different fields have been proven to be a good way to initialize networks and improving performance.
3. *Unsupervised learning*: Generative Adversarial Networks can also be explored for generating new high quality samples from the original dataset. Such sample generation models are able to generate potentially unlimited number of artificial training samples that could allow, not only the training of more powerful models, but also the usage of artificially generated images that do not belong to any particular patient, ie. removing completely potential privacy legal concerns.

4. *Reinforcement Learning*: Adding to the models the possibility of enhancing its performance, designing online learning methods that allow continuous learning of networks from the corrections done by ophthalmologists on inference time. Hospital Universitari Sant Joan de Reus wants to use the classification model developed in this thesis in its daily work. This needs a previous process of integration of computer systems as well as the permission of Catalan Health Care authorities. If it is finally done, learning from online work could be very interesting.
5. *Use of Interpretation Model in other applications*: The designed interpretation model is domain independent, therefore, it would be interesting the study of its application in other domains, ie. for interpretation of other medical imaging classification tasks like for example, radiology, ultrasound, or other related imaging applications.
6. *Interpretation model for unsupervised image segmentation*: Other interesting aspect to explore is its usage in the segmentation domain. For this particular area of expertise U-Net derived networks are working very well but it could be interesting to explore the usage of classification networks amplified with its interpretation model as a alternative way of segmenting images without specifically annotating segmentation masks.

Bibliography

- Aguiree, Florencia et al. (2013). “IDF diabetes atlas”. In:
Aldington, SJ et al. (1995). “Methodology for retinal photography and assessment of diabetic retinopathy: the EURODIAB IDDM complications study”. In: *Diabetologia* 38.4, pp. 437–444.
- Bach, Sebastian et al. (2015). “On pixel-wise explanations for non-linear classifier decisions by layer-wise relevance propagation”. In: *PloS one* 10.7, e0130140.
- Baehrens, David et al. (2010). “How to explain individual classification decisions”. In: *Journal of Machine Learning Research* 11, Jun, pp. 1803–1831.
- Baldi, P. and P. Sadowski (2013). “Understanding Dropout”. In: *Advances in Neural Information Processing Systems (NIPS)*. Ed. by C. J. C. Burges et al. Vol. 26, pp. 2814–2822.
- Bengio, Yoshua (2009). “Learning deep architectures for AI”. In: *Foundations and Trends in Machine Learning* 2.1, pp. 1–127.
- Bengio, Yoshua, Aaron Courville, and Pascal Vincent (Aug. 2013). “Representation Learning: A Review and New Perspectives”. In: *IEEE Trans. Pattern Anal. Mach. Intell.* 35.8, pp. 1798–1828. ISSN: 0162-8828.
- Brain, Google (Nov. 2018). *Diabetic Retinopathy grades (as well as DME and Gradability) for the publically available MESSIDOR-2 fundus image database @ONLINE*. URL: <https://www.kaggle.com/google-brain/messidor2-dr-grades/home>.
- Bushberg, Jerrold T and John M Boone (2011). *The essential physics of medical imaging*. Lippincott Williams & Wilkins.
- Cardoso, Jean-François (2003). “Dependence, correlation and gaussianity in independent component analysis”. In: *Journal of Machine Learning Research* 4, pp. 1177–1203.
- Chollet, François (2017). “Xception: Deep learning with depthwise separable convolutions”. In: *arXiv preprint*, pp. 1610–02357.

- Cireřan, Dan Claudiu et al. (2010). "Deep, Big, Simple Neural Nets for Handwritten Digit Recognition". In: *Neural Computation* 22.12, pp. 3207–3220.
- Clevert, Djork-Arné, Thomas Unterthiner, and Sepp Hochreiter (2015). "Fast and Accurate Deep Network Learning by Exponential Linear Units (ELUs)". In: *CoRR* abs/1511.07289.
- Cohen, Jacob (1960). "A coefficient of agreement for nominal scales". In: *Educational and psychological measurement* 20.1, pp. 37–46.
- (1968). "Weighted kappa: Nominal scale agreement provision for scaled disagreement or partial credit." In: *Psychological bulletin* 70.4, p. 213.
- Cohen, Nadav, Or Sharir, and Amnon Shashua (2016). "On the expressive power of deep learning: A tensor analysis". In: *Conference on Learning Theory*, pp. 698–728.
- Comon, Pierre (1994). "Independent component analysis, a new concept?" In: *Signal processing* 36.3, pp. 287–314.
- Dahl, George E., Tara N. Sainath, and Geoffrey E. Hinton (2013). "Improving Deep Neural Networks for LVCSR using Rectified Linear Units and Dropout". In: *IEEE International Conference on Acoustics, Speech and Signal Processing (ICASSP)*, pp. 8609–8613.
- Decencière, Etienne et al. (Aug. 2014). "Feedback on a publicly distributed database: the Messidor database". en. In: *Image Analysis & Stereology* 33.3, pp. 231–234. ISSN: 1854-5165. DOI: [10.5566/ias.1155](https://doi.org/10.5566/ias.1155). URL: <http://www.ias-iss.org/ojs/IAS/article/view/1155>.
- Deng, J. et al. (2009). "ImageNet: A Large-Scale Hierarchical Image Database". In: *CVPR09*.
- Dumoulin, Vincent and Francesco Visin (2016). "A guide to convolution arithmetic for deep learning". In: *arXiv preprint arXiv:1603.07285*.
- Dundar, Aysegul, Jonghoon Jin, and Eugenio Culurciello (2015). "Convolutional Clustering for Unsupervised Learning". In: *CoRR* abs/1511.06241.
- Eldan, Ronen and Ohad Shamir (2016). "The power of depth for feedforward neural networks". In: *Conference on Learning Theory*, pp. 907–940.
- Escorcia-Gutierrez, José et al. (2016). "Interactive Optic Disk Segmentation via Discrete Convexity Shape Knowledge Using High-Order Functionals". In: *Artificial Intelligence Research and Development - Proceedings of the 19th International Conference of the Catalan Association for Artificial Intelligence, Barcelona, Catalonia, Spain, October 19-21, 2016*, pp. 39–44.

- Esteva, Andre et al. (2017). "Dermatologist-level classification of skin cancer with deep neural networks". In: *Nature* 542.7639, p. 115.
- EyePACS (Nov. 2018). *EyePACS Dataset @ONLINE*. URL: <https://www.kaggle.com/c/diabetic-retinopathy-detection/data>.
- Fairchild, Mark D (2013). *Color appearance models*. John Wiley & Sons.
- Fleiss, Joseph L., Jacob Cohen, and B. S. Everitt (1969). "Large sample standard errors of kappa and weighted kappa". In: *Psychological Bulletin* 72(5), pp. 323–327.
- Fong, Donald S et al. (2004). "Retinopathy in diabetes". In: *Diabetes care* 27.suppl 1, s84–s87.
- Fukunaga, Keinosuke (2013). *Introduction to statistical pattern recognition*. Elsevier.
- Glorot, Xavier and Yoshua Bengio (2010). "Understanding the difficulty of training deep feedforward neural networks". In: *Proceedings of the thirteenth international conference on artificial intelligence and statistics*, pp. 249–256.
- Glorot, Xavier, Antoine Bordes, and Yoshua Bengio (2011). "Deep sparse rectifier neural networks". In: *Proceedings of the fourteenth international conference on artificial intelligence and statistics*, pp. 315–323.
- Goodfellow, Ian, Yoshua Bengio, and Aaron Courville (2016). *Deep Learning*. MIT Press.
- Graham, Benjamin (2014). "Fractional Max-Pooling". In: *CoRR* abs/1412.6071.
- Gulshan, V., L. Peng, and M. Coram (2016). "Development and validation of a deep learning algorithm for detection of diabetic retinopathy in retinal fundus photographs". In: *Journal of the American Medical Association* 316.22, pp. 2402–2410.
- Günther, Klaus P and Yi Sun (1999). "Reliability of radiographic assessment in hip and knee osteoarthritis". In: *Osteoarthritis and Cartilage* 7.2, pp. 239–246.
- He, K. et al. (2015). "Delving Deep into Rectifiers: Surpassing Human-Level Performance on ImageNet Classification". In: *2015 IEEE International Conference on Computer Vision (ICCV)*, pp. 1026–1034.
- He, Kaiming et al. (2016). "Deep residual learning for image recognition". In: *Proceedings of the IEEE conference on computer vision and pattern recognition*, pp. 770–778.

- Hintz, Susan R et al. (2007). "Interobserver reliability and accuracy of cranial ultrasound scanning interpretation in premature infants". In: *The Journal of pediatrics* 150.6, pp. 592–596.
- Howard, Andrew G et al. (2017). "Mobilenets: Efficient convolutional neural networks for mobile vision applications". In: *arXiv preprint arXiv:1704.04861*.
- Hripcsak, George and Daniel F Heitjan (2002). "Measuring agreement in medical informatics reliability studies". In: *Journal of biomedical informatics* 35.2, pp. 99–110.
- Huang, Gao et al. (2017). "Densely Connected Convolutional Networks." In: *CVPR*. Vol. 1, 2, p. 3.
- Hyvarinen, Aapo (1999). "Fast and robust fixed-point algorithms for independent component analysis". In: *IEEE transactions on Neural Networks* 10.3, pp. 626–634.
- Hyvärinen, Aapo and Erkki Oja (2000). "Independent component analysis: algorithms and applications". In: *Neural networks* 13.4-5, pp. 411–430.
- Iandola, Forrest N et al. (2016). "Squeezenet: Alexnet-level accuracy with 50x fewer parameters and < 0.5 mb model size". In: *arXiv preprint arXiv:1602.07360*.
- Ioffe, Sergey and Christian Szegedy (2015). "Batch Normalization: Accelerating Deep Network Training by Reducing Internal Covariate Shift". In: *CoRR abs/1502.03167*.
- Kingma, Diederik P. and Jimmy Ba (2014). "Adam: A Method for Stochastic Optimization". In: *CoRR abs/1412.6980*.
- Klein, Ronald et al. (2009). "The Wisconsin Epidemiologic Study of Diabetic Retinopathy XXIII: the twenty-five-year incidence of macular edema in persons with type 1 diabetes". In: *Ophthalmology* 116.3, pp. 497–503.
- Krizhevsky, Alex, Ilya Sutskever, and Geoffrey E Hinton (2012a). "ImageNet Classification with Deep Convolutional Neural Networks". In: *Advances in Neural Information Processing Systems* 25. Ed. by F. Pereira et al. Curran Associates, Inc., pp. 1097–1105.
- Krizhevsky, Alex, Ilya Sutskever, and Geoffrey E. Hinton (2012b). "ImageNet Classification with Deep Convolutional Neural Networks". In: *Advances in Neural Information Processing Systems* 25. Ed. by F. Pereira et al. Curran Associates, Inc., pp. 1097–1105.
- Kruskal, Joseph B (1964). "Multidimensional scaling by optimizing goodness of fit to a nonmetric hypothesis". In: *Psychometrika* 29.1, pp. 1–27.
- Kullback, Solomon and Richard A Leibler (1951). "On information and sufficiency". In: *The annals of mathematical statistics* 22.1, pp. 79–86.

- La Torre, Jordi de et al. (2018). "Identification and Visualization of the Underlying Independent Causes of the Diagnostic of Diabetic Retinopathy made by a Deep Learning Classifier". In: *CoRR* abs/1809.08567. arXiv: 1809.08567. URL: <http://arxiv.org/abs/1809.08567>.
- Landis, J Richard and Gary G Koch (1977). "The measurement of observer agreement for categorical data". In: *biometrics*, pp. 159–174.
- LeCun, Y. et al. (1998). "Gradient-Based Learning Applied to Document Recognition". In: *Proceedings of the IEEE* 86.11, pp. 2278–2324.
- Lecun, Yann, Yoshua Bengio, and Geoffrey Hinton (May 2015). "Deep learning". In: *Nature* 521.7553, pp. 436–444. ISSN: 0028-0836.
- LeCun, Yann et al. (1989). "Backpropagation applied to handwritten zip code recognition". In: *Neural computation* 1.4, pp. 541–551.
- Liao, Zhibin and Gustavo Carneiro (2015). "Competitive Multi-scale Convolution". In: *CoRR* abs/1511.05635.
- Luo, Wenjie et al. (2016). "Understanding the effective receptive field in deep convolutional neural networks". In: *Advances in Neural Information Processing Systems*, pp. 4898–4906.
- MA, Mazurowski et al. (2008). "Training neural network classifiers for medical decision making: The effects of imbalanced datasets on classification performance". In: *Neural Networks* 21(2-3), pp. 427–436.
- Maaten, Laurens van der and Geoffrey Hinton (2008). "Visualizing data using t-SNE". In: *Journal of machine learning research* 9.Nov, pp. 2579–2605.
- Mehdiyev, Nijat et al. (2016). "Evaluating Forecasting Methods by Considering Different Accuracy Measures". In: *Procedia Computer Science* 95, pp. 264–271.
- Montavon, Grégoire et al. (2017). "Explaining nonlinear classification decisions with deep taylor decomposition". In: *Pattern Recognition* 65, pp. 211–222.
- Murphy, Kevin P. (2012). *Machine Learning: A Probabilistic Perspective*. The MIT Press. ISBN: 0262018020, 9780262018029.
- Nair, Vinod and Geoffrey E Hinton (2010). "Rectified linear units improve restricted boltzmann machines". In: *Proceedings of the 27th international conference on machine learning (ICML-10)*, pp. 807–814.
- Patra, S et al. (2009). "Interobserver agreement between primary graders and an expert grader in the Bristol and Weston diabetic retinopathy

- screening programme: a quality assurance audit". In: *Diabetic Medicine* 26.8, pp. 820–823.
- Pearson, Karl (1901). "Principal components analysis". In: *The London, Edinburgh, and Dublin Philosophical Magazine and Journal of Science* 6.2, p. 559.
- Ramos, Juan (2003). *Using TF-IDF to Determine Word Relevance in Document Queries*. Tech. rep. Department of Computer Science, Rutgers University, 23515 BPO Way, Piscataway, NJ, 08855e.
- Romero-Aroca, Pedro et al. (2006). "Nonproliferative diabetic retinopathy and macular edema progression after phacoemulsification: prospective study". In: *Journal of Cataract & Refractive Surgery* 32.9, pp. 1438–1444.
- Romero-Aroca, Pedro et al. (2018). "A Clinical Decision Support System for Diabetic Retinopathy Screening: Creating a Clinical Support Application". In: *Telemedicine and e-Health*.
- Russakovsky, Olga et al. (2015). "ImageNet Large Scale Visual Recognition Challenge". In: *International Journal of Computer Vision (IJCV)* 115.3, pp. 211–252.
- Saad, David (1998). "Online algorithms and stochastic approximations". In: *Online Learning* 5.
- Sammut, Claude and Geoffrey I Webb (2011). *Encyclopedia of machine learning*. Springer Science & Business Media.
- Sandler, Mark et al. (2018). "MobileNetV2: Inverted Residuals and Linear Bottlenecks". In: *Proceedings of the IEEE Conference on Computer Vision and Pattern Recognition*, pp. 4510–4520.
- Schmidhuber, J. (2015). "Deep Learning in Neural Networks: An Overview". In: *Neural Networks* 61, pp. 85–117.
- SE, Moss et al. (1985). "Comparison Between Ophthalmoscopy and Fundus Photography in Determining Severity of Diabetic Retinopathy". In: *Ophthalmology* 92(1), pp. 62–67.
- Sermanet, Pierre et al. (2014). "Overfeat: Integrated recognition, localization and detection using convolutional networks". In: *International Conference on Learning Representations (ICLR2014), CBLS, April 2014*.
- Shaw, Jonathan E, Richard A Sicree, and Paul Z Zimmet (2010). "Global estimates of the prevalence of diabetes for 2010 and 2030". In: *Diabetes research and clinical practice* 87.1, pp. 4–14.
- Sim, Julius and Chris C Wright (2005). "The kappa statistic in reliability studies: use, interpretation, and sample size requirements". In: *Physical therapy* 85.3, pp. 257–268.

- Simonyan, Karen, Andrea Vedaldi, and Andrew Zisserman (2013). "Deep Inside Convolutional Networks: Visualising Image Classification Models and Saliency Maps". In: *CoRR* abs/1312.6034. arXiv: [1312.6034](https://arxiv.org/abs/1312.6034).
- Simonyan, Karen and Andrew Zisserman (2014). "Very Deep Convolutional Networks for Large-Scale Image Recognition". In: *CoRR* abs/1409.1556.
- (2015). "Very Deep Convolutional Networks for Large-Scale Image Recognition". In: *International Conference on Learning Representations, ICLR 2015*.
- Sudha, L. R. and S. Thirupurasundari (2014). "Analysis and detection of haemorrhages and exudates in retinal images". In: *International Journal of Scientific and Research Publications* 4, pp. 1–5.
- Sugiyama, Masashi, Neil D Lawrence, Anton Schwaighofer, et al. (2017). *Dataset shift in machine learning*. The MIT Press.
- Szegedy, Christian et al. (2015). "Going Deeper with Convolutions". In: *Computer Vision and Pattern Recognition (CVPR)*.
- Szegedy, Christian et al. (2016). "Rethinking the inception architecture for computer vision". In: *Proceedings of the IEEE Conference on Computer Vision and Pattern Recognition*, pp. 2818–2826.
- Szegedy, Christian et al. (2017). "Inception-v4, inception-resnet and the impact of residual connections on learning." In: *AAAI*. Vol. 4, p. 12.
- Tenenbaum, Joshua B, Vin De Silva, and John C Langford (2000). "A global geometric framework for nonlinear dimensionality reduction". In: *science* 290.5500, pp. 2319–2323.
- Torre, Jordi de la, Domenec Puig, and Aida Valls (2018). "Weighted kappa loss function for multi-class classification of ordinal data in deep learning". In: *Pattern Recognition Letters* 105, pp. 144–154.
- Torre, Jordi de la, Aida Valls, and Domenec Puig (2016a). "Diabetic Retinopathy Detection Through Image Analysis Using Deep Convolutional Neural Networks". In: *Artificial Intelligence Research and Development - Proceedings of the 19th International Conference of the Catalan Association for Artificial Intelligence, Barcelona, Catalonia, Spain, October 19-21, 2016*. Ed. by Àngela Nebot, Xavier Binefa, and Ramon López de Mántaras. Vol. 288. *Frontiers in Artificial Intelligence and Applications*. IOS Press, pp. 58–63. ISBN: 978-1-61499-695-8.

- Torre, Jordi de la, Aida Valls, and Domenec Puig (2016b). "Diabetic Retinopathy Detection Through Image Analysis Using Deep Convolutional Neural Networks". In: *Artificial Intelligence Research and Development, Frontiers in Artificial Intelligence and Applications*. Vol. 288. IOS Press, pp. 58–63.
- (2017). "A Deep Learning Interpretable Classifier for Diabetic Retinopathy Disease Grading". In: *arXiv preprint arXiv:1712.08107*.
- Torrents-Barrena, Jordina et al. (2015). "Screening for Diabetic Retinopathy through Retinal Colour Fundus Images using Convolutional Neural Networks". In: *Artificial Intelligence Research and Development - Proceedings of the 18th International Conference of the Catalan Association for Artificial Intelligence*. IOS Press, pp. 259–262.
- Tumer, Kagan and Joydeep Ghosh (1996). "Estimating the Bayes error rate through classifier combining". In: *Proceedings of the International Conference on Pattern Recognition, Vienna, Austria, pages IV*, pp. 695–699.
- Varma, Rohit, William C Steinmann, and Ingrid U Scott (1992). "Expert agreement in evaluating the optic disc for glaucoma". In: *Ophthalmology* 99.2, pp. 215–221.
- Viera, Anthony J, Joanne M Garrett, et al. (2005). "Understanding interobserver agreement: the kappa statistic". In: *Fam Med* 37.5, pp. 360–363.
- Wang, Shui-Hua et al. (2018). "Classification of Alzheimer's Disease Based on Eight-Layer Convolutional Neural Network with Leaky Rectified Linear Unit and Max Pooling". In: *Journal of medical systems* 42.5, p. 85.
- Wilkinson, CP et al. (2003). "Global Diabetic Retinopathy Project Group. Proposed international clinical diabetic retinopathy and diabetic macular edema disease severity scales". In: *Ophthalmology* 110.9, pp. 1677–1682.
- www.diabetes.co.uk (Nov. 2018). *Diabetes Types @ONLINE*. URL: <https://www.diabetes.co.uk/diabetes-types.html>.
- Zeiler, Matthew D and Rob Fergus (2014). "Visualizing and understanding convolutional networks". In: *European conference on computer vision*. Springer, pp. 818–833.
- Zhou, Zhi-Hua (2012). *Ensemble methods: foundations and algorithms*. Chapman and Hall/CRC.
- Zhou, Zhi-Hua, Jianxin Wu, and Wei Tang (2002). "Ensembling neural networks: Many could be better than all". In: *Artificial Intelligence* 137, pp. 239–263.

-
- Zhu, Wentao et al. (2018). "Deeplung: Deep 3d dual path nets for automated pulmonary nodule detection and classification". In: *IEEE Winter Conference on Applications of Computer Vision*.

UNIVERSITAT ROVIRA I VIRGILI

DIABETIC RETINOPATHY CLASSIFICATION AND INTERPRETATION USING DEEP LEARNING TECHNIQUES

Jordi De la Torre Gallart



UNIVERSITAT
ROVIRA i VIRGILI